DEGREE PROJECT IN CHEMICAL SCIENCE AND ENGINEERING,
SECOND CYCLE, 30 CREDITS
STOCKHOLM, SWEDEN 2021

Corrosion behavior of lead-free and dezincification resistant brass alloys in tap water

NAZA ALEXIS

KTH ROYAL INSTITUTE OF TECHNOLOGY
SCHOOL OF ENGINEERING SCIENCES IN CHEMISTRY, BIOTECHNOLOGY AND HEALTH

Abstract

Dezincification resistant (DZR) and lead-free brass alloys continue to be widely applied replacing lead containing brasses in the drinking water sector. Due to the limited number of corrosion studies of these alloys in tap water, the present thesis was initiated with the aim to understand how the water type, its temperature and exposure duration can affect the corrosion behavior. Three DZR brass alloys were studied in order to evaluate their corrosion behavior in tap water of varying characteristics. The alloys included were two lead-free brasses (CW511L and CW724R) and a leaded brass alloy (CW602N) considered as a reference material. A combination of electrochemical, microscopic and surface analytical techniques were adopted to explore the corrosion form, mechanisms and corrosion rate. While these alloys passed the dezincification test as per ISO 6509-1:2014, the aim was to assess their corrosion performance in tap water.

The influence of water chemistry parameters including pH, chloride concentration and alkalinity on the corrosion resistance of the three DZR alloys was investigated in short-term exposures (24 h). Depending on the brass alloy, the corrosivity of the test waters varied. The results show grade CW511L to be more sensitive in tap water of higher chloride concentration (44.7 mg/L) and alkalinity (310 mg/L) compared with low pH (6.9). However, opposite results were obtained for both CW724R and CW602N. The corrosivity of the test water was also affected by the temperature when increased from 22°C to 50°C during 24 h of immersion. While no dezincification features were observed on the surfaces, a combination of general and localized corrosion was observed to a largely variable extent between the alloys. The extent of initiation of localized corrosion varied with test water and alloy composition. While CW724R and CW602N showed similar high susceptibility to localized corrosion in the alkaline (pH 8.2) tap water, CW511L was more prone to pitting corrosion in tap water of low pH (6.9). The effect of exposure duration was explored in the alkaline test water for the three brasses up to 72 days. Corrosion rates based on weight loss showed an expected initial high corrosion rate which declined with continuous immersion, leading to low and similar corrosion rates for all three brass alloys after 72 days. Thus, at given test conditions, the lead-free brasses showed good corrosion behavior being competitive to the performance of lead containing brass. Therefore, lead-free brass alloys are good candidates to substitute lead-containing brasses in tap water applications.

Sammanfattning

Avzinkningshärdiga och blyfria mässingslegeringar används i stor utsträckning för att ersätta blyinnehållande mässingslegeringar som används för dricksvattensapplikationer. På grund av det begränsade antalet korrosionsstudier av dessa legeringar är syftet med denna studie att belysa hur vattensammansättning, temperatur och exponeringstid kan påverka legeringarnas korrosionsegenskaper. Tre avzinkningshärdiga mässingslegeringar studerades i kranvatten; två blyfria mässingslegeringar (CW511L och CW724R) och en blyinnehållande mässingslegering (CW602N) som betraktades som ett referensmaterial. En kombination av elektrokemiska, mikroskopiska och ytanalystekniker användes för att utforska korrosionstyp, mekanismer samt korrosionshastighet. Även om samtliga legeringar visade godkända egenskaper i avzinkningstestet enligt ISO 6509-1:2014 var målet att bedöma deras korrosionsbeteende i kranvatten.

Vattenkemin justerades för att undersöka effekten av pH, kloridkoncentration och alkalinitet hos de tre mässingslegeringarna under kortvarig exponeringstid (24 timmar). Vattnets korrosivitet varierade beroende på mässingslegeringens sammansättning. Det visade sig att CW511L var känsligare för höga kloridkoncentrationer (44.7 mg/L) och hög alkalinitet (310 mg/L) än för lågt pH (6.9). Det motsatta observerades dock för både CW724R och CW602N. Testvattnets aggressivitet påverkades också av temperaturen när den ökades från 22 °C till 50 °C under exponering i 24 timmar. Medan ingen tydlig avzinkning upptäcktes observerades en kombination av både allmän och lokal korrosion i varierande utsträckning mellan de olika legeringarna. Initieringen av det lokala korrosionsangreppet varierade både med testvattnets kemi och med legeringssammansättningen. Medan CW724R och CW602N bägge uppvisade hög känslighet för lokal korrosion i vattnet med högst pH (8.2), var CW511L mer känslig i det vatten med lågt pH (6.9) vid 50 °C. Effekten av exponeringstid undersöktes i vattnet med högst pH (8.2) för de tre mässingslegeringarna upp till 72 dagar. Korrosionshastigheten baserad på viktminskning visade en förväntad hög korrosionshastighet som minskade med kontinuerlig exponeringstid, vilket ledde till en låg korrosionshastighet för alla tre mässingslegeringarna efter 72 dagar. De blyfria mässingslegeringar uppvisade ur detta perspektiv goda korrosionsegenskaper som är konkurrenskraftiga med mässing som innehåller bly.

Table of contents

1. Introduction

1.1 Background

Brass is a copper-zinc alloy commonly used in drinking water systems due to its good corrosion resistance and mechanical properties. The main components made of brass in water systems are valves, connection fittings and faucets. Various grades of brass alloys are developed by combining different amounts of copper, zinc and other additional alloying elements in controlled manufacturing processes. This result in brass alloys with different properties, such as corrosion resistance, mechanical strength, ductility and machinability. [1]

One of the most common alloy constituent in brass alloys is lead (Pb), which provides an improvement in machinability. However, Pb is hazardous and can migrate from the brass due to different chemical and electrochemical processes into the drinking water system. Therefore, the use of Pb as an alloying element is questioned as it poses health concerns. [2] To minimize the probable hazards, a more strict regulation is undergoing around the world to define a threshold limit Pb release into the drinking water. Both WHO and European commission have agreed that the maximum concentration of Pb at the tap that should not exceed 10 ppb (μg/L). This threshold is going to be reduced to 5 ppb by 2036 at the latest. [3] Brass producers and component manufacturers have therefore started to develop a new class of brasses called lead-free (Pb <0.2 wt.-%) brasses of maintained good machinability and corrosion resistance. [4]

Corrosion failures of this new class of brasses have raised the need for further research efforts trying to determine their resistance to dezincification, the typical corrosion type of brasses related to dealloying. [5-7] In terms of laboratory tests, ISO 6509-1:2014 and EN 15664-1:2013 stipulate the main standardized accelerated tests available to screen the resistance of brasses toward dezincification and assess the extent of metal release in drinking water [8,9]. Furthermore, the lack of correlation between field corrosion data and laboratory generated data in accelerated tests has raised some questions about differences in mechanisms involved in the corrosion of this new class of brasses. It is therefore important to understand the corrosion behavior of the new lead-free brass alloys regarding corrosion stimulators. An improved knowledge will enable the development of these Pb-free brass alloys to become as good substitutes for leaded brass alloys as possible, without affecting the corrosion properties, reliability or capacity. [4]

1.2 Aim and methodology

The aim of this master thesis is to investigate the corrosion behavior and mechanisms of two different modern lead-free brass alloys (CW511L and CW724R) which both have passed the ISO 6509-1:2014 dezincification test in stagnant tap water. In parallel a leaded brass alloy (CW602N) was included for comparison. Effects of environmental parameters including pH, chlorides, alkalinity and temperature was investigated from a short-term (up to 24 h) corrosion

behavior perspective. For their long-term corrosion behavior (up to 72 days), only tap water at ambient temperature was considered. The study employed a combination of electrochemical, weight loss, chemical, microscopic and surface analytical techniques to obtain information on kinetics and the mechanisms involved in the corrosion processes of the Pb-free brasses. Furthermore, this master thesis is a part of the Vinnova project OPTIBRASS (2019-02933). The project is a part of the strategic innovation program Metallic materials in committee 10825.

1.3 Sustainability aspect

The present project contributes to two interrelated Sustainable Development Goals (SDGs). This includes goal No. 3 related to good health and well-being as well as goal No. 6 to ensure clean water and sanitation. Indeed, the well-being depends on clean water, which should not contain harmful species such as Pb released from brass alloys. This can be achieved by the minimization of leaded brass alloys use for tap water applications. With this regard, the investigation of the corrosion behavior of lead-free brass alloys aims to ensure both their corrosion resistance as well as the absence of undesirable release of harmful species.

2. Brass metallurgy

2.1. Microstructure

Brass is a copper-zinc (Cu-Zn) alloy in which Zn is the principal alloying element with 5-40 wt.-% Zn. When the Zn concentration is up to 35 wt.-% with a minimum of 63 wt.-% Cu, a material with a face-centered cubic (fcc) microstructure is formed represented by the α-phase. [2] This class of α-phase brasses are known for their higher corrosion resistance compared with brasses of higher Zn content, which contain a second phase enriched in Zn, β-phase. α-brasses, also named cold working brasses, offer good ductility at room temperature, which make their cold forming an easy operation. However, their areas of applications are limited since the machinability deteriorates at higher temperatures and the high Cu content makes them more expensive. [10]

Considering the phase diagram of Cu-Zn shown in Figure 1, the β-phase can form and coexist with the α-phase for a Zn concentration between 35-45 wt.-%. These cheaper brasses are called duplex α + β brasses or “hot working brasses". They are stronger and easier to fabricate compared to α-brasses. The Zn-rich β-phase has a body centered cubic (bcc). [2] These brasses are less formable at room temperature than α-brasses. Still, they are more used in products used for water systems since their machinability is much better at higher temperatures compared with the α-brasses. However, the β-phase present in duplex α + β brasses is more prone to dezincification, a corrosion type further explained in section 1.2.1. [10]

A third phase called the γ-phase develop when the Zn content exceeds 45 wt.-%. The γ-phase typically form in grain boundaries, which increases the brittleness of the brass alloy and limit its commercialization. [10]

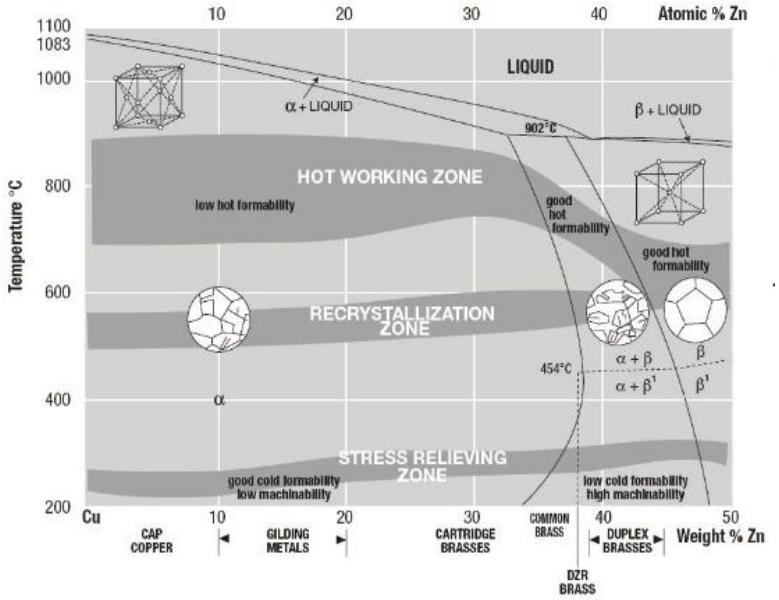

Figure 1: Cu-Zn phase diagram [10]

2.2 Brass alloying

In addition to the Cu and Zn content, other alloying elements, shown in table 1, are added to gain specific properties.

Table 1: Alloying elements added to brass (in wt.-%)

Al	Fe	Ni	Mn	As	Si	Sn	Sb	P	Pb
≤ 2 %	≤ 1 %	≤ 1 %	≤ 1 %	≤ 0.1 %	≤ 3 %	≤ 1 %	≤ 0.1 %	≤ 0.1 %	≤ 3 %

Aluminum (Al)
The addition of Al affects mainly the mechanical properties of the brass alloy resulting in an improvement in hardness and strength of the brass alloy. It affects the microstructure of the material in terms of grain size and morphology, where it stabilizes the β-phase. [11] Al improves the corrosion resistance by forming a protective and self-healing alumina oxide (Al_2O_3). [2][12]

Iron (Fe) and Manganese (Mn)
The addition of Fe and Mn is most common in duplex α + β brasses and contributes to improved hardness and tensile strength of the material without a large effect of the ductility. [12] However, small amounts of Fe have been shown to accelerate the dezincification process of β-brasses. β-brasses with the addition of Fe showed more corrosion products than formed on the same alloy without any addition of Fe. Similar findings have been shown for Mn, although with a slightly lower degree of corrosion compared with the addition of Fe. [13] Furthermore, Fe can form intermetallic compounds with arsenic (As), which can impede the corrosion inhibiting effect and provide poorer protection even in α-brasses. [1]

Nickel (Ni)
Ni is another element that contributes to an increase in hardness and tensile strength of the material without affecting the ductility. The properties of the brass alloy are also improved at higher temperatures. The presence of Ni has been shown to inhibit the dezincification of brasses. [13]

Arsenic (As)
Small amounts of As results in a considerably improved corrosion resistance of the material. Brass alloys containing As are known to be dezincification resistant brasses (DZR), where As dissolves in the α-phase and prevents corrosion of the material. This beneficial impact of As is limited to α-brasses and is not observed for either duplex- or β-brasses. However, As can interact with other elements, which leads to an increased risk for dezincification for 60-40 high purity brasses. [12]

Silicon (Si)
The addition of Si leads to an increased wear resistance and strength of the brass alloy. It is very common that alloying is done with both Si and Mn to build up a manganese silicide, a

hard intermetallic compound, in the base material. As a result, brass alloys exhibit very good wear resistant properties. The addition of Si prevents the unwanted formation of FeAs in dezincification resistant brass alloys containing As because of its reaction with Fe to form intermetallics. Silicon is also a β-phase stabilizer, which affects the corrosion behavior of the brass alloy. [10] The effect of Si toward dezincification depends on the brass alloy, where either inhibition or acceleration can be observed [14]. Furthermore, brass alloys with a high Si content have a structure containing another phase, the κ-phase, beside from α-, β- and γ-phases discussed in section 2.1. The κ-phase is a Si-rich phase with a hexagonal lattice, which leads to an increase in tensile strength and hardness of the alloy. [2]

Tin (Sn)
Sn can be added to the brass alloy to improve the corrosion resistance. It also increases, even though not on a large scale, the hardness and strength of the material. [10]

Antimony (Sb) and Phosphorus (P)
Sb and P additions are known to increase the corrosion resistance. Similar to the effect of As, they dissolve in the α-phase and improve the dezincification resistance. However, interactions with other elements can occur, which can impair the corrosion resistance. [13]

Lead (Pb)
Pb is the most common alloying element in brass alloys to improve their properties, in particular the machinability. Pb is insoluble in brass alloys and will thus not form a solid solution with Cu and Zn. This leads to its precipitation in the form of globules, during solidification. Undissolved Pb-particles are hence present both in the grain boundaries and within the alloy matrix. Alloying with Pb improves the machinability and castability of the alloy but does not affect the hardness and tensile strength of the material. Depending on the brass alloy, Pb has been shown to both enhance and inhibit the extent of dezincification. [14]
However, since Pb is classified as an hazardous element to aquatic life with long lasting effects, any release of Pb from the alloy into solution as a result of electrochemical and chemical processes should be minimized. [10]

3. Corrosion of brass

Corrosion is defined as an irreversible interaction between a material and the surrounding environment, which leads to formation of an oxidized surface layer of metal oxides and other corrosion products (often denoted patina for Cu, Zn and Cu-Zn alloys). Brasses are known to have good corrosion resistance because of their high content of Cu, which is a noble metal. However, brass contains a significant amount of Zn as well, which is a less noble metal. When a noble metal, in this case Cu, interacts with a less noble metal, Zn, the latter will preferentially corrode faster and migrate into solution. In brass, this corrosion mechanism is called dezincification. Different corrosion forms are observed for brass including dezincification (dealloying), stress corrosion cracking (SCC) and intergranular corrosion. The scope of the present thesis is limited to the dezincification, which is the most common corrosion process of brass in drinking water applications. [10]

3.1 Dezincification

Dezincification of brass corresponds to the selective dissolution of Zn, which with time leaves behind a weak porous Cu matrix. Different Cu-rich corrosion products, such as copper oxides, gradually form and predominate at the surface, of e.g. water systems (valves and fittings), because of the removal of Zn. As a result, a pink surface appearance can be observed and the mechanical properties are affected badly, which with time lead to cracks and failure of the material. Dezincification is one of the main reasons behind leaking taps, which limits the applications of brass alloys. The higher Zn content in the alloy, the higher risk for dezincification. [10]

3.1.1 Dezincification types

There are two kinds of dezincification processes: plug-type dezincification and uniform-layer dezincification. Plug-type dezincification occurs at surfaces that are mainly not affected to any large extent by corrosion and can be observed on, for example, the sides of valves and fittings. The problem with plug-type attack is that the penetration through the sides results in leakage of water and a reduced mechanical strength of the material. Uniform-layer dezincification involves the migration of Zn from a larger surface area of the product. As a result, the wall thickness of the valve or fitting is reduced and the probability of fracture under mechanical stress is increased.

3.1.2 Dezincification mechanisms

There are many theories about the prevailing mechanisms and the characterization of the structures of dezincification. Two main mechanisms prevail; selective dissolution and dissolution-redeposition. Selective dissolution represents a process of Zn in the absence of electrochemical involvement of Cu. The most common selective dissolution theories include surface diffusion, volume diffusion of Zn/Cu and the percolation mechanism. [15] Duplex α + β brass alloys exposed to water of high chloride concentration and/or in CO_2, are most likely to undergo this type of dezincification. [16] On the contrary, the dissolution-redeposition of Cu

theory includes dissolution of both Cu and Zn. This process includes that Cu, which is more noble, redeposited onto the surface of the alloy forming corrosion products. As a result, an insufficient layer of Cu layer is formed. [15] Studies have shown that both categories do not occur simultaneously, but overlap in the potential regimes as illustrated in Figure 2. The solid diffusion of Zn, which is essential for the selective dissolution, has been shown to be too slow to constitute for the high rates of penetration observed through experiments. Hence, it is feasible that dezincification arises by both redeposition and simultaneous dissolution where selective dissolution also takes place, but without being involved in the rate control. [16]

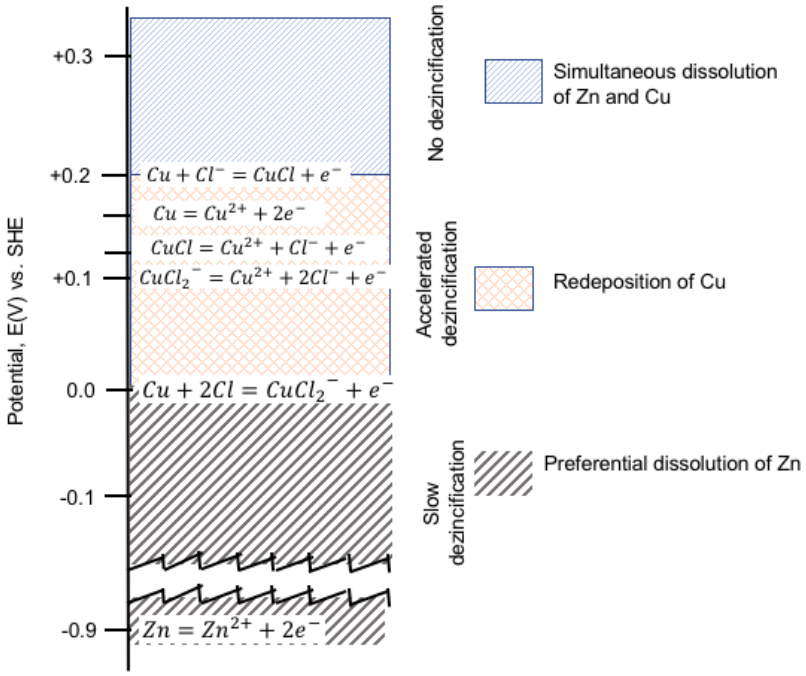

Figure 2: Potential regions for simultaneous and separate dissolution of Cu and Zn and redeposition of Cu in chloride-rich solutions adapted from [16].

A complication observed when trying to identify the corrosion mechanisms of brass is the complex composition of the oxide and Zn metallic layers. The research of dezincification has mostly been done in acidic solutions, which have shown no oxide formation. Moreover, experiments in tap water, with its near-neutral pH value, have however shown more complex corrosion and dezincification although of lower corrosion rates. The reason behind this is the development of a multi-layered dezincification composition, which includes Zn- and Cu containing corrosion products together with a Zn depleted layer. [15]

3.1.3 Prevention of dezincification

Dezincification can be prevented mainly by designing the metallurgical microstructure of the brass by adding some of the alloying elements discussed in section 1.1.1. As and P have a positive influence against dezincification due to their capability to prevent from Cu redeposition by reducing Cu^{2+} ions to Cu^{+}. Improved dezincification resistance observed by adding these elements to the alloy are predominantly observed on α-brasses. As also show

positive effects on duplex α + β brasses and the addition of Sb is another way to prevent dezincification of α-brasses. However, both As and Sb are toxic elements and therefore used in very small quantities. The addition of Sn and Al improves the dezincification resistance in duplex α + β brasses, especially together with Ni in the case of Sn addition. The reason behind the positive effect of these elements is the formation of a protective film, SnO_2 film for Sn and Al_2O_3 film for Al. The same case is shown for Pb-free brasses containing 3 wt.-% Si together with 0.05 wt.-% P for which a Si-rich protective oxide is formed. [2]

Practically, dezincification is promoted by high temperatures, presence of chlorides and stagnant water. It can though be difficult to limit these environmental factors. The simplest way to prevent dezincification is to choose a dezincification resistant brass alloy. The sensitivity to dezincification is affected by the Zn content and the presence of the α-phase. Less sensitive alloys contain less Zn and alloys with Cu concentration above 85 wt.-% are alleged to be immune to dezincification. The least sensitive alloys contain pure α-phase because β-phase is the most sensitive to dezincification. The addition of As, P or Sb, as mentioned above, can make the α-phase less sensitive. The alloys with both phases, duplex α + β brasses, should be in isolated fragments instead of forming a continuous network. This can be done by thermomechanical treatments to prevent corrosion penetration through a continuous β-phase network. [10]

3.2 Brass in tap water

3.2.1 Water characteristics

An important factor in corrosion research is the chemistry of the water, which is a main factor influencing the metal release and the corrosion mechanisms. Understanding corrosion of brass in water applications passes by the understanding of the effect of water characteristics on both kinetics and mechanisms. Therefore, it is important to determine the behavior of brass alloys in different water types. Both chemical and physical water parameters affect corrosion of brass. The chemical parameters include for example pH, alkalinity, hardness, and chloride concentration whereas examples of physical parameters include temperature and duration. It is well established that brass may suffer from non-uniform corrosion which is influenced by three categories of factors i.e. water chemistry, material properties and installation (water temperature, velocity). [17]

3.2.1.1 pH

The pH value of the water is one of the most common parameters affecting the corrosion of brass. pH is the concentration of hydrogen ions on a logarithmic scale and determines the acidity of the water. The hydrogen ions are involved in cathodic reaction and other interactions that affect the stability of the surface layer. For example, drinking water must have a pH value 7.5-9 to prevent corrosion attacks on the pipes. Research findings [10, 18-20] show that water of lower pH is generally more corrosive and leads to more corrosion and metal release into the water. A low pH value contributes to the development of non-protective corrosion products on

Cu-based alloys, and hence higher corrosion rates. [21] However, in the case of dezincification, most Zn has been shown to be released in water of pH 8. [18]

The solution pH, together with its redox conditions and potential, is related to the metal stability in solution. Pourbaix diagrams, which are potential-pH diagrams, can be used to predict the stability of corrosion products of a metal at different pH-values. Figure 3 illustrates the Pourbaix diagram of Cu in water at 25°C, which possibly is a good approximation for brass since Cu is the main element in brass. The orange area in the figure is where Cu is stable and immune. As can be observed, for pH values 7-13 at higher potential values, Cu forms oxides (Cu_2O and CuO). This area reflects the passive area where the corrosion process is slow and the material is protected by stable oxides. For pH values lower than 7 or higher than 13, Cu^{2+} or CuO_2^{2-} ions will form respectively, i.e. the material readily corrodes. Very high pH levels can also dissolve protective layers. [10]

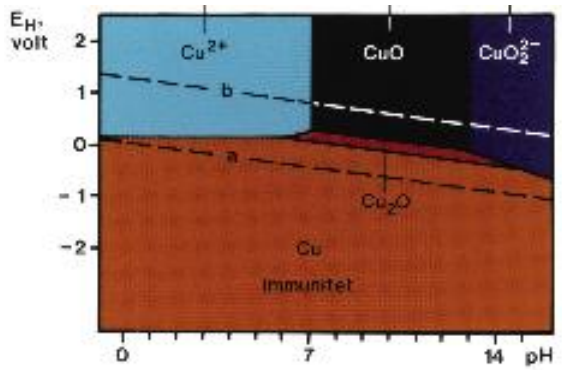

Figure 3: Pourbaix diagram of copper in pure water at 25°C [10]

3.2.1.2 Alkalinity

Alkalinity of aqueous solutions is defined with regard to the bicarbonate ion, HCO_3^- concentration. The beneficial impact of alkalinity is that it leads to the stabilization of the pH value and formation of corrosion layers which protects the brass alloy. However, the formation of these layers is also affected by other parameters such as the total organic carbon content (TOC) in water. TOC can contribute to the formation of a biofilm that may prevent the formation of these protective layers. [10] The extent of Zn dissolution has been shown to decrease with increasing alkalinity [18, 20] and Cu to form more protective corrosion products in water of higher alkalinity. [21] Nowadays, adjustment of pH and alkalinity is the most common method for corrosion control. The thermodynamic properties of the carbonate system are affected when the pH and the alkalinity are adjusted in order to achieve a less corrosive environment of the water. [22]

3.2.1.3 Hardness

The definition of hardness is the total sum of the mineral ions Ca^{2+} and Mg^{2+} and is expressed in mg/L Ca or °dH, where 1 °dH = 7.12 mg/L Ca. Water can be divided into three groups; very soft and soft with a value of 0-8 °dH, moderately soft and middle hard: 8-18 °dH and hard 18-30 °dH. [10]

$CaCO_3$ dissolves in water forming Ca^{2+} and HCO_3^- ions (equation 1), which is the definition of both alkalinity and hardness. HCO_3^- contributes to the formation of a protective layer on the surface, which hinders corrosion and reduces the extent of metal dissolution into the water.

$$CaCO_3 + CO_2 + H_2O \leftrightarrows Ca^{2+} + 2HCO_3^- \quad (1)$$

3.2.1.4 Chlorides

The chloride concentration in water increases the probability of dezincification. Several research findings [10][16][19] show that a high chloride concentration promotes dezincification. In fact, the presence of chloride leads to an increase in the solubility of zinc and interfere with the formation of protective layers. At high chloride concentrations, more corrosion products and an increase in weight loss were observed. [16] On the other hand, it is common to explore the effect of chloride concentration together with alkalinity as done with the Turner diagram. This diagram used as a dezincification risk assessment tool is shown in Figure 4 and describes potential conditions for brass dezincification depending on the chloride concentration and alkalinity where different types of dezincification can be expected such as meringue dezincification where a white bulky layer is formed on the surface [23].

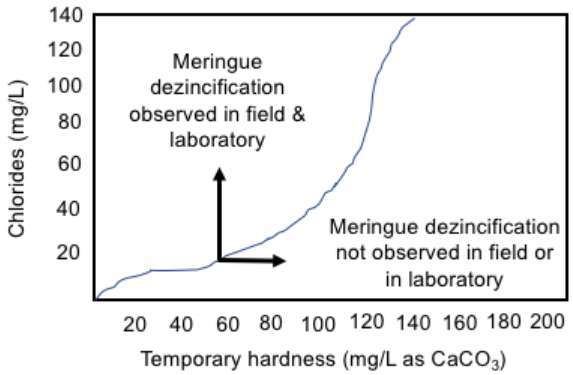

Figure 4. Influence of the content of chlorides and alkalinity in water to meringue dezincification adapted from [23].

3.2.2 Water temperature

Another factor influencing the extent of corrosion is the temperature of the water. Higher temperatures promote dezincification [10] and have been shown to result in more Cu release from the brass alloy. [20] Experiments in water with higher temperatures are very common and easy to perform in order to accelerate the corrosion of brass alloys.

3.2.3 Exposure duration

The exposure duration also has an important role in terms of corrosion. The corrosion rate of brass alloys has shown to be the highest in the first period of the exposure according to previous studies. [22]

4. Electrochemistry

Electrochemical techniques are commonly used to determine the corrosion behavior and mechanisms of different alloys in aqueous environment. Aqueous corrosion is an electrochemical reaction occurring at the metal-electrolyte interface with a heterogenous charge transfer. A corrosion reaction is a combination of two partial and complementary processes i.e. anodic and cathodic. The anodic process consists of the metal oxidation generating electrons that are transported from anodic surface sites to the cathodic sites where they contribute to the cathodic reduction reactions (Figure 5). The type of the cathodic reaction depends on the electrolyte characteristics and the metal surface potential. For instance, in neutral to alkaline water, oxygen reduction is the main cathodic reaction that drives the corrosion process. When the partial processes are uniformly distributed in time and location over the surface, a homogeneous mixed electrode is formed resulting in uniform corrosion. However, when they are spatially separated, a heterogeneous mixed electrode generating localized corrosion is present. [24]

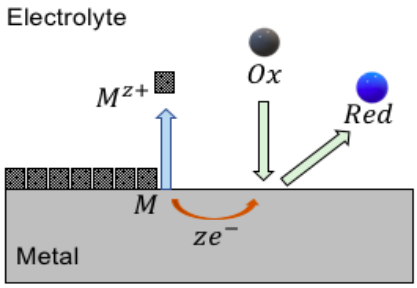

Figure 5. Corrosion process at the metal-electrolyte interface adapted from [22].

The overall corrosion reaction can be studied/characterized in terms of thermodynamic and kinetic parameters. The free corrosion potential (E_{corr}) or open circuit potential (OCP) are the thermodynamic corrosion parameters which represent a mixed potential between the reversible (equilibrium) potential of metal oxidation and the one of the cathodic process. The corrosion rate is the kinetic corrosion parameter that reflects the progress (rate) of the corrosion. In electrochemical corrosion, the instantaneous corrosion rate that can be determined at different time points is discussed. In addition to the anodic and cathodic reactions, other processes can be involved such as mass transport (by diffusion) or adsorption of reaction species. This represents corrosion mechanisms that can be investigated with specific techniques.

Two types of electrochemical techniques are mainly distinguished that can be used in complementary ways to explore the above-mentioned aspects of corrosion. This includes direct current (DC) and alternative current (AC) techniques. [25] The measurements are done by having a three-electrode electrochemical cell. Firstly, a working electrode (WE) is needed representing the metal/alloy to be studied. Secondly, a reference electrode (RE) is required because of its constant potential, which makes it possible to measure the difference between it and the WE. Lastly, a counter electrode (CE) is essential to the measurement because it allows current to flow through the cell, which enables the application or measurement of a current to the WE.

4.1 Direct current (DC) techniques

Direct current techniques include potential, current and polarization measurements. In the present study, the former consists of measurements of the free corrosion potential (E_{corr}) or open circuit potential (OCP). Practically, this thermodynamic corrosion parameter corresponds to the voltage difference between a WE (metal) and a non-polarized RE measured using a high-input resistance voltmeter. E_{corr} evolution provides an indication whether the corrosion system is in a passive or active state and how the surface is affected by the environmental (electrolyte) variations. [25]

The current measurements can include corrosion, cathodic and anodic currents. In the present thesis the scope is limited to the corrosion current which can be converted into the corrosion rate using Faraday Law assuming a uniform (general) corrosion process. Corrosion current cannot be measured directly but can acquired graphically from potentiodynamic scans as discussed below. [26]

Polarization measurements are destructive and simply a way to scan the potential far from the equilibrium potential of the metal while recording the corresponding current. Detailed information of the set-up and test procedure is given in ISO 17475 [24]. The obtained curve can be presented in a linear or logarithmic (Tafel plot) form. Corrosion parameters that can be extracted from polarization curves include corrosion potential (E_{corr}), corrosion current (i_{corr}), Tafel slopes and linear polarization resistance (R_p). R_p is the slope of the linear portion of the polarization curve at the vicinity of E_{corr} (Figure 6). E_{corr} and i_{corr} are obtained graphically by means of an extrapolation method on Tafel plots as shown in Figure 7. Tafel slopes are determined for each linear Tafel plot branch (anodic slope (right) and cathodic slope (left) in Figure 7) and expressed in mV/decade. [26]

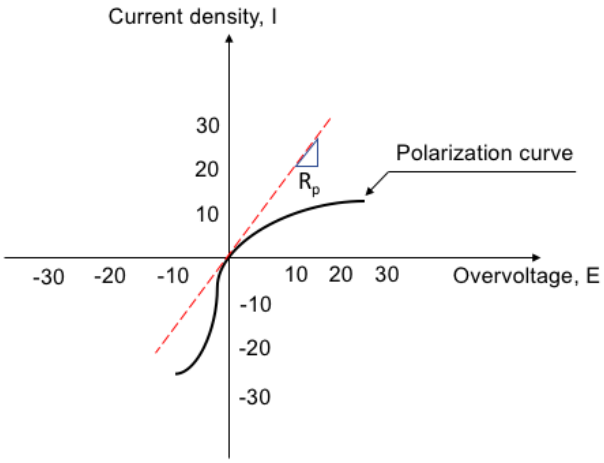

Figure 6. Polarization resistance (R_p) determination adapted from [25].

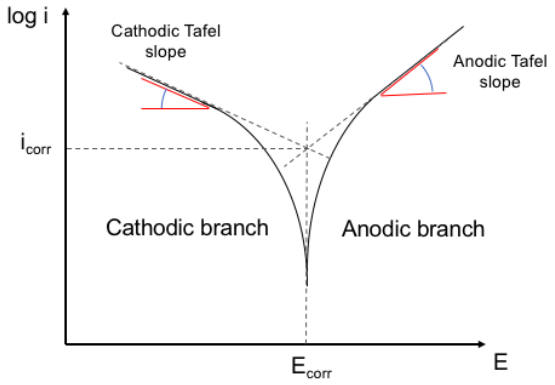

Figure 7. Determination of corrosion potential and corrosion current by extrapolation method adapted from [25].

4.2 Alternative current (AC) techniques

The main AC technique is electrochemical impedance spectroscopy (EIS). This technique continues to be developed and used to assess different corrosion mechanisms due to its non-invasive character. Practically, a small amplitude potential signal perturbation is applied on the corroding metal at E_{corr} recording the current flow across the electrochemical cell in a defined frequency range. The ratio of the potential and the current corresponds to the electrochemical impedance response of different processes participating at the surface/interface. This includes the corrosion layer properties, adsorption of reacting species, charge transfer and diffusion from electrolyte to the surface and vice versa. EIS is given in the form of complex numbers with real and imaginary parts with different graphical representations. The most adopted representations are the Nyquist and Bode (phase and magnitude) diagrams (Figure 8). [27]

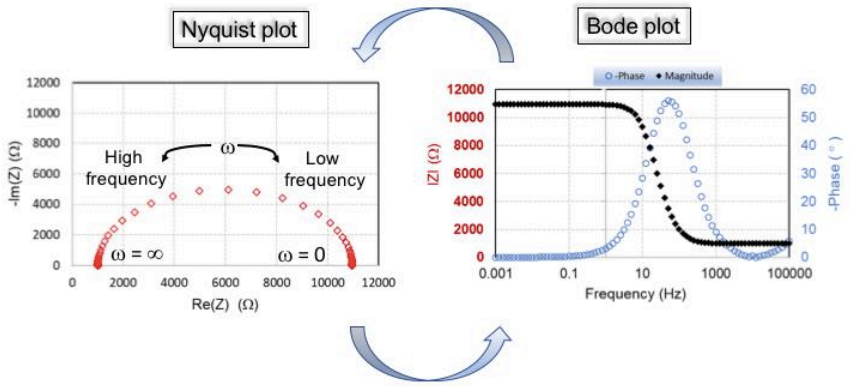

Figure 8. Typical EIS graphical representations: Nyquist and Bode diagrams adapted from [25]

To obtain the characteristics of the different corrosion processes, EIS data is subject to analysis by different methods (direct and indirect) that vary in complexity depending on the investigated corrosion system. Usually, an equivalent electrical circuit (EEC) with an overall impedance equation is used to fit the experimental impedance data. It is important to know that EEC components need to have a physical meaning and be supported by results of other characterization techniques (surface analysis, microscopic data). Further discussions of the EIS technique and its capabilities and limitations are given in the literature [27].

5. Experimental

In order to get an overview of the corrosion process and its mechanisms of the three different brass alloys in water, both short-term and long-term exposure experiments were performed. In terms of environment, three test waters with different characteristics were considered investigating also the effect of temperature. In one of the test waters the effect of exposure duration was explored. Electrochemical experiments including OCP, EIS and Potentiodynamic (PDP) measurements were performed in the different environments and for different durations. In addition, the weight loss method was used to determine corrosion rates. Light Optical Microscopy (LOM), Scanning Electron Microscopy-Energy Dispersive Spectroscopy (SEM-EDS) and X-Ray Photoelectron Spectroscopy (XPS) were used for surface characterization. The experimental set up is illustrated in Figure 9.

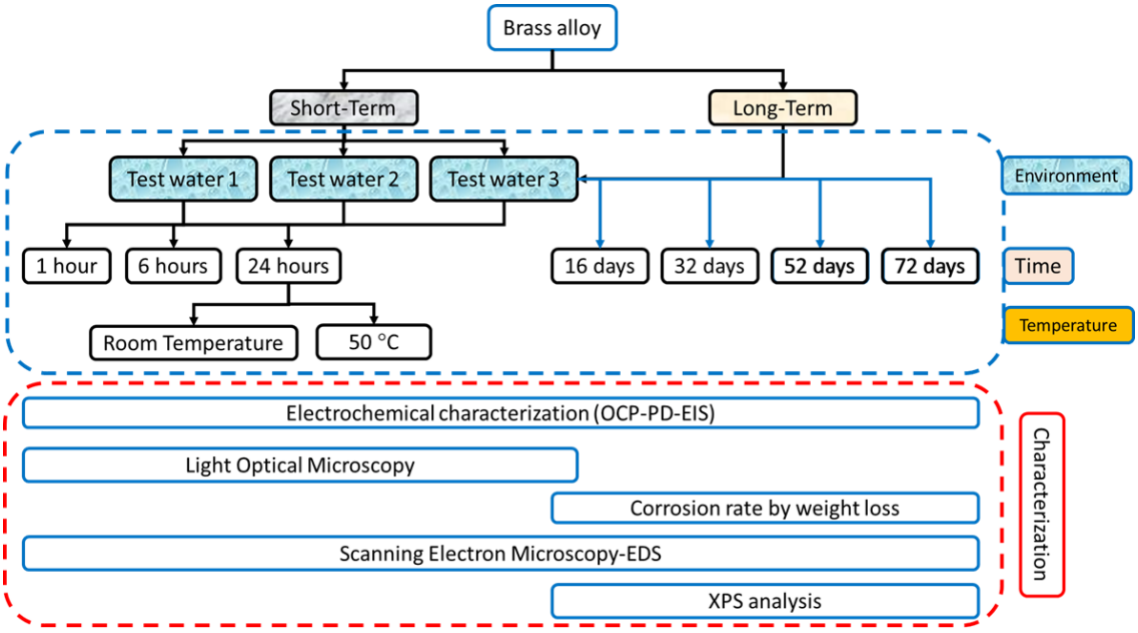

Figure 9. Illustration of the experimental set up

5.1 Materials

Three different commercial dezincification resistant (DZR) brasses of different composition focusing on their lead content were investigated. Two of the alloys (CW511L and CW724R) are lead-free while the third one (CW602N) contains lead and considered as a reference material.

CW511L

The first brass alloy, CW511L (CuZn38As), also known as *AquaNordic*, is a Pb-free and dezincification resistant grade. The material is produced at *Nordic Brass Gusum AB* as rods with a diameter of 19 mm. It contains As to improve its corrosion resistance, as discussed in section 1.1.1. It has a microstructure with nearly 100% α-phase. The chemical composition in wt.-% of elements is shown in Table 2.

Table 2: Chemical composition of CW511L in wt.-% determined by *Degerfors Laboratorium AB*

CW511L Chemical composition (wt.%)							
Cu	**Zn**	**Al**	**Fe**	**Ni**	**Mn**	**As**	**Si**
63.5	36.3	0.003	0.05	0.08	0.001	0.03	0.0003
Sn	**Sb**	**Pb**	**B**	**Bi**	**Mg**	**Cr**	
0.01	0.0004	0.1	0.001	0.001	0.001	0.001	

CW724R

CW724R (CuZn21Si3P), also known as *EcoBrass*, was the second studied Pb-free and dezincification resistant alloy. This material is produced at *Wieland Werke AG* as rods with a diameter of 50 mm. This alloy is characterized by a higher Cu amount, considerable amounts of Si and a minor content of P (Table 3). In terms of microstructure, this alloy consists of approximately 60% α-phase and 40% κ-phase.

Table 3: Chemical composition of CW724R in wt.-% determined by *Degerfors Laboratorium AB*

CW724R Chemical composition (wt.%)							
Cu	**Zn**	**Al**	**Fe**	**Ni**	**Mn**	**As**	**Si**
75.8	20.6	0.0005	0.07	0.003	0.005	0.0005	3.4
Sn	**Sb**	**Pb**	**B**	**Bi**	**Mg**	**Cr**	**P**
0.02	0.0007	0.03	0.0005	0.001	0.0005	0.0005	0.05

CW602N

CW602N (CuZn36Pb2As) was the reference brass alloy in this study due to its Pb content. This alloy is produced by *Nordic Brass Gusum AB* as rods with a diameter of 30 mm. CW602N has similar chemical composition as CW511L, doped with 0.03 As %, but with a higher content of Pb (Table 4). The microstructure of this alloy is similar to CW511L with nearly 100% α-phase.

Table 4: Chemical composition of CW602N in wt.-% determined by *Degerfors Laboratorium AB*

CW602N Chemical composition (wt.%)							
Cu	**Zn**	**Al**	**Fe**	**Ni**	**Mn**	**As**	**Si**
61.7	36.4	< 0.01	0.1	0.03	0.007	0.03	0.01
Sn	**Sb**	**Pb**	**Bi**	**Cr**			
0.04	< 0.005	1.7	0.01	< 0.005			

5.2 Environment (Test waters)

Three test waters (TW1, TW2, TW3) including a collected tap water (test water 3 collected at *RISE KIMAB,* Kista, Stockholm) were investigated to explore the short-term corrosion resistance of the commercial DZR brasses. The test water chemistries are based on ISO 15664-2 with variable pH, conductivity, alkalinity and chloride concentration covering the chemistry of typical tap waters relevant for Europe [28]. Literature findings show that test water 1 of neutral pH, high conductivity and high alkalinity is the most corrosive towards copper alloys [29]. Test water 3 was used for the long-term corrosion behavior studies. Table 5 summarizes the water chemistry for each test water analyzed by *ALS Scandinavia AB.* The effect of water temperature was investigated only for the short-term exposure investigation. A temperature of 50 °C was considered since it is a common temperature for domestic tap water installations that brass parts can face.

Table 5. Test waters parameters (average values with standard deviation).

	pH	**Conductivity (µS/cm)**	**Alkalinity (mg/L)**	**Chlorides (mg/L)**	**Total hardness (°dH)**	**TOC (mg/L)**
TW1	7.3 ± 0.2	1120 ± 110	310 ± 24	44.7 ± 6.7	6.2	4.9 ± 0.9
TW2	6.9 ± 0.2	290 ± 29	74 ± 5.9	17.1 ± 2.6	6.4	4.8 ± 0.9
TW3	8.2 ± 0.2	257 ± 26	63 ± 5.1	15.5 ± 2.3	5.5	4.1 ± 0.8

5.2.1 Preparation of test waters

Test water 3 was collected from the tap in the building at *RISE KIMAB*, Kista, Stockholm. This water was considered as the base for the preparation of the other test waters. Test water 2 was prepared from test water 3, where the pH was adjusted by bubbling carbon dioxide (CO_2). To minimize the risk of pH changes, the pH was monitored and adjusted if needed before, during and after the experiments. Test water 1 was prepared by adding 284.08 mg $NaSO_4$, 43.25 mg NaCl and 316.70 $NaHCO_3$ for 1 liter of test water 3 and adjusting the pH value by bubbling

CO_2. To obtain the same water chemistry for all the repeated experiments, 100 L of test water 3 were collected from the tap before starting all the experiments and 15 L of test waters 1 and 2 were prepared for all the experiments.

5.3 Methods

5.3.1 Electrochemical tests

5.3.1.1 Sample preparation

Samples for electrochemical experiments for the long-term and short-term exposure were cut from the rod into smaller sections. Electrical connection of the brass was ensured by using an electrical wire with a conductive paint (*Bare Conductive Electric Paint)*. They were then cold mounted in *Epoxy Resin* to define the exposed surface to the electrolyte (Figure 10). Next, they were wet grinded with silicon carbide abrasive paper in the order of: 320p, 600p, 1200p, 2500p and 4000p using a *Buehler Phoenix Alpha* manual grinding machine for the four first grinding steps and a *Struers LaboPol-21* manual grinding machine for the last two grinding steps. The samples were then polished by adding diamond-paste to three different polishing cloths, one per diamond size: 3 µm for 30 s, 1 µm for 60 s and 0.25 µm for 90 s using a manual polishing machine (*Buehler PoliMet 1000 polisher* with polishing cloths *Struers MD Mol*^{TM} for 3 µm, *Struers MD Chem*^{TM} for 1 µm and *Struers MD Nap*^{TM} for 0.25 µm). The polishing is done because the electrochemical tests are more accelerated (higher active surface) compared with e.g. weight loss samples where the surface roughness represent realistic components surface appearance. The samples were rinsed with ethanol and dried with hot air convection after each grinding and polishing step. The final step was an ultrasound cleaning, using *Ney ULTRAsonik*, with ethanol for 15 min. All steps described above were performed to obtain a clean surface and ensure the reproducibility of the results.

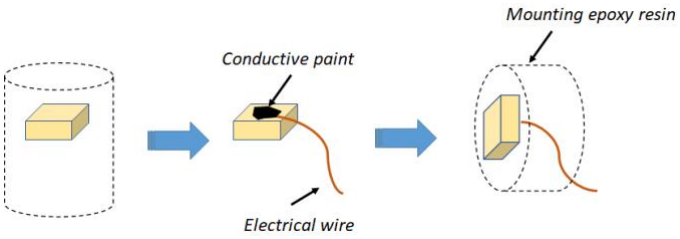

Figure 10. Illustration of the preparation of the samples used for electrochemical tests

5.3.1.2 Procedure

A configuration of three electrodes was adopted for the electrochemical investigations which consist of a working electrode (WE), a reference electrode (RE), and a counter electrode (CE). The brass sample was the WE, an Ag/AgCl electrode the RE and a platinum mesh or wire the CE. A multichannel potentiostat *(AMETEK, US)* from *Princeton Applied Research* combined with the *VersaStudio* software was used for both DC and AC measurement techniques. Potentiodynamic tests were conducted from -300 V vs OCP up to +700 V vs OCP with a scan rate of 0.16 mV/s as recommended by ISO 17475 [26]. EIS tests were performed by imposing

a 10 mV amplitude sine wave of potential at E_{corr} for a frequency range between 10^5 Hz to 1 mHz with 10 points per decade. All electrochemical tests were repeated at least once to ensure reproducibility and accurate results.

5.3.2 Weight loss

5.3.2.1 Sample preparation

Weight loss samples were cut into approximately 10 x10 x10 mm cubes. The instrument used for the cutting was firstly a *Buehler AbrasiMatic 300 Abrasive Cutter* for cutting the materials into smaller pieces from which cubes were acquired using an automatic cutting machine, *Struers Accutom-50 (feed 0.050 mm/s and speed 5000 rpm)*. Each side of the cube was then grinded with wet silicon carbide abrasive paper in the order of: 320p, 600p, 1200p, 2500p and 4000p. Here, polishing was not performed since this method is less accelerated with a surface roughness representing realistic components surface compared with the electrochemical samples (higher active surface). The grinding was performed using the same manual grinding machines as described for the electrochemical samples (section 5.3.1.1). The samples were rinsed with ethanol and dried with hot air convection after each grinding step. Lastly, all samples were rinsed in ethanol in an ultrasonic bath, using the same instrument as in section 5.3.1.1, for 15 minutes. The initial weight of each cube was obtained using *Sartorius BP 211D* analytical balance (±0.0001 mg). The samples were then placed on a sample holder in a water container (Figure 11).

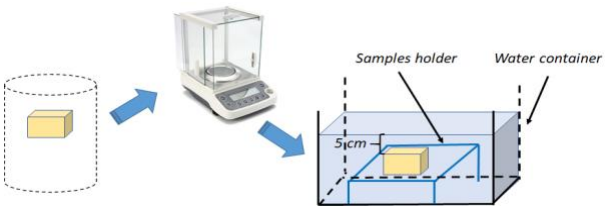

Figure 11. Illustration of the procedure for the weight loss samples.

5.3.2.2 Procedure

The weight loss method allows the determination of time dependent corrosion rates. The samples were placed at a plastic sample holder in water containers of the different test waters to get the samples immersed five cm below the water surface as recommended in ISO 2812-2 [30], illustrated in Figure 11. One side of the cube was therefore not fully exposed to the water. The water was changed once every two weeks to maintain the same water chemistry. The cubes were collected after 16, 32, 52 and 72 days of exposure into test water 3 before cleaned following the standard procedure described in ISO 8407 [31]. This was done by adding 25 g of sulfonic acid to distilled water to make 500 ml and expose the samples to the solution for five minutes. The samples were then weighed to determine the total weight loss. The cleaning procedure was repeated until no significant difference in weight loss was observed. The initial and final mass are considered in the calculation of the corrosion using the following equation:

$$CR = \frac{k*W}{A*t*\rho} \quad (2)$$

where: CR: corrosion rate (mm/y)
k: constant ($8.76*10^4$),
W: mass loss (g),
A: exposed surface area (cm^2)
t: exposure duration (h)
ρ: density (8.41[1], 8.25[2], 8.38[3] g/cm^3)

5.4 Surface analysis

5.4.1 Sample preparation

Samples for surface analysis were prepared following the same procedure of samples used for electrochemical tests (section 3.2.1) except for the electrical connection and the cold mounting. These samples were instead mounted in the phenolic resin compound *Buehler TransOptic™ Compression Mounting Compound* using the *Buehler SimpliMet™ XPS1 Mounting System* machine.

5.4.2 Procedure

Light optical microscopy (LOM) was used to characterize the corrosion type and its depth from cross-sectional images using a *LEICA DM IRM* instrument with the software *Kappa ImageBase*.

Scanning Electron Microscopy (SEM) combined with Energy Dispersive Spectroscopy (EDS) analysis were used to explore the morphology and chemistry of corrosion products. The information depth is in the order of 1 µm and an acceleration voltage of 10-15 kV was used. The instrument used was a *Zeiss Sigma 300 VP* microscope with a 50 mm^2 *X-Max* Silicon Drift Detector (SDD) from *Oxford Instruments* for the EDS.

X-ray photoelectron spectroscopy (XPS) was another surface analysis used, which is a technique widely used in corrosion and surface science to explore the corrosion layer chemistry and track its thickness. The XPS analysis provides the chemical composition and oxidation state of elements within the outermost surface layer (5-10 nm depth). The instrument used was an *UltraDLD spectrometer, Kratos Analytical Manchester, UK* with a monochromatic *Al K(alpha) X-ray source (150 W)*. Wide spectra and detailed spectra (pass energy 80 eV) of all alloy constituents > 0.1 wt.% in the nominal bulk composition as well as oxygen and carbon were acquired, i.e. of Zn 2p, Cu 2p, Ni 2p, Fe 2p, Pb 4f, Sn 3d, Ni 2p, Mn 2p, Si 2p, As 3d, O 1s, and C 1s (as energy reference at 285.0 eV).

[1] Density of CW511L
[2] Density of CW724R
[3] Density of CW602N

6. Results

6.1 Short time exposure

6.1.1 Effect of test water

6.1.1.1 Electrochemical tests

DC techniques

CW511L

The open circuit potential (OCP) was monitored in the different test waters at different short-term durations. The obtained values are shown in Table 6. OCP is a thermodynamic corrosion parameter that can give indication on surface activity and should be correlated with kinetic information. Based on the mixed potential theory, the OCP gives indication on the redox processes which affect the corrosion process. In all test waters, similar negative potentials were obtained for the different immersion durations. The figure implies that more negative potentials were measured in the highly conductive TW1 up to 6 h, however, these differences were after 24 h less than 4 mV vs Ag/AgCl.

Table 6. OCP in mV vs. Ag/AgCl of CW511L immersed for 1, 6 and 24 h in the different test waters.

Test water\exposure duration (h)	**1**	**6**	**24**
OCP TW1	-30.0 ± 0.9	-35.0 ± 1.0	-21.0 ± 2.0
OCP TW2	-20.0 ± 1.0	-20.0 ± 0.3	-19.0 ± 1.0
OCP TW3	-18.0 ± 3.0	-25.0 ± 5.0	-23.0 ± 1.0

Following the OCP measurements, potentiodynamic scans were performed for the CW511L alloy to explore the cathodic and anodic processes in the different test waters at different durations. The Tafel representation showed the same shape at the different times and only the 24 h results are shown in Figure 12 (results after 1 and 6 h in Figure A1 in Appendix). The examination of the Tafel plots after 24 h of immersion showed a higher cathodic current density in TW1 compared to the other waters. While the anodic branch form was similar in TW2 and TW3, it showed the presence of a current plateau at 0.24 V vs Ag/AgCl only in TW1 (Figure 12). Such a plateau means a current which is independent of the potential and implies a diffusion process or passive domain.

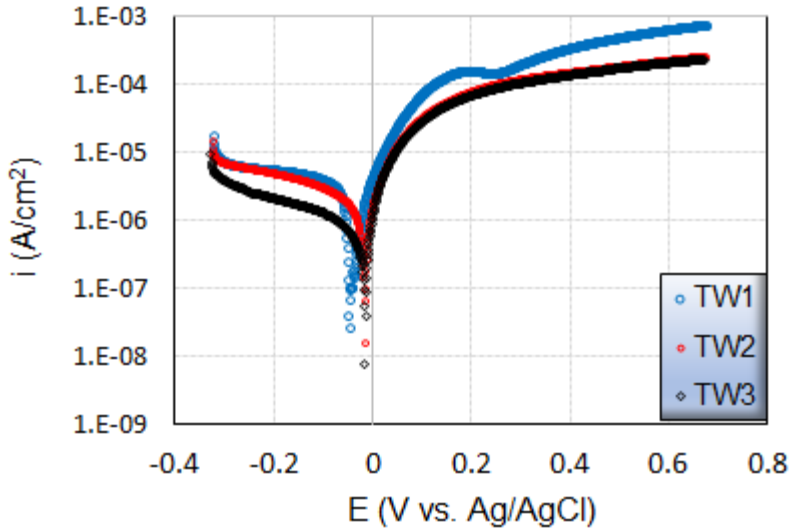

Figure 12. Tafel plots of CW511L after 24 h of exposure at stagnant conditions in the different test waters at room temperature.

The extraction of corrosion parameters by the Tafel extrapolation method was done with the aim to distinguish differences in corrosion kinetics and mechanisms in the three test waters. The free corrosion potentials (E_{corr}), determined via the polarization method, are summarized in Table 7 for the different test waters and investigated time periods.

Table 7. Corrosion potential in mV vs. Ag/AgCl of CW511L immersed for 1, 6 and 24 h in the different test waters.

Test water\exposure duration (h)	**1**	**6**	**24**
E_{corr} TW1	-35.0 ± 5.0	-33.0 ± 1.0	-44.0 ± 1.0
E_{corr} TW2	-19.0 ± 0.5	-24.0 ± 8.0	-12.0 ± 1.0
E_{corr} TW3	-14.0 ± 4.0	-28.0 ± 8.0	-14.0 ± 2.0

E_{corr} shifted slightly to more negative values in TW1 compared to the values obtained in TW2 and TW3. After 24 h of immersion, the largest difference between E_{corr} in the test waters did not exceed 32 mV vs Ag/AgCl which is still considered as a small difference. The findings of E_{corr} agree well with what was obtained for OCP and the differences between OCP and E_{corr} values remained small which shows an negligible effect of the potentiodynamic scan on the corrosion process.

From the corrosion currents, compiled in Table 8, it is evident that CW511L corrodes at different rates in the different test waters and varies with exposure duration. After 24 h of exposure, corrosiveness of the test waters can be ranked from the highest to the lowest as follows: TW1>TW2>TW3, changing to TW1≈TW2>TW3 after 6 h and to TW2>TW1>TW3 after 1 h.

Table 8. Corrosion current density in μA/cm^2 of CW511L immersed for 1, 6 and 24 h in the different test waters.

Test water\exposure duration (h)	**1**	**6**	**24**
i_{corr} TW1	0.97 ± 0.02	1.65 ± 0.10	2.24 ± 0.00
i_{corr} TW2	1.61 ± 0.01	1.61 ± 0.03	1.84 ± 0.01
i_{corr} TW3	0.75 ± 0.01	0.43 ± 0.00	0.44 ± 0.02

Linear polarization resistances (extracted from E_{corr} zone in the potentiodynamic scans) are shown in Table 9. Similarly to i_{corr}, CW511L showed different polarization resistance (R_p) depending on the test water and exposure duration. Obtained values are in the same order of magnitude as reported in the literature for similar conditions [2]. Usually, a high R_p corresponds to a low corrosion rate. After 24 h of exposure, the degree of test water corrosivity agreed with the i_{corr} results (Table 8).

Table 9. Polarization resistance in kΩ cm^2 of CW511L immersed for 1, 6 and 24 h in the different test waters.

Test water\exposure duration (h)	**1**	**6**	**24**
R_p TW1	20.0 ± 0.0	11.1 ± 0.0	14.6 ± 0.0
R_p TW2	10.0 ± 0.0	11.8 ± 0.9	15.4 ± 1.6
R_p TW3	18.2 ± 0.9	50.0 ± 0.0	28.6 ± 1.6

In the same way, mechanistic information can be obtained from the Tafel slopes summarized in Tables 10 and 11. The anodic slope values agree with literature findings for copper and brass in fresh or saline waters [32,33]. The highest value after 24 h of immersion was observed in test water 1.

Table 10. Anodic Tafel slopes (B_a) in mV/decade of CW511L immersed for 1, 6 and 24 h in the different test waters.

Test water\exposure duration (h)	**1**	**6**	**24**
B_a TW1	50.5 ± 0.7	51.4 ± 0.7	87.9 ± 1.4
B_a TW2	58.4 ± 0.7	70.9 ± 4.2	76.9 ± 1.4
B_a TW3	45.9 ± 4.2	60.4 ± 4.9	30.9 ± 2.8

The observed cathodic slopes (Table 11) were higher than the theoretical value of 120 mV/dec (proposed for a process governed by pure charge transfer). This supports a contribution of diffusion on the cathodic process during this first exposure period. Similar to findings for the anodic Tafel slope, the highest value after 24 h of immersion was noticed in test water 1.

Table 11. Cathodic Tafel slopes (B_c) in mV/decade of CW511L immersed for 1, 6 and 24 h in the different test waters.

Test water\exposure duration (h)	**1**	**6**	**24**
B_c TW1	245.8 ± 12.6	263.3 ± 0.7	253.3 ± 0.6
B_c TW2	292.8 ± 7.0	197.3 ± 21.0	232.3 ± 0.7
B_c TW3	262.3 ± 14.7	250.8 ± 7.0	219.3 ± 9.0

CW724R

Similar electrochemical investigations as presented for the CW511L alloy were performed for CW724R. Observed open circuit potentials (OCP) in the different test waters at different durations are summarized in Table 12. For TW1 and TW2, the OCP shifted from negative to positive values between 1 and 24 h. The opposite findings were observed for TW3.

Table 12. OCP in mV vs. Ag/AgCl of CW724R immersed for 1, 6 and 24 h in the different test waters.

Test water\exposure duration (h)	**1**	**6**	**24**
OCP TW1	-40.0 ± 0.0	2.0 ± 4.0	4.0 ± 2.0
OCP TW2	-29.0 ± 2.0	12.0 ± 0.6	4.0 ± 0.1
OCP TW3	4.0 ± 1.0	-4.0 ± 2.0	-0.1 ± 1.0

Since the Tafel plots of the results in the three different test waters and times periods showed the same trend, only the result obtained after 24 h is shown in Figure 13 (results from 1 and 6 h in Figure A2 in Appendix). While the lowest cathodic current density was observed in TW3, it was almost similar in TW1 and TW2. For the anodic branch, TW1 showed the highest anodic current density. A difference in both the anodic and the cathodic slopes were observed, which indicates different corrosion mechanisms for CW724R in the different test waters. A clear difference in shape was observed in TW3 compared with TW1 and TW2, findings which are consistent with observed changes in OCP with time (see Table 12).

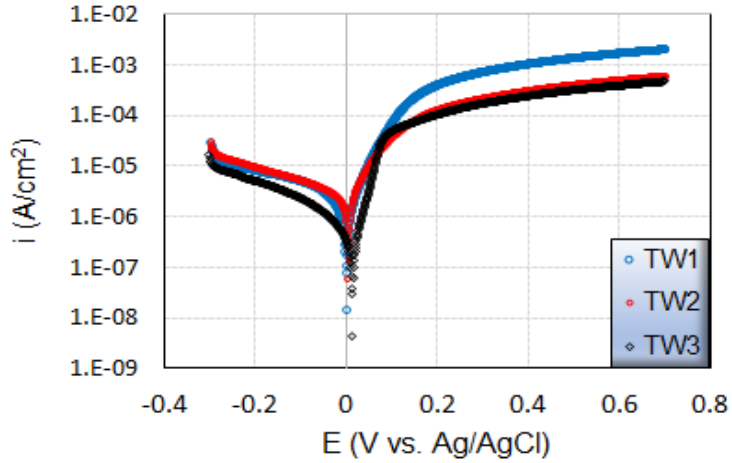

Figure 13. Tafel plots of CW724R after 24 h of exposure at stagnant conditions in the different test waters at room temperature.

The free corrosion potential (E_{corr}) values determined from the polarization measurements of CW724R in the different test waters with time are compiled in Table 13. E_{corr} shifted between 1 and 24 h from negative to positive values in all test waters. These changes agree well with observed OCP potentials in TW1 and TW2 but not for TW3, see Table 12.

Table 13. Corrosion potential in mV vs. Ag/AgCl of CW724R immersed for 1, 6 and 24 h in the different test waters.

Test water\exposure duration (h)	**1**	**6**	**24**
E_{corr} TW1	-34.0 ± 1.0	-28.0 ± 0.1	3.0 ± 1.0
E_{corr} TW2	-24.0 ± 3.0	-0.7 ± 2.0	8.0 ± 2.0
E_{corr} TW3	8.0 ± 1.0	6.0 ± 0.0	11.0 ± 3.0

Table 14 summarizes the different corrosion current densities in the different test waters and time periods. The corrosiveness of the waters was after 24 h ranked from highest to lowest as TW2>TW1>TW3. Similar findings were observed after 6 h. The ranking was different after 1h; TW1>TW2>TW3.

Table 14. Corrosion current density in µA/cm^2 of CW724R immersed for 1, 6 and 24 h in the different test waters.

Test water\exposure duration (h)	**1**	**6**	**24**
i_{corr} TW1	3.54 ± 0.04	1.46 ± 0.01	1.56 ± 0.08
i_{corr} TW2	2.56 ± 0.10	1.60 ± 0.00	2.44 ± 0.10
i_{corr} TW3	0.77 ± 0.01	0.35 ± 0.02	0.48 ± 0.02

Table 15 shows a difference in polarization resistance (R_p) in different test waters at different exposure durations. A considerable difference was observed for TW3 compared with TW1 and TW2. Since a higher R_p corresponds to a lower corrosion rate, could the corrosiveness of the test waters after 24 h be ranked in the same order as the i_{corr} after 24 h (Table 14). However, in the case of both 1 and 6 h, the ranking was different: TW1>TW2>TW3, which is expected in short time exposure durations.

Table 15. Polarization resistance in kΩ cm^2 of CW724R immersed for 1, 6 and 24 h in the different test waters.

Test water\exposure duration (h)	**1**	**6**	**24**
R_p TW1	4.0 ± 1.2	10.0 ± 0.0	11.8 ± 0.9
R_p TW2	6.7 ± 3.5	11.8 ± 0.9	6.7 ± 0.0
R_p TW3	25.0 ± 0.0	50.0 ± 0.0	33.3 ± 0.0

In terms of anodic Tafel slopes shown in Table 16 after 24 h of immersion, no significant difference was observed between the values for TW1 and TW2 compared for TW3, which showed considerably lower values (Figure 13). This behavior was clearly observed when examining the anodic branch shape characterized by a sharp increase for TW3. Moreover, the trend observed between the test waters in terms of anodic Tafel slopes (Table 16) was also observed for the cathodic slopes shown in Table 17. This suggests more pure active control in the test water TW3 compared to the remaining waters. Similar to the findings for CW511L, the order of Tafel slopes agreed with the test water ranking.

Table 16. Anodic Tafel slopes (B_a) in mV/decade of CW724R immersed for 1, 6 and 24 h in the different test waters.

Test water\exposure duration (h)	**1**	**6**	**24**
B_a TW1	69.6 ± 0.9	61.9 ± 0.0	63.9 ± 0.0
B_a TW2	61.0 ± 0.0	61.5 ± 0.7	70.9 ± 0.0
B_a TW3	36.5 ± 2.1	25.9 ± 0.0	34.0 ± 1.3

Table 17. Cathodic Tafel slopes (B_c) in mV/dec of CW724R immersed for 1, 6 and 24 h in the different test waters.

Test water\exposure duration (h)	**1**	**6**	**24**
B_c TW1	163.0 ± 4.2	126.9 ± 1.4	235.5 ± 6.3
B_c TW2	254.5 ± 0.7	177.9 ± 2.8	300.9 ± 0
B_c TW3	175.4 ± 3.6	124.5 ± 0.7	163.5 ± 9.0

CW602N

The OCP values for the Pb-containing CW602N alloy in the different test waters at different exposure durations are summarized in Table 18. The OCP became more negative with time for all waters. A minor difference (≤ 15 mV vs. Ag/AgCl) in potential were observed after 24 h of immersion in the three test waters.

Table 18. OCP in mV vs. Ag/AgCl of CW602N immersed for 1, 6 and 24 h in the different test waters.

Test water\exposure duration (h)	**1**	**6**	**24**
OCP TW1	-11.0 ± 1.0	-19.0 ± 1.0	-29.0 ± 0.0
OCP TW2	7.0 ± 5.0	-7.0 ± 1.0	-14.0 ± 2.0
OCP TW3	0.1 ± 0.2	-18.0 ± 4.0	-16.0 ± 2.0

Tafel plots of CW602N immersed in the three test waters for 24 h are shown in Figure 14 (results from 1 and 6 h in Figure A3 in Appendix). A more considerable change for the cathodic Tafel slopes was observed compared with the anodic slopes. While the highest cathodic current was observed in TW2, the highest anodic current was observed in TW1.

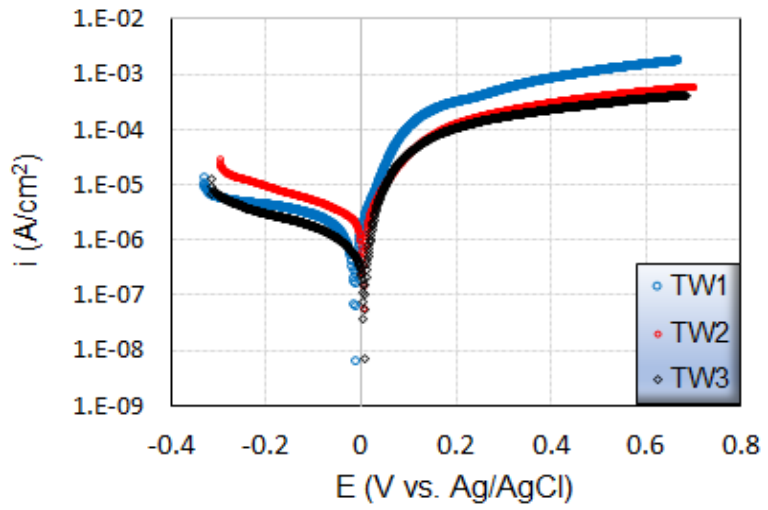

Figure 14. Tafel plots of CW602N after 24 h of exposure at stagnant conditions in the different test waters at room temperature.

Table 19 summarizes the free corrosion potential (E_{corr}) values, determined from the polarization measurements of CW602N in the different test waters for different immersion times. E_{corr} was clearly shifting positively towards the noble direction (copper reversible potential) in TW2 and TW3, whereas the values in TW1 remained negative. The observed difference of E_{corr} in the test waters vary from 2 to 18 mV vs. Ag/AgCl. This difference was judged negligible since the same level was obtained between replicas (same alloy in the same test water). The comparison between changes in E_{corr} and OCP showed a clear discrepancy which is typical for this alloy as it seems that the potentiodynamic scan considerably affected the thermodynamics of the corrosion process in the presence of Pb.

Table 19. Corrosion potential in mV vs. Ag/AgCl of CW602N immersed for 1, 6 and 24 h in the different test waters.

Test water\exposure duration (h)	**1**	**6**	**24**
E_{corr} TW1	-13.0 ± 3.0	-35.0 ± 7.0	-13.0 ± 4.0
E_{corr} TW2	15.0 ± 1.0	2.0 ± 1.0	3.0 ± 0.0
E_{corr} TW3	12.0 ± 6.0	-4.0 ± 5.0	5.0 ± 2.0

Table 20 shows CW602N corrosion current densities in the different test waters and exposure durations. After 24 h of exposure, the corrosiveness of the test waters could be ranked from the highest to the lowest as follows: TW2>TW1>TW3. This ranking was not observed after 1 h (TW1>TW3>TW2). This supports well the fact that corrosion rate depends on exposure time where surface phenomena vary in a very active way, especially visible in short-term tests.

Table 20. Corrosion current density in $\mu A/cm^2$ of CW602N immersed for 1, 6 and 24 h in the different test waters.

Test water\exposure duration (h)	**1**	**6**	**24**
i_{corr} TW1	2.08 ± 0.03	0.38 ± 0.05	0.90 ± 0.00
i_{corr} TW2	0.48 ± 0.05	1.38 ± 0.01	1.59 ± 0.01
i_{corr} TW3	0.95 ± 0.01	0.63 ± 0.01	0.64 ± 0.05

For corrosion resistance based on R_p values shown in Table 21, an agreement was observed with i_{corr} results after 24 h in terms of test water corrosivity. The ranking of R_p for CW602N from the lowest to the highest was: TW2<TW1<TW3, a ranking also observed after 6 h but not after 1 h of immersion (TW3<TW1<TW2).

Table 21. Polarization resistance in kΩ cm^2 of CW602N immersed for 1, 6 and 24 h in the different test waters.

Test water\exposure duration (h)	**1**	**6**	**24**
R_p TW1	16.7 ± 0.8	33.3 ± 2.5	15.4 ± 0.2
R_p TW2	22.2 ± 1.5	10.0 ± 0.0	12.5 ± 0.0
R_p TW3	12.5 ± 0.9	40.0 ± 2.5	22.2 ± 1.4

The anodic Tafel slopes shown in Table 22 varied between 30 and 52 mV for all the test waters with only minor differences. However, considerable variations were observed on the cathodic Tafel slopes (Table 23) with higher values after 24 h. These observation implies more diffusion contribution/control in the cathodic process.

Table 22. Anodic Tafel slopes (B_a) in mV/decade of CW602N immersed for 1, 6 and 24 h in the different test waters.

Test water\exposure duration (h)	**1**	**6**	**24**
B_a TW1	41.9 ± 1.4	48.5 ± 0.7	42.5 ± 0.7
B_a TW2	37.5 ± 0.6	45.5 ± 0.7	52.0 ± 1.4
B_a TW3	30.9 ± 0.0	44.0 ± 2.8	31.5 ± 0.7

Table 23. Cathodic Tafel slopes (B_c) in mV/decade of CW602N immersed for 1, 6 and 24 h in the different test waters.

Test water\exposure duration (h)	**1**	**6**	**24**
B_c TW1	191.0 ± 5.6	114.5 ± 0.7	202.1 ± 0.0
B_c TW2	197.1 ± 2.8	236.1 ± 12.6	316.1 ± 8.5
B_c TW3	234.5 ± 4.9	259.0 ± 1.3	256.6 ± 10.4

Electrochemical Impedance spectroscopy (EIS)

Electrochemical impedance results were analyzed qualitatively with focus on low frequency impedance that corresponds to the polarization resistance and its correlation with R_p extracted from the potentiodynamic scan. Some observations on phase angle and Nyquist diagrams are mentioned as guidance for future exploitation of generated results.

CW511L

The EIS response was recorded in the different test waters with the aim to get indications on the different processes involved in the corrosion mechanism. At the immersion times investigated, two main processes are expected i.e. charge transfer at high frequency (HF) followed by mass transport (diffusion) appearing at low frequencies (LF).

Figure 15 shows EIS in Nyquist representation after 1 h of immersion in the test waters. The response is characterized by depressed semi-circles and an incomplete high frequency (HF) semi-circle. While the depression indicates a constant phase element (CPE) behavior, explained by surface inhomogeneities, the incomplete HF semi-circle indicates a non-uniformity of current distribution on the electrode surface [35]. HF semi-circles for TW2 and TW3 are matching, which is indicative of similar processes in this frequency range. However, at low frequency the response starts to vary with different size of the semi-circles, which may be related to the diffusion processes affected by the difference in pH and alkalinity between these two test waters. The response in TW1 is distinguished by a smaller HF semi-circle that is mainly affected by the higher water conductivity.

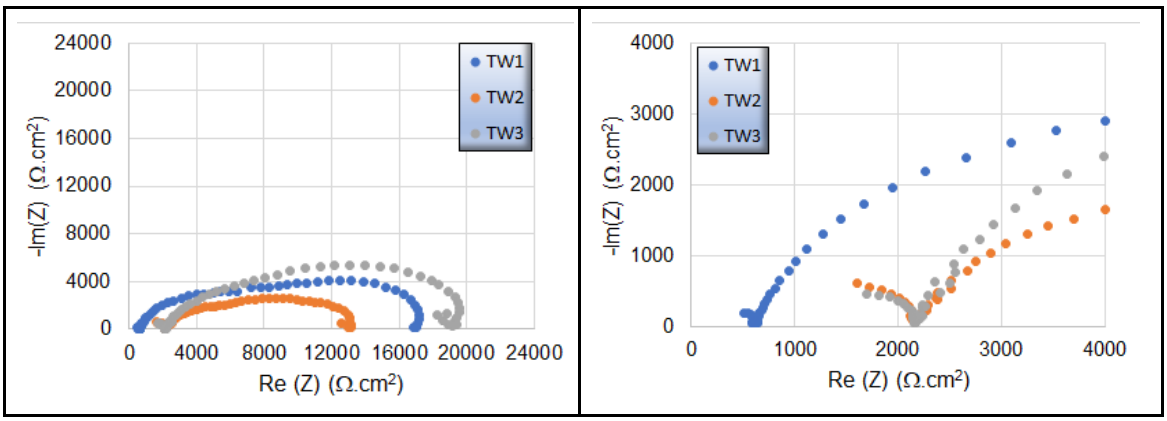

Figure 15. Nyquist diagram of CW511L at E_{corr} in the different test waters after 1 h of immersion at room temperature: left: full frequency range, right: high frequency region.

Figure 16 shows generated Bode diagrams (phase and impedance magnitude) in the test waters. The number of different processes can be checked through the number of slope changes in Bode magnitude representation or the number of phase angle maxima. However, when the kinetics of two processes are very similar it is difficult to distinguish them from each other, in this study as mixed peaks in the Bode phase diagram (Figure 16, left). The maximum value of the phase angle at HF showed a typical diffusion value of 45° for TW1 and lower in the case of TW2 and TW3. This indicates different diffusion characteristics in these waters, findings that are consistent with cathodic Tafel slopes shown in Table 11. On the other hand, the HF limit of Bode magnitude corresponds to the electrolyte resistance which is significantly lower in the case of the highly conductive TW1 compared with the other test waters (Figure 16, right).

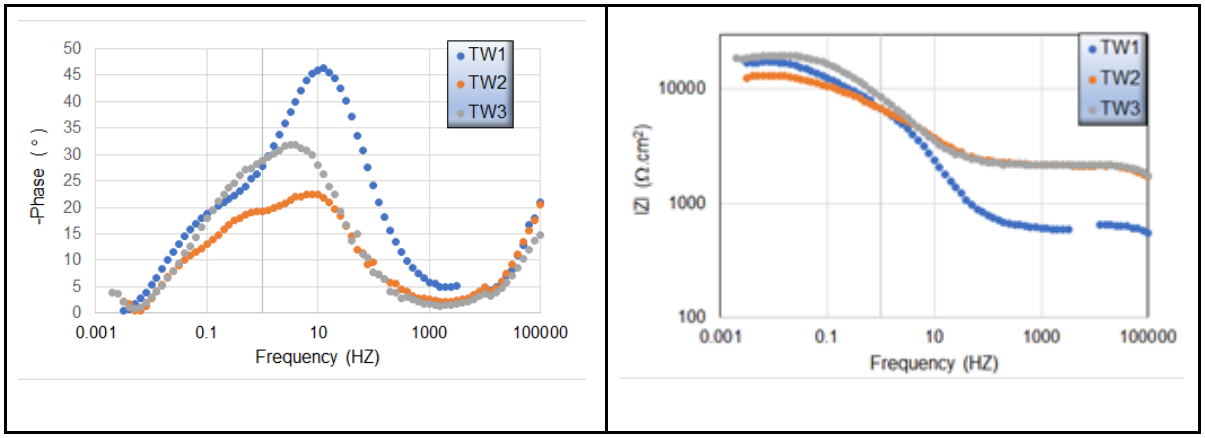

Figure 16. Bode diagram of CW511L at E_{corr} in the different test waters after 1 h of immersion at room temperature.

The current distribution across the metal surface and CPE took place also after 24 h of immersion (Figure 17). Indeed, the surface inhomogeneity, zinc element distribution and ohmic drop continue to affect EIS response moving towards the typical behavior of porous electrodes discussed in the literature [36]. The initiation of localized corrosion cannot be excluded at this stage and may contribute to EIS response. This hypothesis can be verified depending on surface characterization. On the other hand, the lowest LF impedance, which represents polarization resistance, was obtained in TW1 followed by TW2 and TW3. These findings are consistent with the observed trend of the i_{corr} and R_p values obtained from the potentiodynamic investigations (Tables 8 and 9).

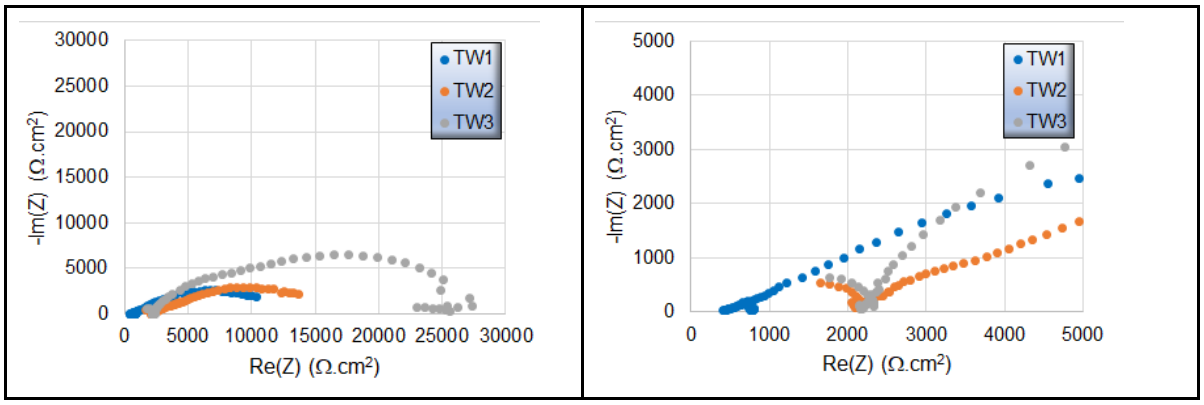

Figure 17. Nyquist diagram of CW511L at E_{corr} in the different test waters after 24 h of immersion at room temperature: left: full frequency range, right: high frequency region.

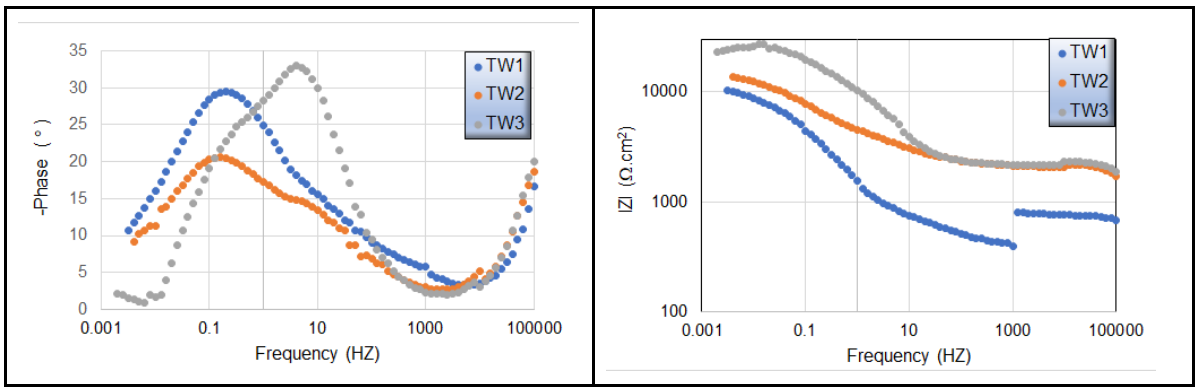

Figure 18. Bode diagram of CW511L at E_{corr} in the different test waters after 24 h of immersion at room temperature.

CW724R

Figure 19 shows EIS in Nyquist representation after 1 h of immersion in the test waters. Similar to CW511L, the results are characterized by a similar HF response for TW1 and TW2 and a different one in the case of TW3. At LF, the response showed an open and larger semi-circle in TW3 making the determination of polarization resistance challenging. However, the LF response for TW1 and TW2 seemed to converge to the same limit.

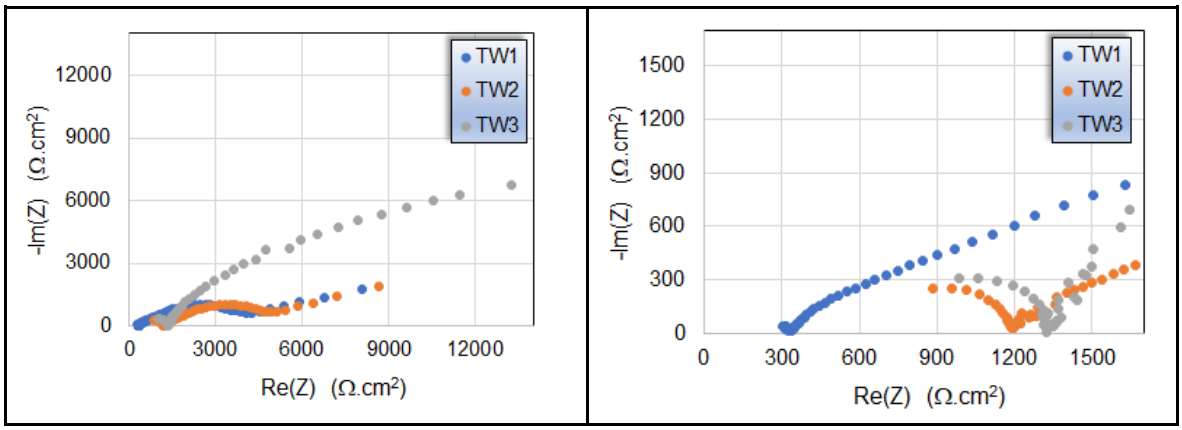

Figure 19. Nyquist diagram of CW724R at E_{corr} in the different test waters after 1 h of immersion at room temperature: left: full frequency range, right: high frequency region.

The Bode phase diagrams shown in Figure 20 indicate two visible maxima (two processes) and a third incomplete one at low frequencies. The results show a lower HF limit for TW1 than for TW2 and TW3 which is related to the high conductivity of TW1.

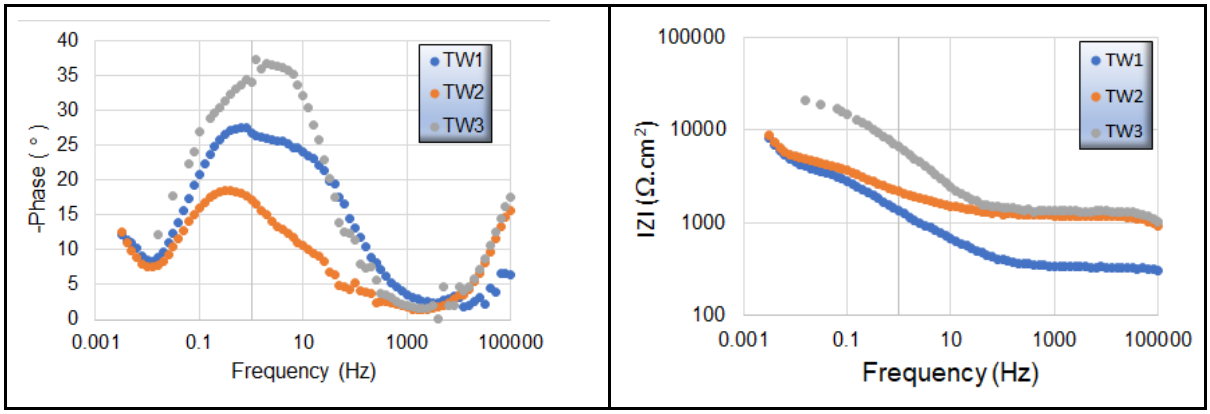

Figure 20. Bode diagram of CW724R at E_{corr} in the different test waters after 1 h of immersion at room temperature.

A similar Nyquist response was observed for CW724R after 24 h in the three test waters with a smaller HF semi-circle in TW1 and less depressed semi-circles and higher impedance values (Figure 21). The HF response in TW2 and TW3 was close with a slight shift towards higher values compared to the response after 1 h of immersion. The LF response in TW3 continued to show an open semi-circle as observed after 1 h of immersion. The shape of Nyquist diagram may suggest three processes observed by means of EIS.

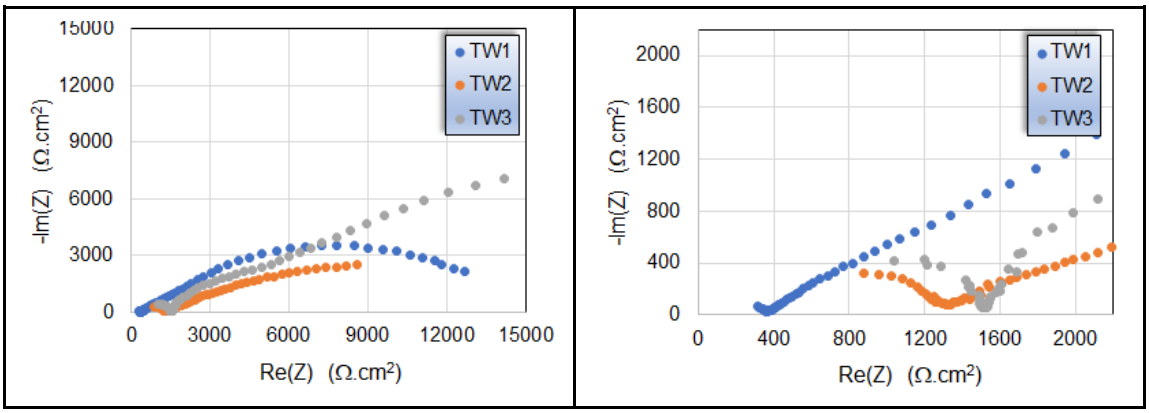

Figure 21. Nyquist diagram of CW724R at E_{corr} in the different test waters after 24 h of immersion at room temperature: left: full frequency range, right: high frequency region.

The examination of the Bode phase diagram (Figure 22) revealed double peaks that were easier to distinguish in TW3 compared to TW1 and TW2. This indicates that the processes for TW1 and TW2 should have very similar kinetics (time constants) compared to the behavior in TW3. Moreover, the response in TW2 showed the lowest phase angle, which could be correlated to the highest corrosion current density and the lowest R_p determined from the Tafel plot. The impedance limit at LF ranking was possible to correlate with the corrosion parameters obtained from the Tafel plot (i_{corr}, R_p, slopes) following: TW2-TW1-TW3.

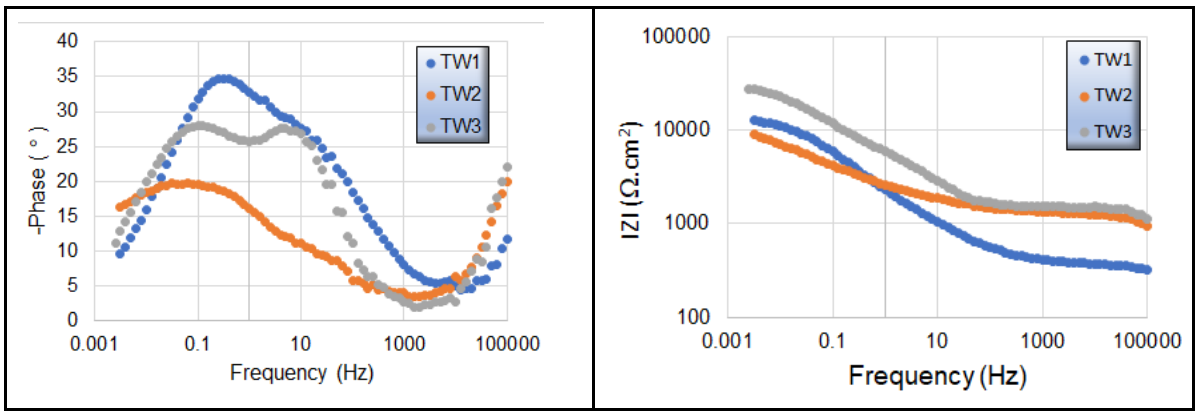

Figure 22. Bode diagram of CW724R at E_{corr} in the different test waters after 24 h of immersion at room temperature.

CW602N

Figure 23 shows the EIS results of CW602N in Nyquist representation after 1 h of immersion in the test waters. The results are characterized by more highly depressed semi-circles in TW2 compared to TW1 and TW3. A more complete, smaller and less depressed HF semi-circle was observed in TW1 compared to TW2 and TW3. The HF limit of impedance, representing the electrolyte resistance, was very different from the observations of the other alloys in the same water and exposure duration. This result indicates a considerable role of the alloy composition on EIS response for a given environment. The size of this HF semi-circle size was large and became smaller in the order TW3>TW2>TW1, findings which correspond to the order of anodic and cathodic Tafel slopes extracted from the potentiodynamic scans.

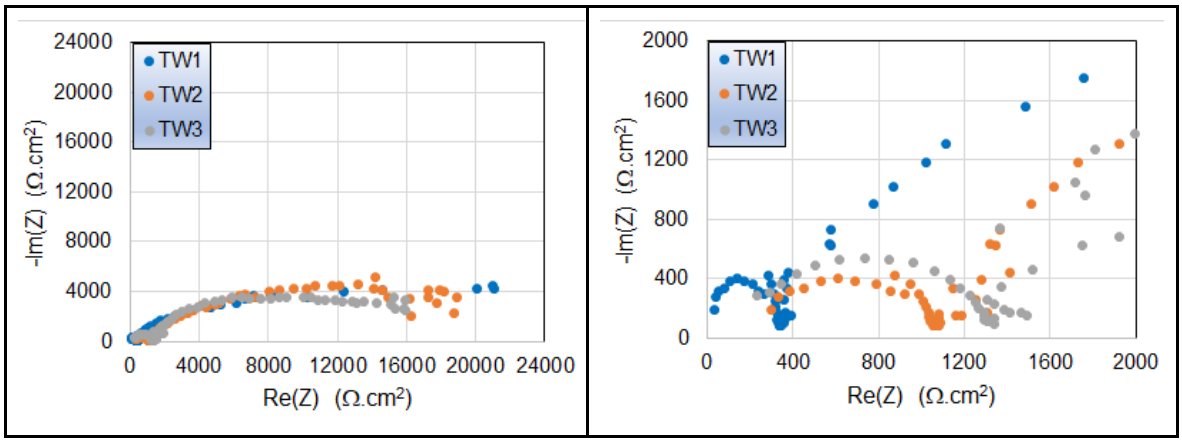

Figure 23. Nyquist diagram of CW602N at E_{corr} in the different test waters after 1 h of immersion at room temperature: left: full frequency range, right: high frequency region.

Examination of the Bode diagram (Figure 24, left) showed a starting at high phase angle values at HF associated to capacitive behavior seen from the Bode Magnitude (Figure 25, right). This response may be attributed to the presence of a surface layer. A very high maximum phase angle was observed in TW1 (> 70°) while lower for TW2 and TW3 (≈45°). Findings in TW1 showed a lower HF limit of the Bode magnitude compared with TW2 and TW3, which had almost identical curves.

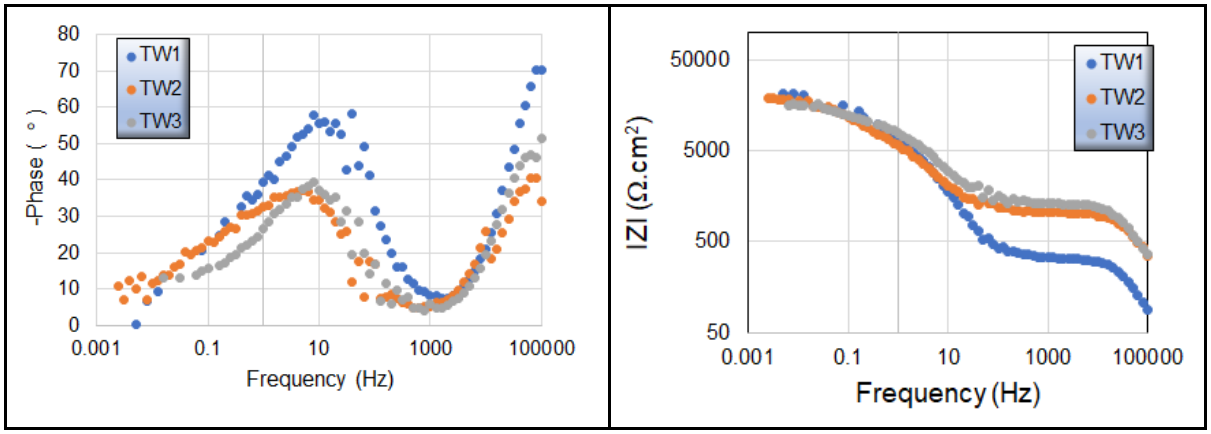

Figure 25. Bode diagram of CW602N at E_{corr} in the different test waters after 1 h of immersion at room temperature.

The Nyquist diagrams (Figure 26) for the different test waters looked after 24 h of exposure similar to findings after 1 h, with the smallest HF semi-circle in TW1 and similar results in in TW2 and TW3. At LF, closed semi-circles of larger size were observed in TW3. The trend of the impedance limits at LF seemed to follow the trends observed for i_{corr} and R_p obtained from the potentiodynamic results after 24 h (Tables 20 and 21).

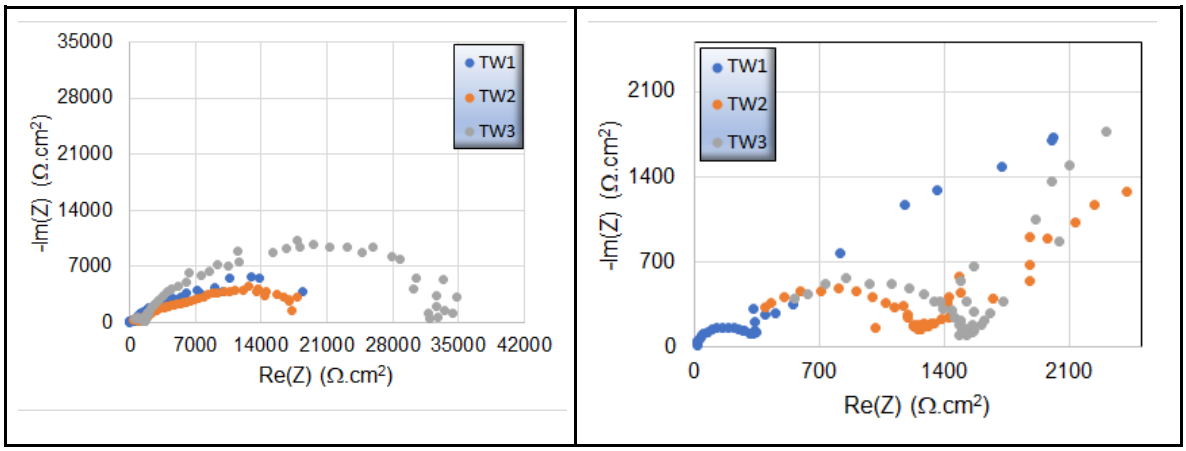

Figure 26. Nyquist diagram of CW602N at E_{corr} in the different test waters after 24 h of immersion at room temperature: left: full frequency range, right: high frequency region.

The similarity is also shown in the Bode diagrams (Figure 27) with the highest phase angle and lowest HF limit of Bode magnitude observed in TW1 compared with TW2 and TW3. The form of the Bode phase curve obtained in TW2 with the second maximum phase angle changed from 38° to 28°.

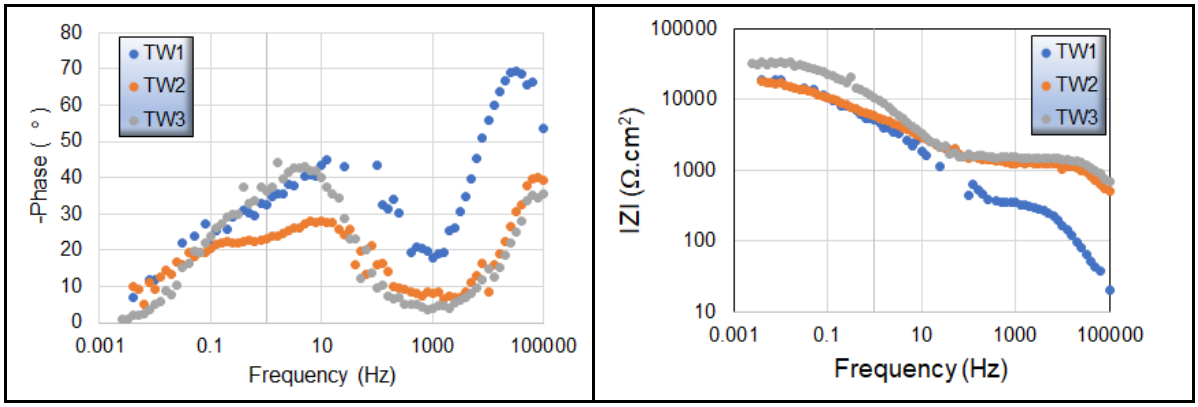

Figure 27. Bode diagram of CW602N at E_{corr} in the different test waters after 24 h of immersion at room temperature.

Summary of electrochemical results

Water corrosivity ranking for short-term exposure was determined in consistent way based on corrosion current densities, polarization resistance and low frequency electrochemical impedance limit. Water corrosivity ranking varies with immersion time and brass alloy. After 24 hours of immersion, water corrosivity was the same for lead-free CW724R and lead CW602N grades (TW2>TW1>TW3) contrary to the lead-free CW511L (TW1>TW2>TW3), which showed a different behavior. Anodic and cathodic Tafel slopes ranking after 24 hours followed test water corrosivity ranking for all alloys except in one case which is the cathodic Tafel slope for lead-containing brass CW602N. Moreover, all cathodic Tafel slope values were high, showing a significant contribution of the diffusion process as expected for this short immersion time. The evolution of OCP potential during 24 hours of immersion varies according to the brass alloy and the test water with two main behaviors. The lead-free (CW511L) and lead containing (CW602N) alloys showed similar evolution direction with a shifting to negative potential values. However, the lead-free CW724R showed a potential ennoblement in all test waters except in TW3. The agreement between OCP and E_{corr} was respected for all alloys except for lead containing brass CW602N. This discrepancy is caused by the potentiodynamic scan that significantly affected the thermodynamics of the corrosion process when lead is present.

6.1.1.2 LOM

Light optical microscope (LOM) was used to characterize the surface after exposure to the corrosive waters. It is important to notice that microscopic analysis of corrosion has to be done in at least two perspectives, in this study corrosion density (number of areas of localized corrosion per surface area) and corrosion depth. Cross-sectional samples were also investigated under LOM, however no substantial corrosion depths were observed, which was expected due to the short immersion time. Investigations of the corrosion density was made in a qualitative way.

CW511L

Figure 28 shows differences in terms of corrosion for CW511L immersed into the different test waters. The surface exposed to TW1 showed a combination of both small and large areas of localized corrosion. The LOM image of the surface exposed to TW2 shows both black corroded areas as well as reddish areas that may be attributed to the bulk copper. The surface immersed in TW3 showed isolated fine smaller-sized corroded areas (black). Qualitatively, TW1 would correspond to the most corrosive water with its large areas of localized corrosion attacks. Figure 29 confirms this overall view observation by showing the corroded areas at higher magnification. These findings agrees with the R_p and i_{corr} results acquired using potentiodynamic scans and EIS LF impedance values.

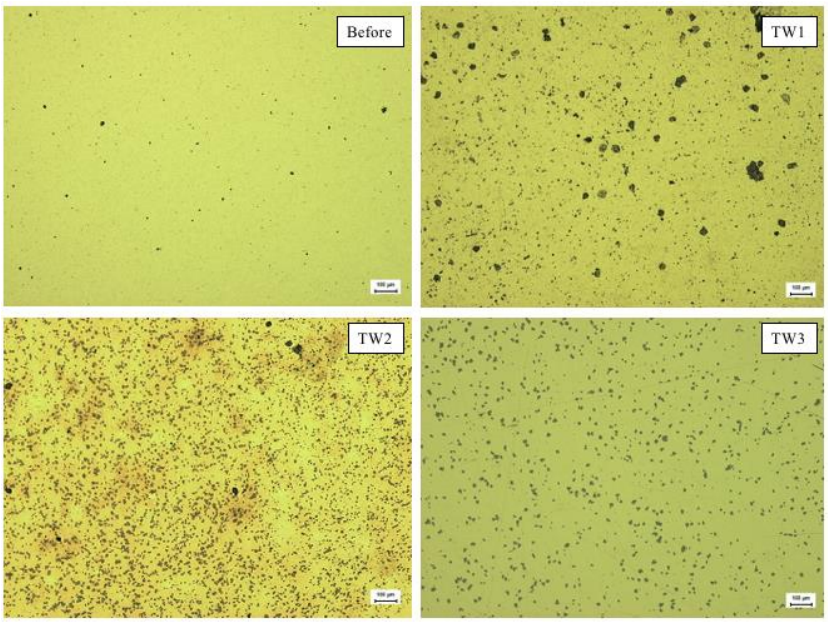

Figure 28. LOM micrographs of CW511L before and after 24 h exposure to three test waters TW1, TW2 and TW3 respectively at room temperature.

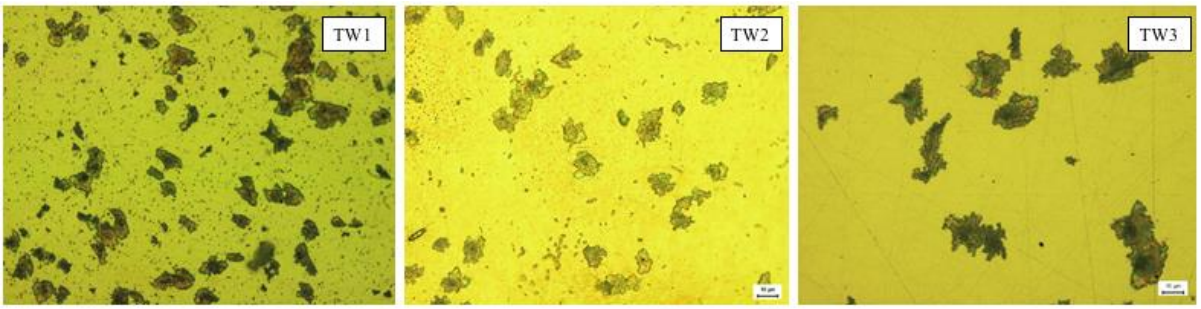

Figure 29. Higher magnification LOM micrographs of CW511L after 24 h exposure to three test waters at room temperature.

CW724R

Figure 30 shows the surface appearance before and after exposure to the three test waters. The surface exposed to TW3 was clearly the least affected, which is consistent with the lowest i_{corr} shown in Table 14. However, the surface immersed in TW1 showed significant redness that may be related to copper-rich corrosion products. The surface exposed in TW2 showed severe

corrosion with some copper redeposition. These findings agree well with i_{corr} and R_p values order in terms of water corrosivity ranking (TW2> TW1>TW3).

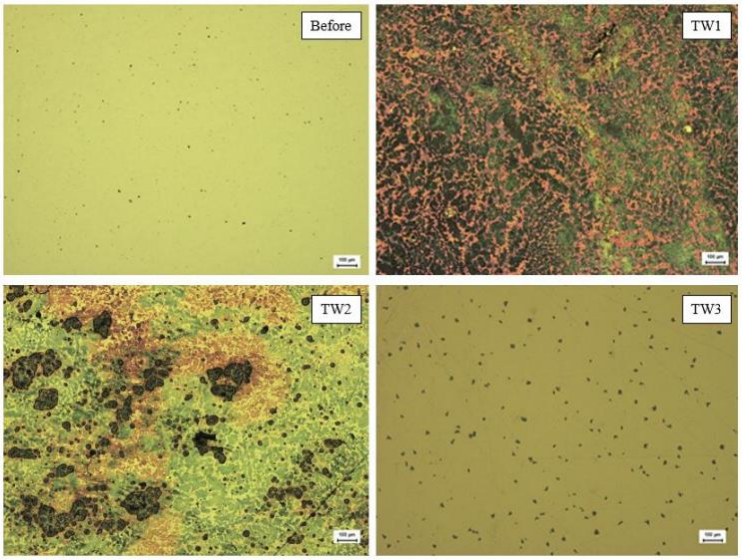

Figure 30. LOM micrographs of CW724R before and after 24 h exposure to three test waters TW1, TW2 and TW3 respectively at room temperature.

CW602N

Figure 31 shows the surface appearance before and after exposure to the three test waters. Exposure in TW3 resulted in the least corroded surface, which can be related to the i_{corr} values observed in Table 20. Exposure in TW1 resulted in large corroded (black) areas while only small corroded areas were a result of exposure in TW2 and TW3. A light reddish color appears within the corroded regions of the surface exposed in TW2, which may be related to copper. For CW602N it was not straight forward to rank the test waters corrosivity from the LOM images, as done for CW511L and CW724R. Ranking was therefore based on the quantitative information generated by the electrochemical investigations.

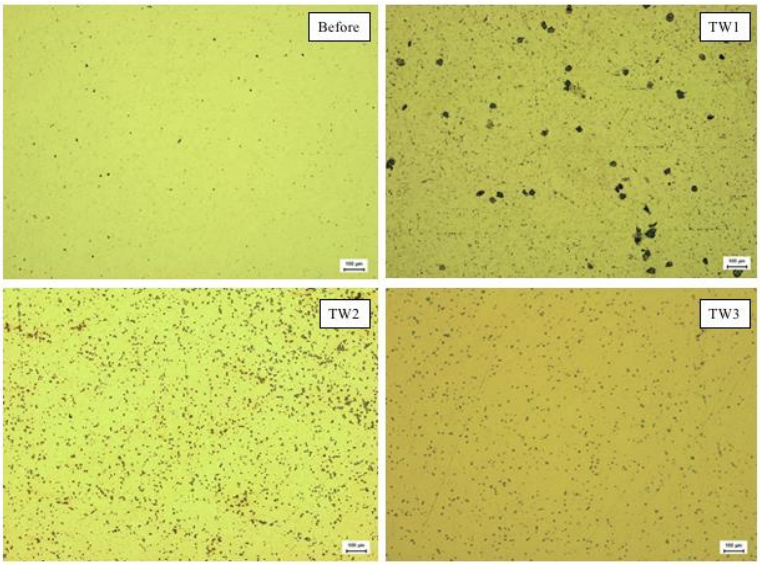

Figure 31. LOM micrographs of CW602N before and after 24 h exposure to three test waters TW1, TW2 and TW3 respectively at room temperature.

6.1.1.3 SEM-EDS

CW511L

SEM-EDS was used to characterize the type of corrosion and investigate the morphology and chemistry of the corrosion products. Figure 32 shows the SEM images of CW511L after exposure in TW1 for 24 h. Selected areas seem to be locally corroded while adjacent areas remains less corroded and smooth. The presence of pits was predominantly present in the corroded areas.

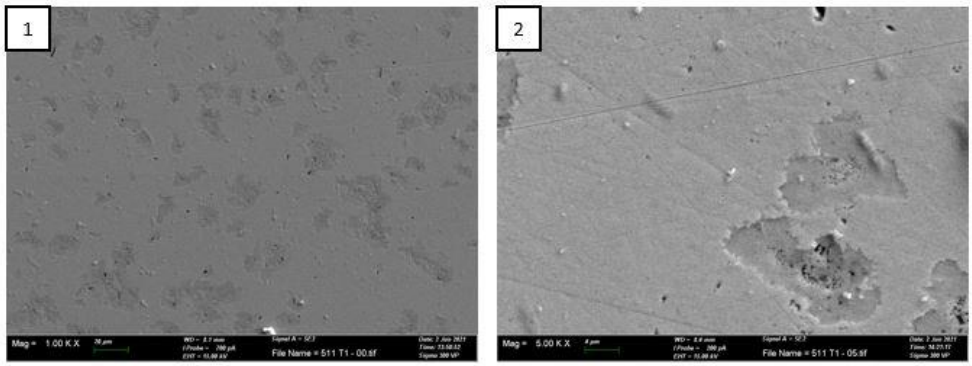

Figure 32. SEM image of CW511L exposed for 24 h at stagnant conditions in TW1 at 22 °C at 1: 1000x magnification 2: 5000x magnification.

Areas of localized corrosion were analyzed by means of EDS. Results based on area analysis of corroded areas are shown in Figure 33 and the results presented in Table 24. Spectrum 1 and 2 correspond to deep, superficial corroded areas respectively and spectrum 3 to the smooth less corroded area. While the result of the smooth area (Spectrum 3) suggests a low-corroded area, spectrum 1 (at the edge of a pit) suggests a more corroded area dominated by zinc with a sulfur content, possibly a poorly zinc-sulfur-containing corrosion product. Spectrum 2 implies a predominance of copper and chlorine.

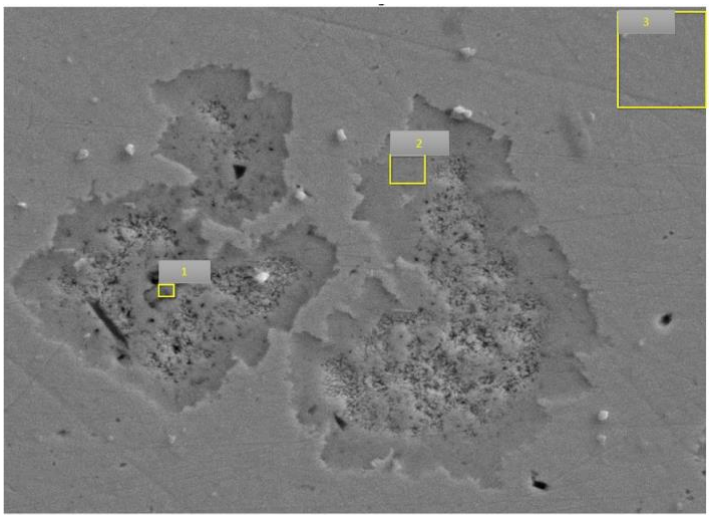

Figure 33. SEM image (10 000x magnification) of CW511L exposed for 24 h in TW1 and corresponding areas of EDS analysis.

Table 24. Elemental analysis of CW511L after 24 h immersion at stagnant conditions in TW1 at 22 °C.

wt.-%	Cu	Zn	O	Cl	S
Bulk	63.5	36.3	-	-	-
Spectrum 1	31.6	43.7	5.2	-	19.6
Spectrum 2	75.8	18.5	5.4	0.3	-
Spectrum 3	61.2	38.1	0.6	-	-

Figure 34 shows SEM images obtained for CW511L after 24 h of immersion in TW2 at different magnifications. Similar types of corrosion were observed with the presence of pits and locally corroded areas.

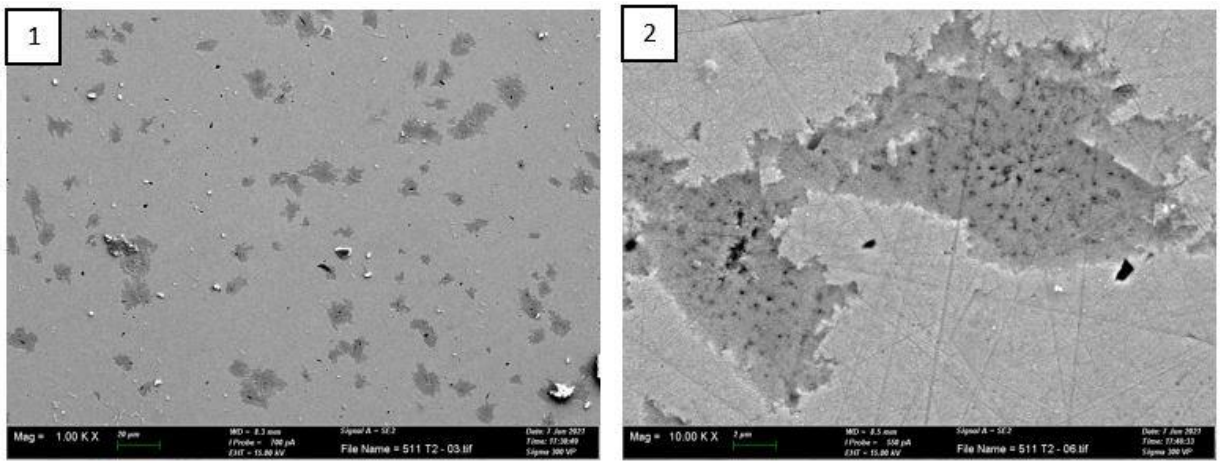

Figure 34. SEM images of CW511L exposed for 24 h at stagnant conditions in TW2 at 22 °C 1: 1000x magnification 2: 10 000x magnification.

EDS analysis conducted on three areas (uniform and locally corroded) showed the presence of chlorine in the locally corroded areas and a similar proportion of elements in the less corroded area as obtained in TW1 (Spectrum 3-Table 24). Traces of sulfur and calcium (<0.01 wt.-%) were detected at the location related to spectrum 3 but is not presented in Table 25.

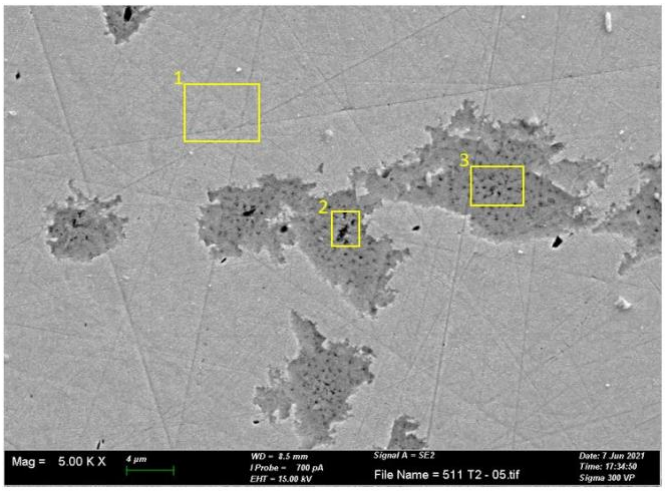

Figure 34. SEM image (5000x magnification) of CW511L after 24 h exposure in TW2 and areas for EDS analysis.

The presence of chlorine (assumed to be present as chloride) enhances the pitting process which leads to the formation of a very corrosive micro-environment. A low content of zinc (<5 wt.%) was observed within the heavily corroded areas compared with the less corroded smooth area.

Table 25. Elemental analysis of CW511L after 24 h immersion at stagnant conditions in TW2 at 22 °C.

wt.-%	Cu	Zn	O	Cl
Bulk	63.5	36.3	-	-
Spectrum 1	61.8	37.5	0.8	-
Spectrum 2	84.2	4.1	10.2	0.9
Spectrum 3	87.4	2.2	9.7	0.7

Similar corrosion features were observed on CW511L exposed for 24 h in TW3 at 22 °C, Figure 35.

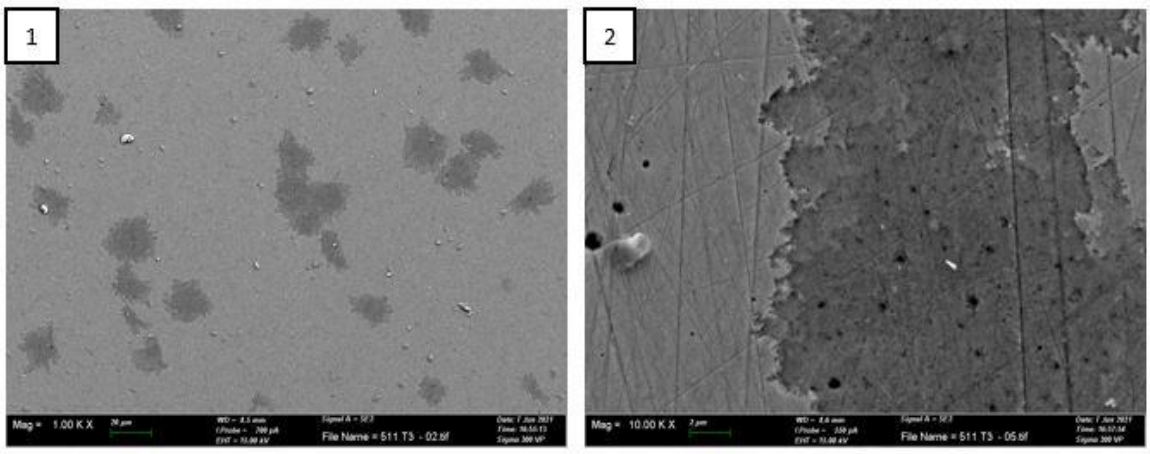

Figure 35. SEM images of CW511L exposed for 24 h at stagnant conditions in TW3 at 22 °C 1: 1000x magnification 2: 10 000x magnification.

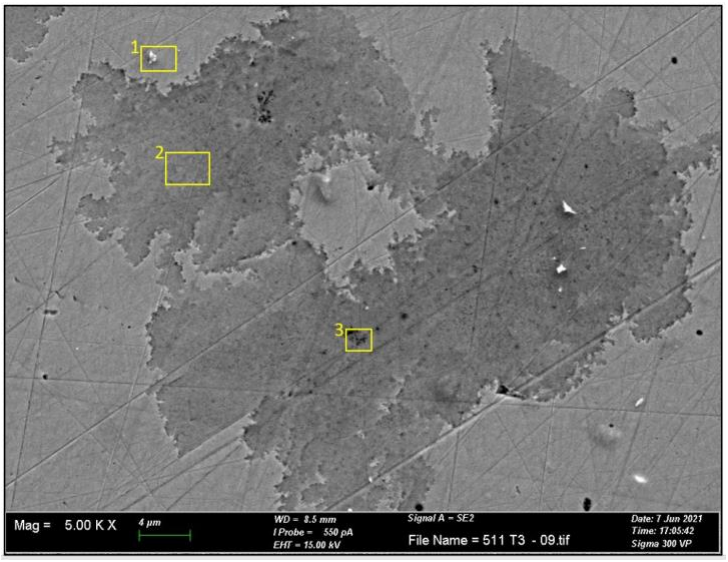

Figure 36. SEM image (5000x magnification) of CW511L after 24 h in TW3 –EDS analysis at marked areas.

EDS analysis of selected areas from the surface of the sample after 24 h immersion in TW3 (Figure 36) are shown in Table 26. The corroded areas are predominantly composed of copper-rich corrosion products combined with traces of chlorine (<1 wt.-%) (Spectrum 2 and 3).

Table 26. Elemental analysis of CW511L after 24 h immersion at stagnant conditions in TW3 at 22 °C.

wt.-%	Cu	Zn	O	Cl
Bulk	63.5	36.3	-	-
Spectrum 1	60.9	37.9	1.2	-
Spectrum 2	82.9	9.2	7.6	0.3
Spectrum 3	86.9	2.8	9.6	0.7

CW724R

SEM images of CW724R after immersion in TW1 for 24 h are shown in Figure 37. The darker and lighter areas shown in picture 1 in Figure 37 can be related to the two phases of this alloy (α (lighter) and κ (darker)), where both phases show the presence of pits. The darker areas are more compact compared with the lighter areas (picture 2 in Figure 37).

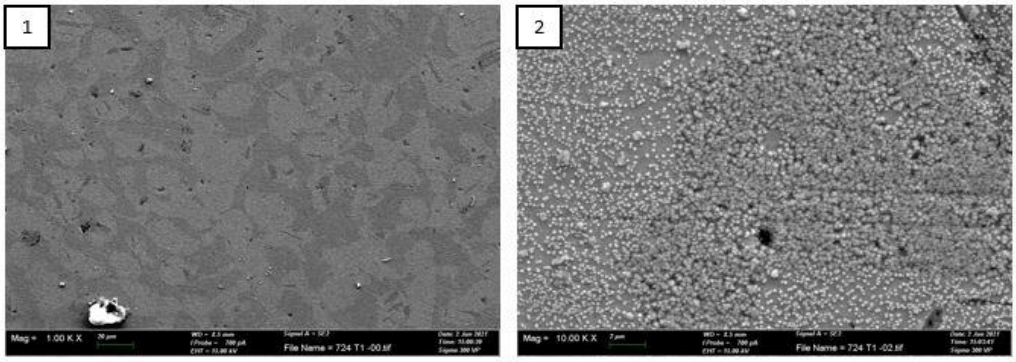

Figure 37. SEM image of CW724R exposed to stagnant TW1 at 22 °C after 24 hours at 1: 1000x magnification 2: 10 000x magnification.

EDS analysis was conducted to determine the chemistry of pit areas (Figure 38). The results are presented in Table 27 where the corrosion products of the deepest pit (Spectrum 2) were copper-rich (possibly a copper oxide) as well as small amounts of phosphorus, chlorides and sulfur. The presence of silicon in relatively high concentrations within the corrosion products raises its potential role in corrosion and merits further investigations. Slightly more Si was present shown in the darker areas (Spectrum 1 and 5), which can be connected to the silicon-rich *κ*-phase of less Zn content compared with the lighter areas (Spectrum 3 and 4).

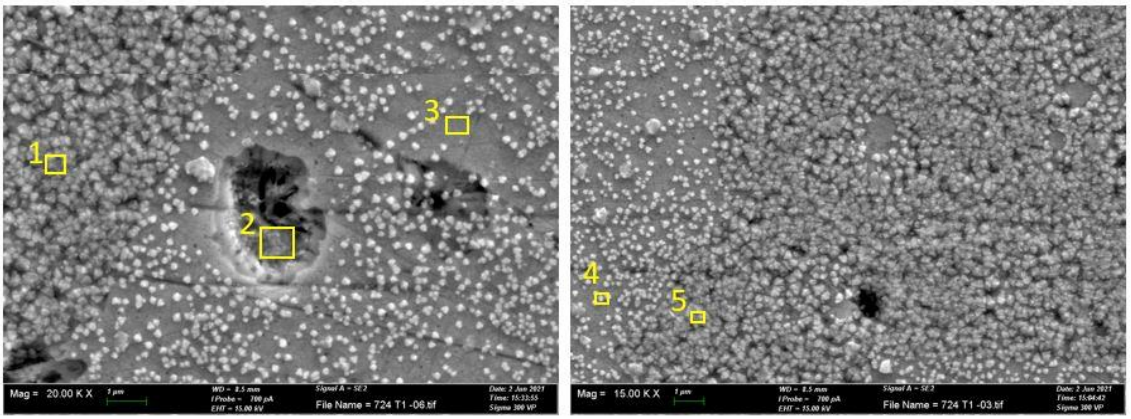

Figure 38. SEM images (20 000x and 15 000x magnification) of CW724R exposed for 24 h in TW1 and marked areas for EDS analysis.

Table 27. Elemental analysis of CW724R after 24 h immersion at stagnant conditions in TW1 at 22 °C.

wt.-%	Cu	Zn	O	Si	P	Cl	S
Bulk	75.8	20.6	-	3.4	0.05	-	-
Spectrum 1	77.1	13.6	5.7	3.5	0.1	-	-
Spectrum 2	81.5	6.6	9.7	1.1	0.04	0.6	0.2
Spectrum 3	72.6	23.9	0.9	2.6	0.03	-	-
Spectrum 4	72.1	22.3	2.6	2.7	-	-	0.3
Spectrum 5	76.7	14.0	5.8	3.5	-	-	-

CW724R exposed in TW2 for 24 h showed a surface morphology as shown in Figure 39. Substantial amounts of corrosion products were observed with the formation of a thick layer and oriented corrosion taking place that created parallel openings (crevices), which makes it easier for the water to penetrate.

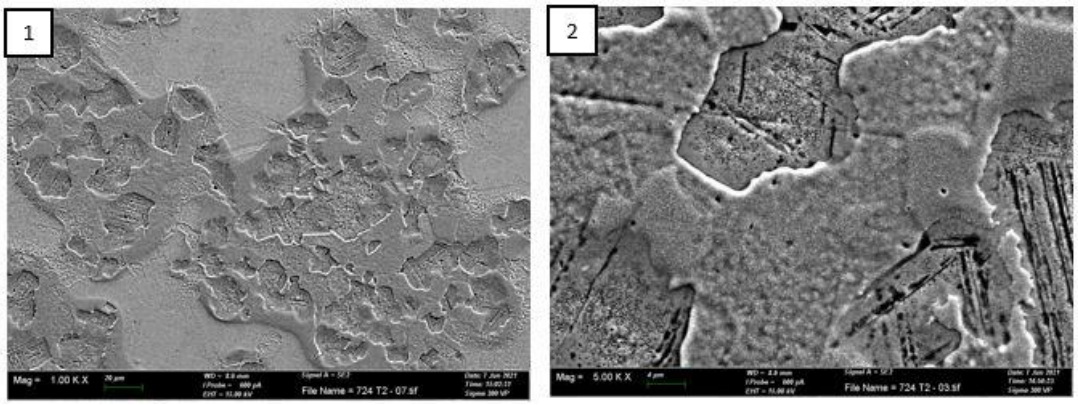

Figure 39. SEM image of CW724R exposed for 24 h at stagnant conditions in TW2 at 22 °C. 1: 1000x magnification 2: 5 000x magnification.

EDS analysis was conducted on four representative areas as shown in Figure 40 and the obtained results are shown in Table 28. The less corroded area (Spectrum 4) is dominated by copper and contains higher silicon content compared with the other spectra.

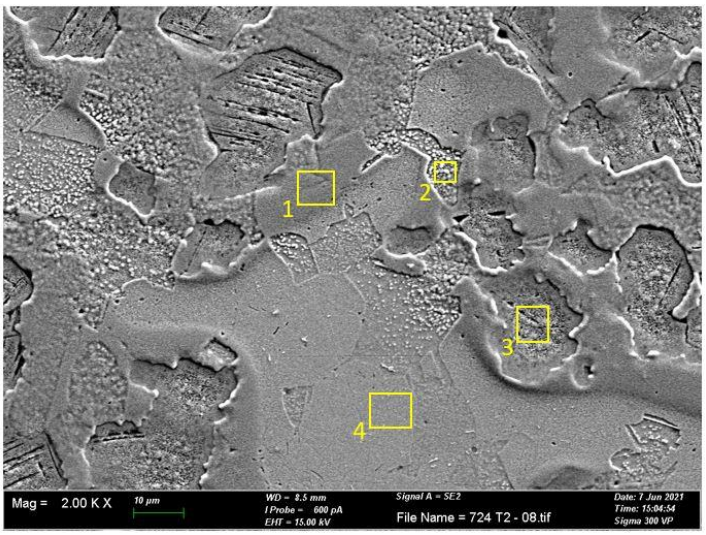

Figure 40. SEM image of CW724R in TW2 after 24 hours considered for EDS analysis at 2000x magnification.

The thick layer formed between what may be κ-phase and α-phase (Spectrum 1) is also dominated by copper and contains some silicon and traces of chlorine with a higher oxygen content compared to the less corroded α-phase. An oxide predominantly rich in copper was detected at all locations with the presence of detectable amounts of chlorine at the crevices (Spectrum 3).

Table 28. Elemental analysis of CW724R after 24 h immersion at stagnant conditions in TW2 at 22 °C.

wt.-%	Cu	Zn	O	Si	Cl
Bulk	75.8	20.6	-	3.4	-
Spectrum 1	84.4	4.1	10.4	0.9	0.2
Spectrum 2	84.5	3.9	9.6	1.8	0.2
Spectrum 3	86.7	1.5	10.4	0.5	0.8
Spectrum 4	75.9	17.4	4.3	2.5	-

SEM images of CW724R after immersion in TW3 for 24 h showed less corroded surfaces compared to TW1 and TW2 (Figure 41). Localized corrosion seems to affect both the α-phase and the κ-phase with some continuity between corroded areas.

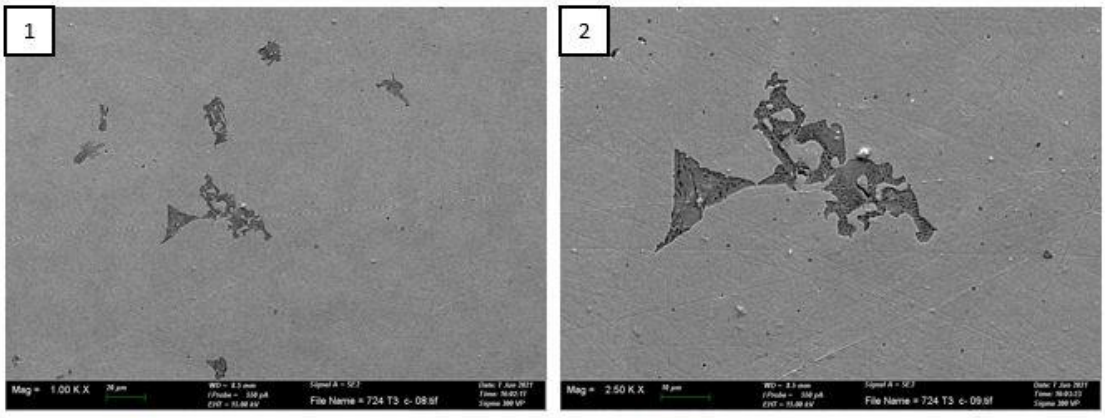

Figure 41. SEM images of CW724R exposed for 24 h at stagnant conditions in TW3 at 22 °C 1: 1000x magnification 2: 2500x magnification.

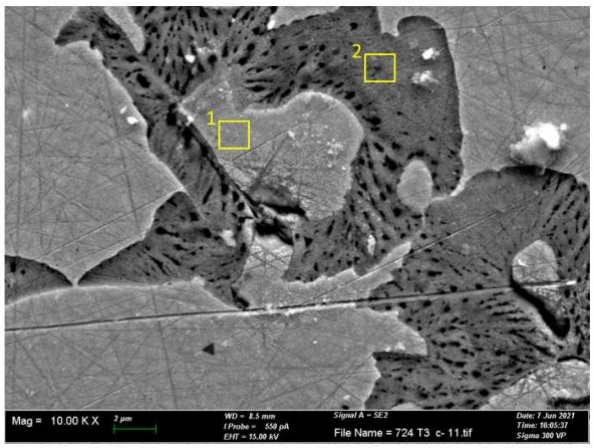

Figure 42. SEM image (10 000x magnification) of CW724R exposed for 24 h in TW3 and marked areas for EDS analysis.

EDS analysis was performed on locally corroded areas in two locations as shown in Figure 42. The results (Table 29) show the deepest corroded area (Spectrum 2) to consist of a corrosion product with the dominance of copper and presence of the silicon. However, the less-corroded area (smooth) was characterized by a very low oxygen content. The copper and zinc composition was similar to the alloy content with silicon (Spectrum 1), which implies a thin layer of corrosion products.

Table 29. Elemental analysis of CW724R after 24 h immersion at stagnant conditions in TW3 at 22 °C.

wt.-%	Cu	Zn	O	Si	Cl
Bulk	75.8	20.6	-	3.4	-
Spectrum 1	70.8	22.5	0.7	6.0	-
Spectrum 2	82.7	3.3	11.2	2.0	0.8

CW602N

SEM images of CW602N after immersion in TW1 for 24h showed locally corroded surface areas (Figure 43). Some pits were locally observed, also in less corroded (smooth) areas.

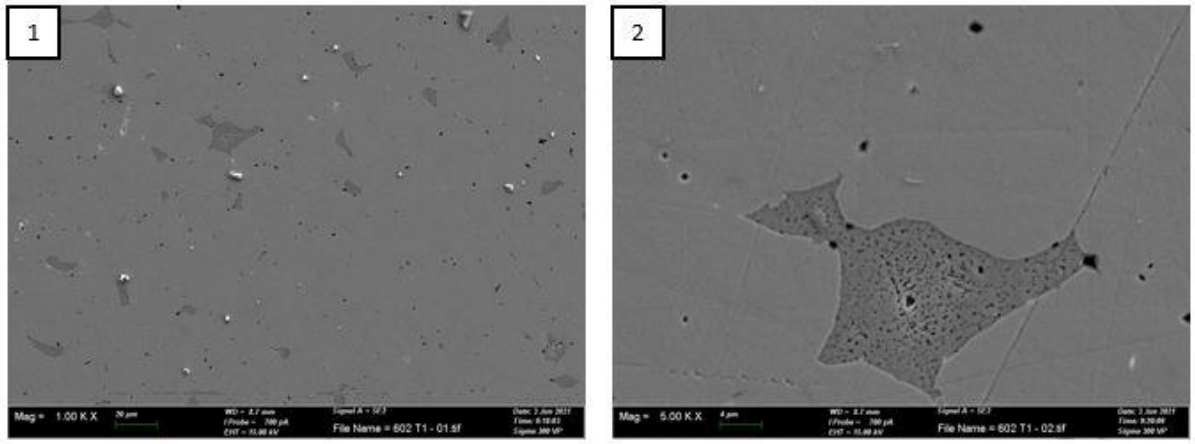

Figure 43. SEM images of CW602N exposed for 24 h at stagnant conditions in TW1 at 22 °C
1: 1000x magnification 2: 5000x magnification.

EDS analysis was performed on selected locally corroded and less corroded (smooth) areas (Figure 44). The results are summarized in Table 30. No information on the corrosion products could be gained in the less corroded areas due to their thin thickness and constraints of the information depth of EDS. However, the composition of the locally corroded areas (Spectrum 2) was dominated by copper with traces of lead and chlorine. Traces of iron, silicon and tin were observed though not included in Table 30.

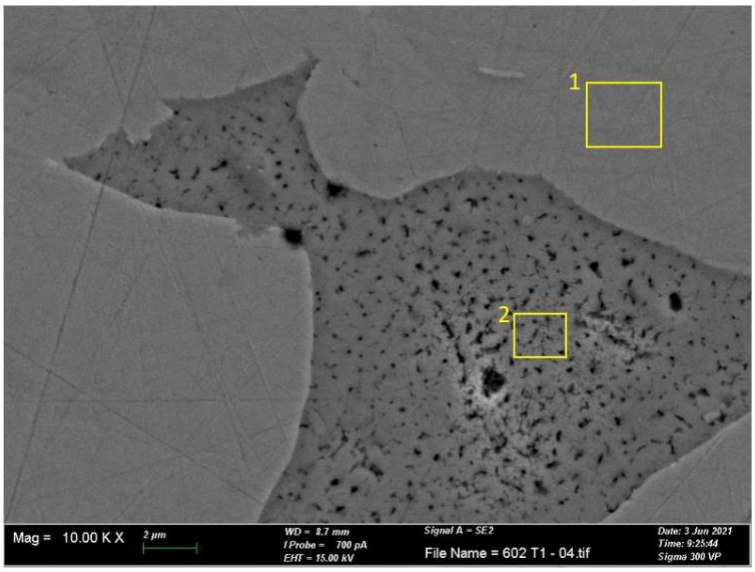

Figure 44. SEM image (10 000x magnification) of CW602N after immersion for 24 h in TW1 and marked areas of EDS analysis

Table 30. Elemental analysis of CW602N after 24 h immersion at stagnant conditions in TW1 at 22 °C.

wt.-%	Cu	Zn	O	Pb	Cl
Bulk	61.7	36.4	-	1.7	-
Spectrum 1	61.1	38.9	-	-	-
Spectrum 2	85.4	2.2	9.6	0.9	0.9

SEM images of CW602N after immersion in TW2 for 24 h showed a more locally corroded surface areas (Figure 45). Some pits of larger size could be clearly observed both within the locally corroded areas as well as in-between the locally and less-corroded (smooth) areas.

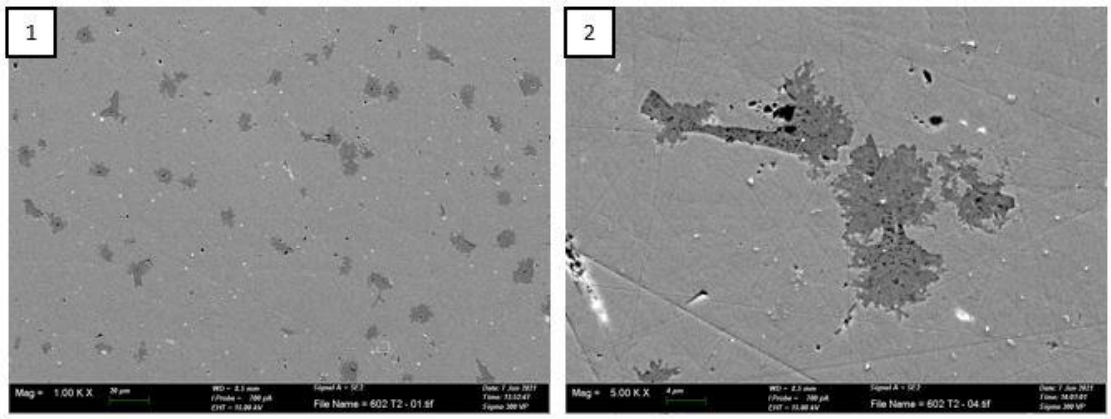

Figure 45. SEM images of CW602N exposed for 24 h in stagnant TW2 at 22 °C
1: 1000x magnification 2: 5000x magnification.

EDS analysis was performed on a selected locally corroded areas (Figure 46). The results are compiled in Table 31. Two locally corroded areas (Spectrum 1 and 3) showed corrosion

products that are Cu-Zn based with a copper dominance. Area 1 revealed the presence of some lead and had a higher silicon content compared with area 2, which only contained a small amount of silicon and no lead. However, spectrum 2 showed the dominance of zinc with a high presence of both lead and sulfur.

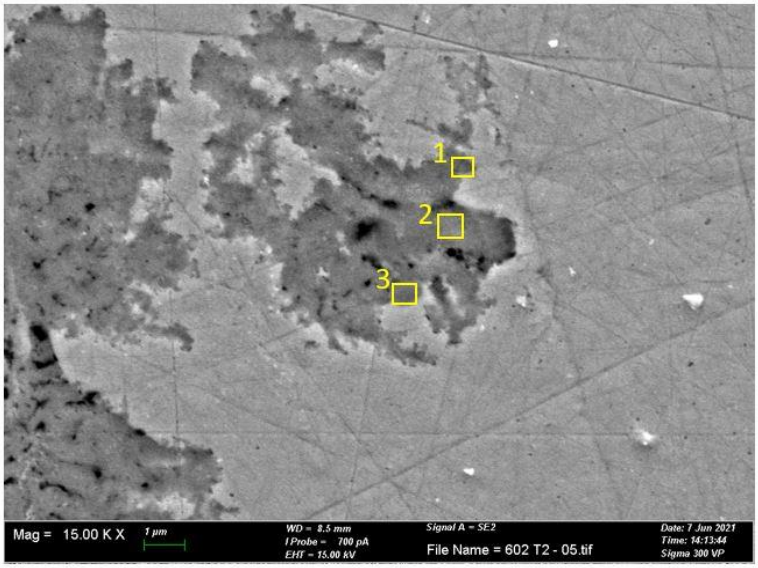

Figure 46. SEM image (15 000x magnification) of CW602N exposed for 24 h in TW2 and marked areas for EDS analysis.

Table 31. Elemental analysis of CW602N 24 h immersion at stagnant conditions in TW2 at 22 °C.

wt.-%	Cu	Zn	O	Pb	S	Si
Bulk	61.7	36.4	-	1.7	-	0.01
Spectrum 1	69.5	20.4	2.3	1.0	-	6.8
Spectrum 2	18.6	47.1	3.8	11.7	18.7	-
Spectrum 3	84.0	12.1	3.1	-	-	0.7

SEM of CW602N in TW3 showed less occurrence of localized corrosion. This type of corrosion had a more circular form compared with their appearance in TW1 and TW2 (Figure 47). Pitting was taking place at different locations over the surface.

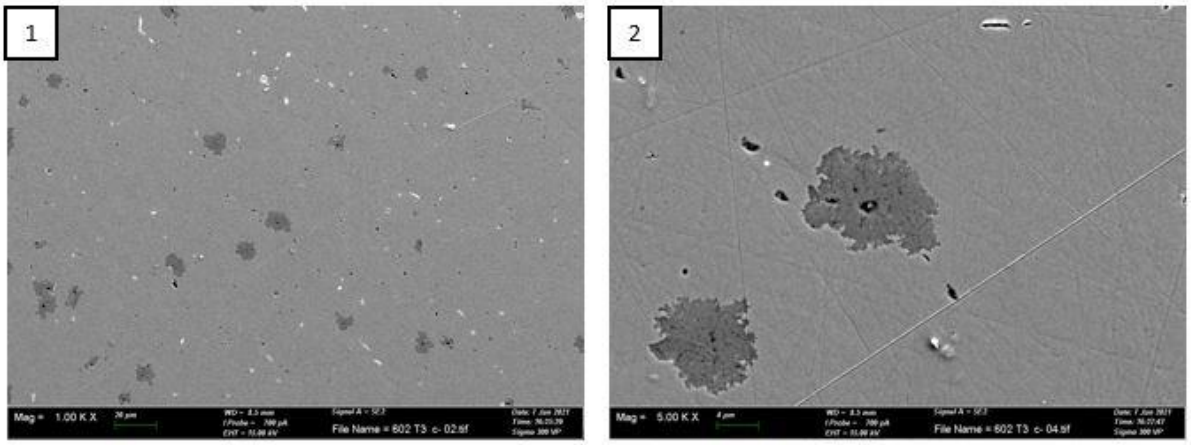

Figure 47. SEM image of CW602N exposed for 24 h at stagnant conditions in TW3 at 22 °C. 1: 1000x magnification 2: 5000x magnification.

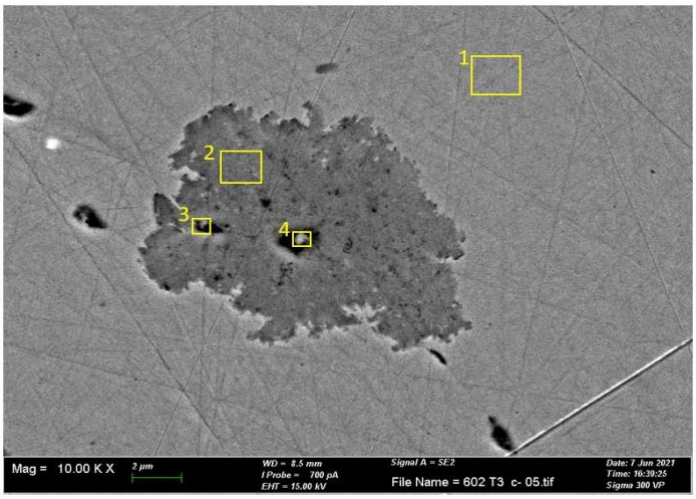

Figure 48. SEM image (10 000x magnification) of CW602N exposed for 24 h in TW3 and marked areas for EDS analysis.

EDS analysis was performed on selected locally corroded and less corroded (smooth) areas (Figure 48). The results are shown in Table 32. The pit locations (Spectrum 3 and 4) showed a predominance of copper as well as zinc and lead. The less corroded area (Spectrum 2), revealed corrosion products primarily composed of copper and minor amounts of zinc.

Table 32. Elemental analysis of CW602N after 24 h immersion at stagnant conditions in TW3 at 22 °C.

wt.-%	Cu	Zn	O	Pb	Cl
Bulk	61.7	36.4	-	1.7	-
Spectrum 1	61.2	38.8	-	-	-
Spectrum 2	85.0	5.6	8.9	-	0.4
Spectrum 3	61.6	20.9	6.4	10.9	0.2
Spectrum 4	60.1	0.03	0.1	0.3	-

6.1.2 Temperature effect

CW511L

The open circuit potential values measured at 22 °C and 50 °C are summarized in Table 33. The temperature increase caused a shift of OCP values to less negative values (the noble direction) in all the three test waters.

Table 33. OCP potentials in mV of CW511L in the different test waters at 22 and 50°C.

	TW1	**TW2**	**TW3**
OCP 22 °C	-18.7	-23.0	-22.7
OCP 50 °C	-8.9	-14.2	-16.8

Potentiodynamic curves (Tafel plot) of CW511L after 24 h of immersion in the three test waters at 50 °C are shown in Figure 49. A clear difference in shape was observed for the anodic slope of TW1 indicating a different corrosion mechanism compared with TW2 and TW3. A sharp current density increase was noticed for the three different test waters at characteristic potentials (denoted pitting potentials). Thus, the results indicate that a temperature increase enhance the extent of localized corrosion.

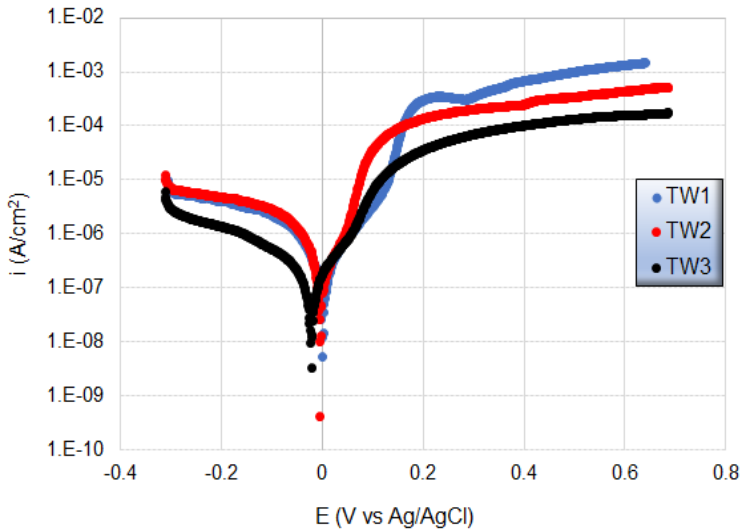

Figure 49. Tafel plots of CW511L after 24 h of exposure at stagnant conditions in the different test waters at 50 °C.

The Tafel plots at 22 and 50 °C are shown in Figure 50. Depending on the test water, the difference in terms of cathodic current density varied significantly in TW1 and TW3 but remained non-affected by temperature in TW2. The sharp increase of the anodic current (at the pitting potential) exceeded the anodic current at 25 °C in both TW1 and TW2, but remained below the anodic current in the case of TW3.

Table 34 summarizes the corrosion parameters of CW511L exposed in the different test waters for 24 h at 50°C and 22°C. As can be observed, a decreased corrosion rate (i_{corr} decrease, R_p increase) was obtained by an increased temperature, and in all cases associated with a reduced cathodic slope. However, the corrosion form changed from a dominance of general corrosion to more localized corrosion with increased temperature, and the ranking of the test water corrosivities is based on the localized corrosion indicator (E_{pit}). Similar to the observations for OCP, the corrosion potential E_{corr} shifted towards less negative values. The pitting potential, which is a localized corrosion resistance indicator of the material, was used to rank the corrosivity of the test waters; TW2>TW3>TW1. The results show TW2 to be the most corrosive test water for CW511L at 50 °C.

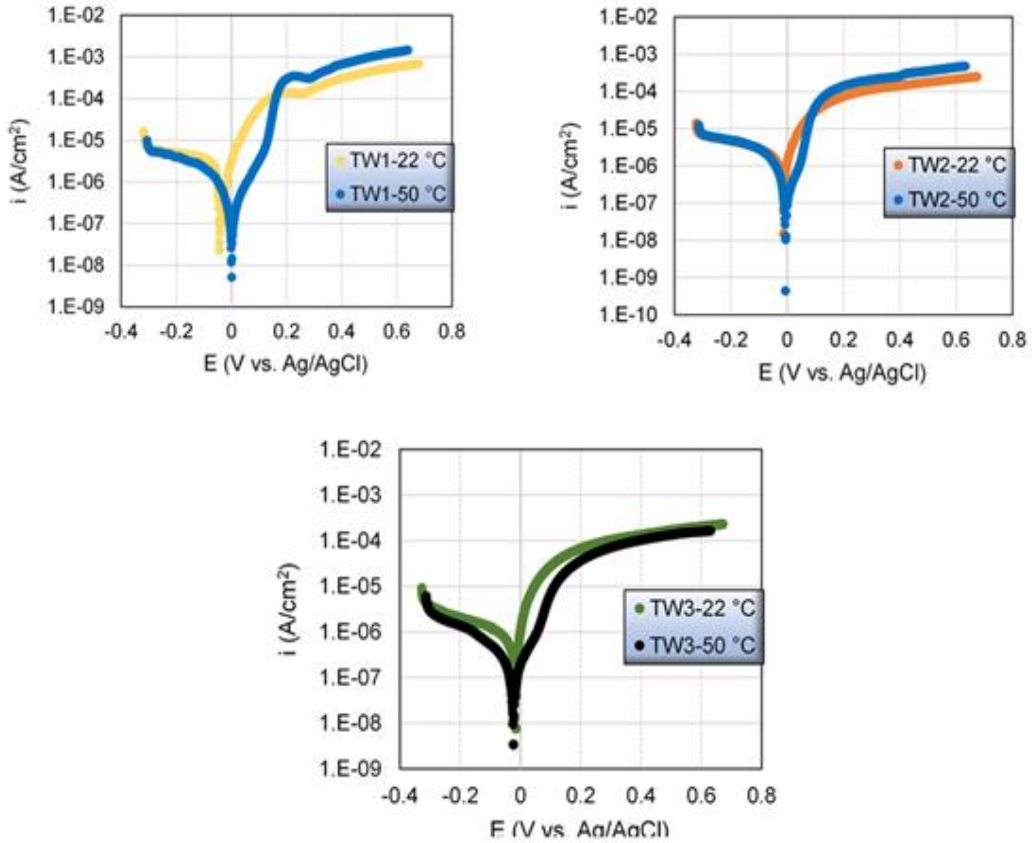

Figure 50. Tafel plots of CW511L after 24 h exposure at stagnant conditions in the different test waters at 22 °C and 50 °C.

Table 34. Different corrosion parameters of CW511L after 24 h exposure in the different test waters at 22°C and 50°C.

	22 °C			50 °C		
	TW1	**TW2**	**TW3**	**TW1**	**TW2**	**TW3**
E_{corr} [mV vs. Ag/AgCl]	-44.0	-12.0	-14.0	-1.0	-3.0	-19.0
i_{corr} [µA/cm^2]	2.2	1.8	0.4	0.3	0.6	0.2
R_p [kΩ cm^2]	20.0	15.4	28.6	66.7	50.0	100.0
B_c [mV/dec]	253.3	232.2	219.3	76.4	87.9	111.4
B_a [mV/dec]	87.9	76.9	30.9	97.9	52.9	81.4
E_{pit} [mV vs. Ag/AgCl]	-	-	-	128.0	45.0	67.0

CW724R

Measured OCP values at 22 and 50 °C are summarized in Table 35. The temperature increase caused a shift in OCP to less negative values (the noble direction) in the test waters TW2 and TW3 in contrast to findings in TW1.

Table 35. OCP potentials in mV of CW724R in different test waters at 22 and 50°C.

	TW1	**TW2**	**TW3**
OCP 22 °C	4.0	3.0	-0.1
OCP 50 °C	-7.0	14.0	18.0

The Tafel plots of CW724R in the different test waters at 50°C after 24 h exposure are shown in Figure 51. Immersion in TW3 resulted in the lowest cathodic current density and pitting potential compared to TW1 and TW2. Similar findings were observed in TW1 and TW2 despite their substantial difference in conductivity (Table 5).

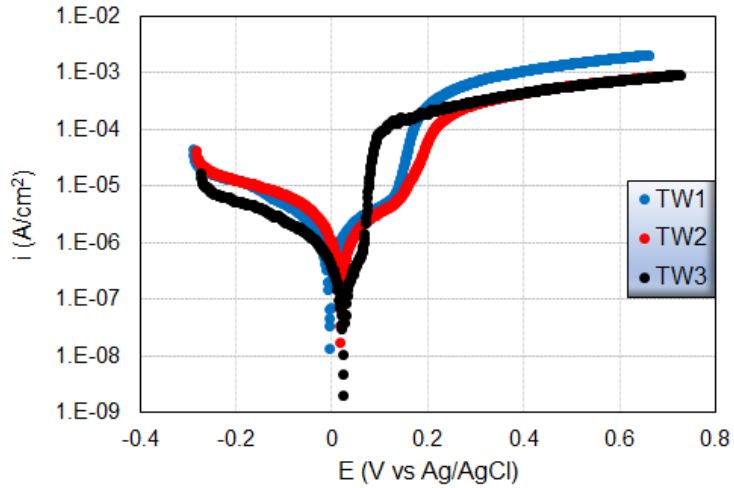

Figure 51. Tafel plots of CW724R after 24 h exposure at stagnant conditions in the different test waters at 50°C

Figure 52 shows Tafel plots at room temperature and 50 °C. Different behavior was observed for this alloy in terms of cathodic current when comparing the results acquired at room temperature and 50 °C. While the cathodic branches were similar in WP3, a slight increase was observed in TW1 and TW2 at 50 °C. Moreover, a double current plateau was noticed in TW1 at 50 °C which suggests two cathodic reactions. The anodic current at 50 °C after the pitting potential exceeds the anodic current at ambient temperature to variable levels depending on the test waters.

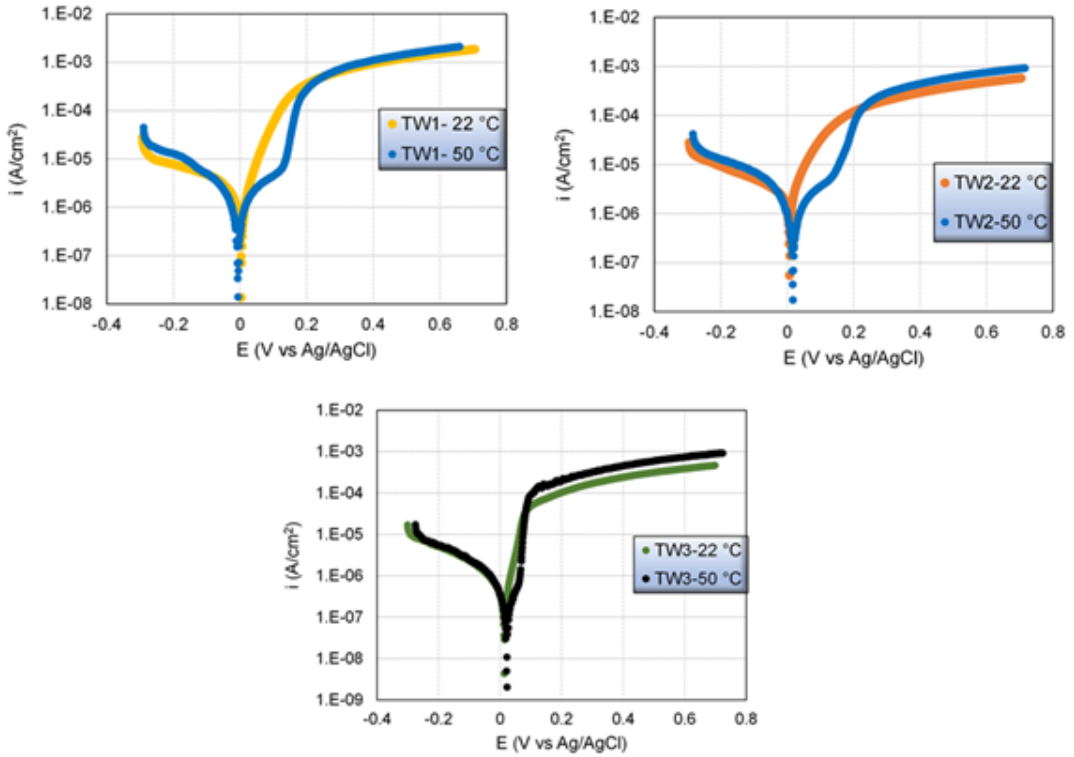

Figure 52. Tafel plots of CW724R after 24 h of exposure at stagnant conditions in the different test waters at 22 °C and 50 °C.

The different corrosion parameters of CW724R extracted from the Tafel plots at room temperature and at 50 °C after 24 h exposure in the different test waters are shown in Table 36. Similar to the OCP variations, the E_{corr} values shifted to higher potentials in TW2 and TW3 with increased temperature while the opposite was the case in TW1. Furthermore, the i_{corr} values decreased and the R_p values increased with the temperature, which indicates a reduced general corrosion rate. Decreased cathodic Tafel slopes were also observed.

The lowest pitting potential was obtained in TW3, clearly observed in Figure 51. These results show that the TW3 was at 50°C after 24 hours of exposure the most corrosive water for this alloy, followed by TW1 and TW2.

Table 36. Different corrosion parameters of CW724R after 24 h exposure in the different test waters at 22°C and 50°C

	22 °C			**50 °C**		
	TW1	**TW2**	**TW3**	**TW1**	**TW2**	**TW3**
E_{corr} [mV vs. Ag/AgCl]	3.0	8.0	11.0	-18.0	18.0	21.0
i_{corr} [µA/cm^2]	1.6	2.4	0.5	1.3	1.2	0.4
R_p [kΩ cm^2]	11.8	6.7	33.3	20.0	18.2	66.7
B_c [mV/dec]	235.5	300.9	163.5	168.5	109.5	145.9
B_a [mV/dec]	63.9	70.9	34.0	194.0	128.5	34.5
E_{pit} [mV vs. Ag/AgCl]	-	-	-	130.0	145.0	54.0

CW602N

Measured OCP values at 22 and 50 °C are summarized in Table 37. The temperature increase caused for all waters a shift in OCP to less negative values (the noble direction).

Table 37. OCP potentials in mV of CW602N in different test waters at 22 and 50°C .

	TW1	**TW2**	**TW3**
OCP 22 °C	-29.0	-14.0	-16.0
OCP 50 °C	-9.0	-6.0	1.0

Figure 53 shows Tafel plots of CW602N in the different test waters at 50°C after 24 h exposure. The highest cathodic current density was obtained in TW2, whereas the anodic current density was the highest in TW1.

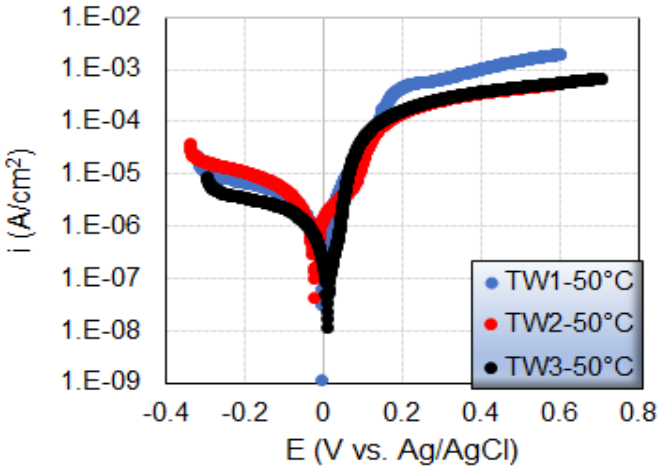

Figure 53. Tafel plots of CW602N after 24 h of exposure at stagnant conditions in the different test waters at 50°C.

Figure 54 shows the comparison of the Tafel plots generated at room temperature and 50 °C. An increased cathodic current density at 50 °C was obvious in TW2 and slightly in increased in TW1. These findings are in contrast to the results in TW3 which resulted in almost similar cathodic current at 22 and 50 °C. The appearance of the pitting potential was more pronounced with an increased temperature TW1 and TW2 compared with TW3.

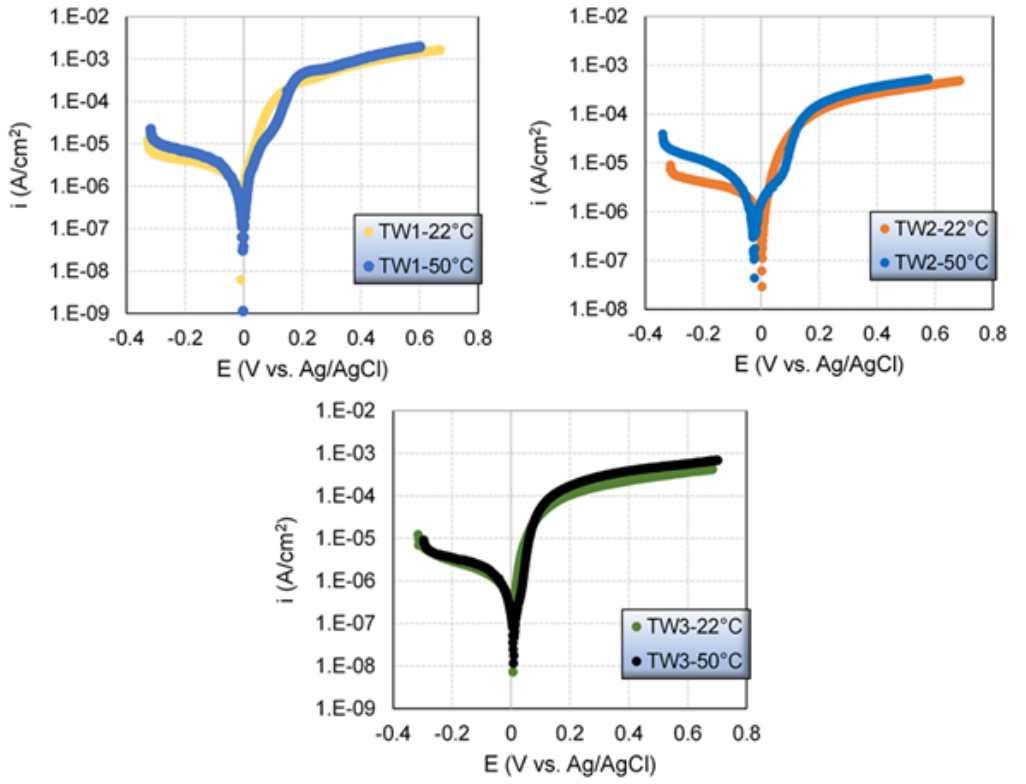

Figure 54. Tafel plots of CW602N after 24 h of exposure at stagnant conditions in the different test waters at 22 and 50 °C.

The different corrosion parameters extracted from the Tafel plots at room temperature and 50 °C after 24 h exposure in the different test waters are summarized in Table 38. Changes in corrosion potential with increased temperature from 22 to 50 °C did not follow the same trend (shift towards less negative values) as observed for the OCP values. The difference between OCP and E_{corr} values did not exceed 17 mV in the worst case at 22 °C and 13 mV at 50 °C. While these differences may appear small, they are within the same range as the changes observed in OCP with increased temperature. The potential scan of CW602N seems to affect the position of E_{corr} significantly considering the development of micro galvanic cells between the three electroactive elements (Cu, Zn and Pb) of this alloy.

The general corrosion rate decreased as indicated by decreased i_{corr} and increased R_p associated with decreased cathodic Tafel slopes. In terms of localized corrosion indicator, the lowest pitting potential was observed in TW3 followed by TW2 and TW1. TW3 was hence at 50 °C and after 24 h exposure the most corrosive water for this alloy.

Table 38. Different corrosion parameters of CW602N after 24 h exposure in the different test waters at 22°C and 50°C

	22 °C			**50 °C**		
	TW1	**TW2**	**TW3**	**TW1**	**TW2**	**TW3**
E_{corr} [mV vs. Ag/AgCl]	-13.0	3.0	5.0	-15.0	-14.0	6.0
i_{corr} [µA/cm^2]	0.9	1.6	0.6	0.8	1.3	0.5
R_p [kΩ cm^2]	15.4	12.5	22.2	25.0	15.0	50.0
B_c [mV/dec]	202.1	316.1	256.6	151.1	122.5	126.0
B_a [mV/dec]	42.5	52.0	31.5	73.0	128.5	31.5
E_{pit} [mV vs. Ag/AgCl]	-	-	-	92.0	78.0	31.0

6.1.2.1 LOM

CW511L

LOM was used to characterize the surface of the brass alloys exposed for 24 h at 50 °C to the three test waters. LOM images before and after exposure are presented in Figure 55. The results showed that TW2 was the most corrosive test water with most corroded areas compared with TW1 and TW3. These results are consistent with the lowest pitting potentials, see Table 34. Qualitatively, ranking of the corrosivity of the test waters at 50 °C according to the LOM images; TW2>TW3>TW1, agrees well with the ranking based on E_{pit} values.

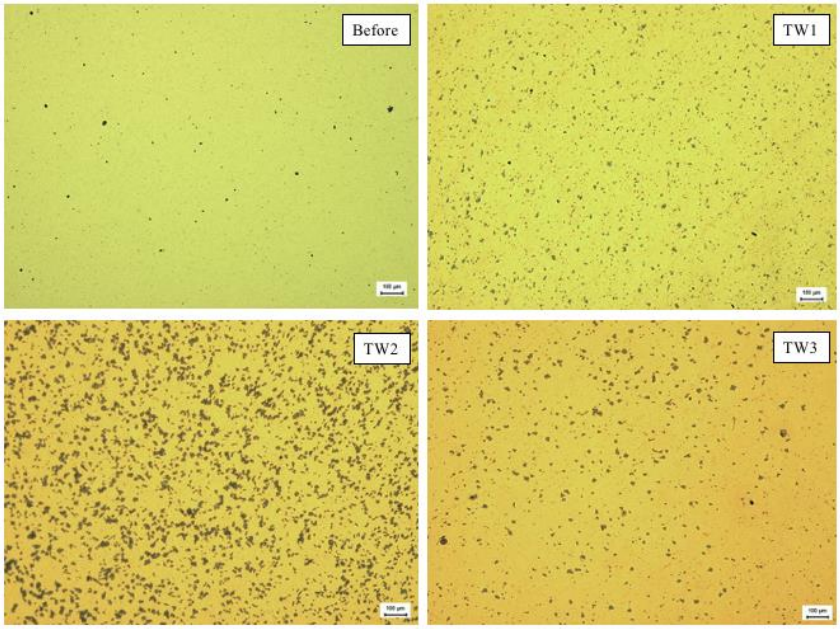

Figure 55. LOM micrographs of CW511L before and after 24 h exposure to three test waters TW1, TW2 and TW3 respectively at 50°C.

CW724R

LOM images before and after exposure at 50°C are presented in Figure 56. Exposure in TW3, resulted in localized corrosion, also confirmed visually. Thus, TW3 was the most corrosive test water. These findings agree well with the lowest pitting corrosion potential determined from the electrochemical investigation (Table 36). For TW2 and TW3 a dark red color could be observed which can be related to copper-rich corrosion products. The relative similarity in terms of surface appearance upon exposure in TW1 and TW2 may be related to their similarities in terms of general corrosion resistance performance as observed through their i_{corr} and R_p values (Table 36). However, pitting corrosion in TW1 and not in TW2 is consistent with the relatively lowest E_{pit} in TW1 compared to TW2.

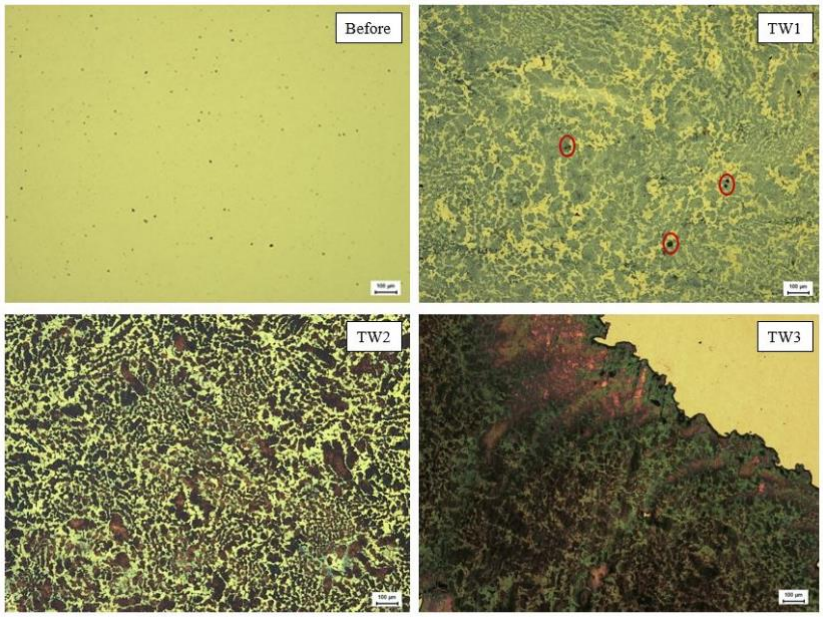

Figure 56. LOM micrographs of CW724R before and after 24 h exposure to three test waters TW1, TW2 and TW3 respectively at 50°C.

CW602N

The surface appearance of CW602N before and after exposure in the three test waters at 50 °C are shown in Figure 57. Exposure in TW3 resulted in the most corroded surface in terms of density and extent (large black corroded areas). These results showed the TW3 test water to be the most corrosive water at 50 °C. TW1 was shown to be the least corrosive test water, findings that are consistent with the pitting potential values shown in Table 38.

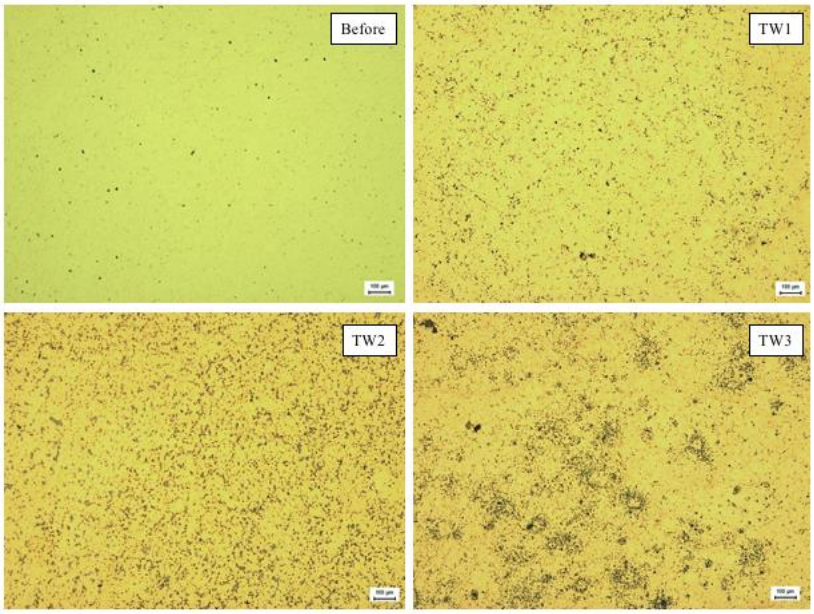

Figure 57. LOM micrographs of CW602N before and after 24 h exposure to three test waters TW1, TW2 and TW3 respectively at 50°C.

6.2 Long term exposure

6.2.1 Electrochemical tests

CW511L

The OCP of CW511L was monitored during 72 days of immersion in TW3, Figure 58. Three stages could be observed starting with a shift toward more negative potentials, stabilization at an average of -40 mV vs Ag/AgCl, followed by a final shift to the positive direction after 32 days of immersion.

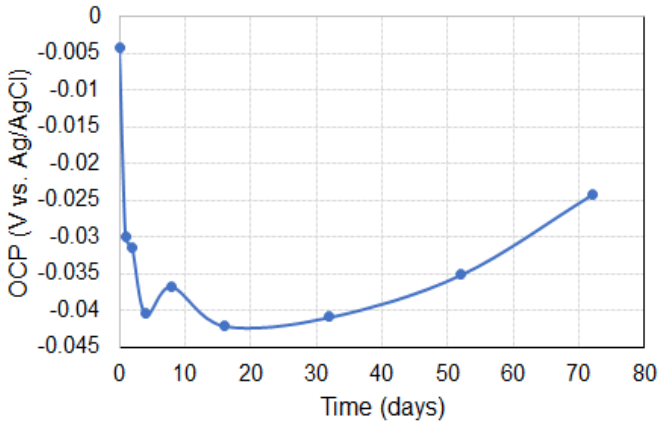

Figure 58. OCP evolution of CW511L in TW3.

Potentiodynamic scans were conducted at different exposure times to investigate the corrosion kinetics at different surface status conditions. Figure 59 shows the obtained results in the Tafel plot. A clear difference is shown in the cathodic branch with slopes moving from a diffusion contribution/control to a pure active control after 72 days of immersion. For the anodic branch, considerable variation occurred after 52 days indicated by a sharp increased current density that may be attributed to a pitting corrosion. This was though not observed after 72 days.

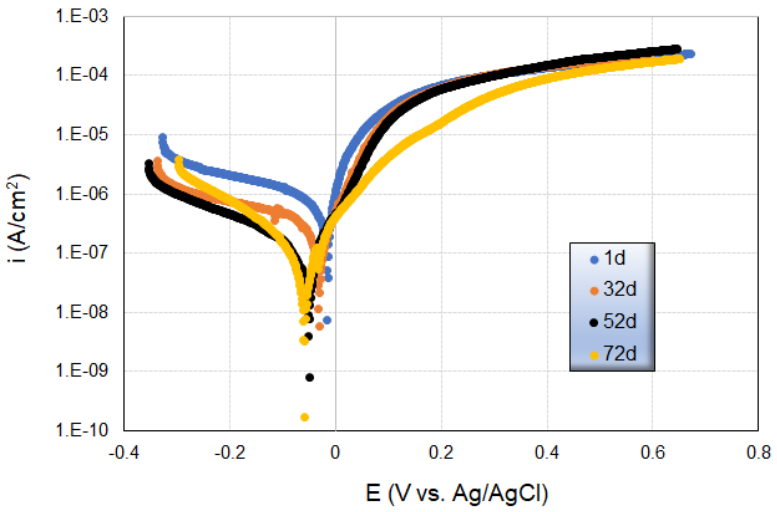

Figure 59. Tafel plots of CW511L after 1, 32, 52 and 72 days of exposure in TW3.

Corrosion parameters extracted from the potentiodynamic investigations are summarized in Table 39. The results obtained after 1 day are added for comparison with long-term durations. Changes in E_{corr} values agrees well with variations in the OCP discussed above. These changes are associated with decreased instantaneous corrosion rates (i_{corr}) and increased polarization resistance (R_p) which can be attributed to the formation of corrosion products.

Table 39. Corrosion parameters of CW511L after 1, 32, 52 and 72 days in TW3

	1d	**32d**	**52d**	**72d**
E_{corr} [mV vs. Ag/AgCl]	-14.0	-31.0	-51.0	-59.0
i_{corr} [µA/cm^2]	0.4	0.2	0.1	0.1
R_p [kΩ cm^2]	28.6	60.2	181.5	271.7
B_c [mV/dec]	219.3	123.9	162.9	153.9
B_a [mV/dec]	30.9	49.9	64.9	99.9
E_{pit} [mV vs. Ag/AgCl]			7.0	

CW724R

Changes in OCP were monitored during 72 days of immersion in TW3, Figure 60. Three stages could be observed starting by an initial shift to the negative potential values region followed by a reverse shift to the noble direction at two rates (fast and slow). The noble potential values region corresponds to the reversible potential of pure copper which indicates that this alloy (with higher copper content) on a long-term perspective behaves as copper when exposed to TW3.

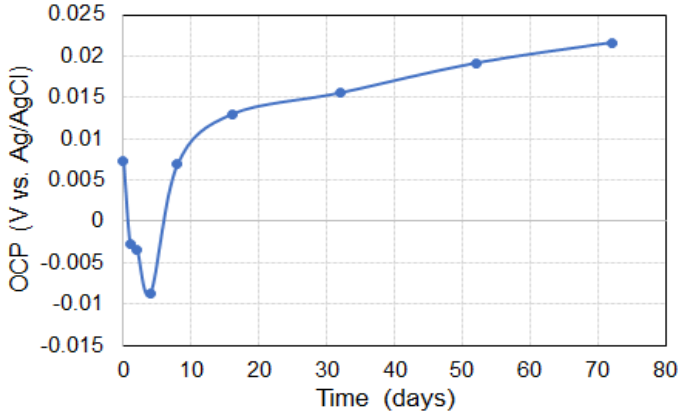

Figure 60. OCP evolution of CW724R in TW3

Results of the potentiodynamic scans conducted for CW724R at different exposure times are presented in Figure 61. The figure shows changes in both cathodic and anodic currents. The cathodic current density changed in two ways, a reduction from 1 to 32 days followed by an increase between 32 to 72 days of immersion. For the anodic branch, a slight decreased anodic current and appearance of a sharp increased current was only observed at 0.068 V vs. Ag/AgCl after 52 days.

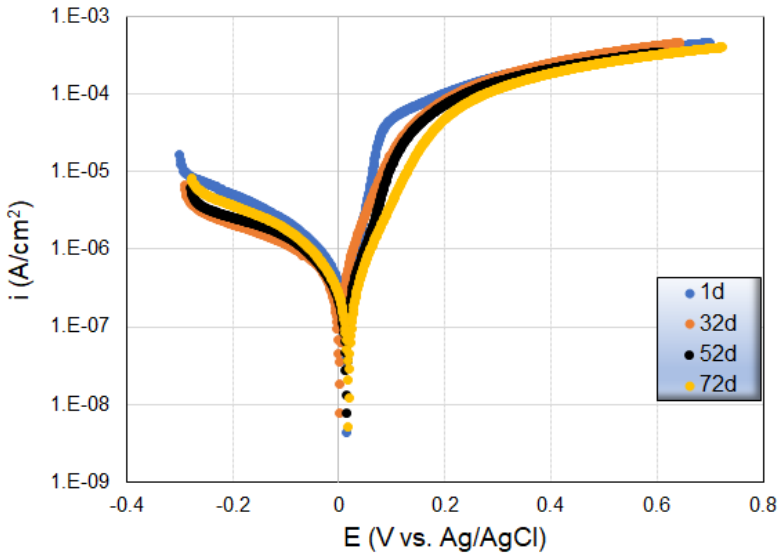

Figure 61. Tafel plots of CW724R after 1, 32, 52 and 72 days of exposure in TW3

Corrosion parameters extracted from the potentiodynamic scans are summarized in Table 40. The corrosion current density decreased with time and associated with a shift of E_{corr} towards the copper corrosion potential (+340 mV) and increased polarization resistance R_p, related to formation of corrosion products.

Table 40. Corrosion parameters of CW724R after 1, 32, 52 and 72 days in TW3

	1d	**32d**	**52d**	**72d**
E_{corr} [mV vs. Ag/AgCl]	11.0	1.0	12.0	18.0
i_{corr} [µA/cm²]	0.5	0.4	0.3	0.2
R_p [kΩ cm²]	33.3	37.2	46.5	62.1
B_c [mV/dec]	163.5	226.9	122.9	133.9
B_a [mV/dec]	34.0	53.0	53.9	62.0
E_{pit} [mV vs. Ag/AgCl]	-	-	68.0	-

CW602N

Changes in OCP were monitored during 72 days of immersion in TW3, Figure 62. The OCP shifted initially towards more negative values region followed by a relative constant potential of approximately -20 mV vs. Ag/AgCl up to 32 days. An increased OCP was observed after 52 days followed by a decreased levels up to 72 days.

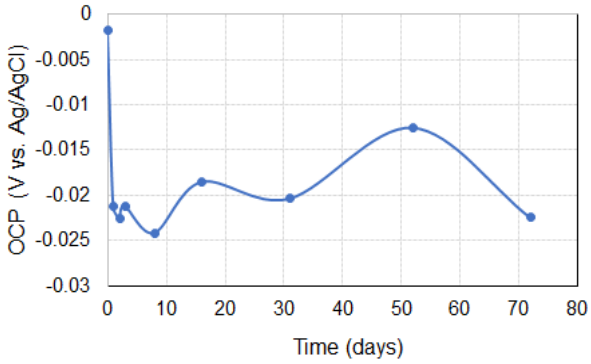

Figure 62. OCP evolution of CW602N in TW3.

Potentiodynamic scans were conducted after different exposure times, Figure 63. Main changes were predominantly observed for the anodic process whereas the cathodic processes seemed to be relatively stable.

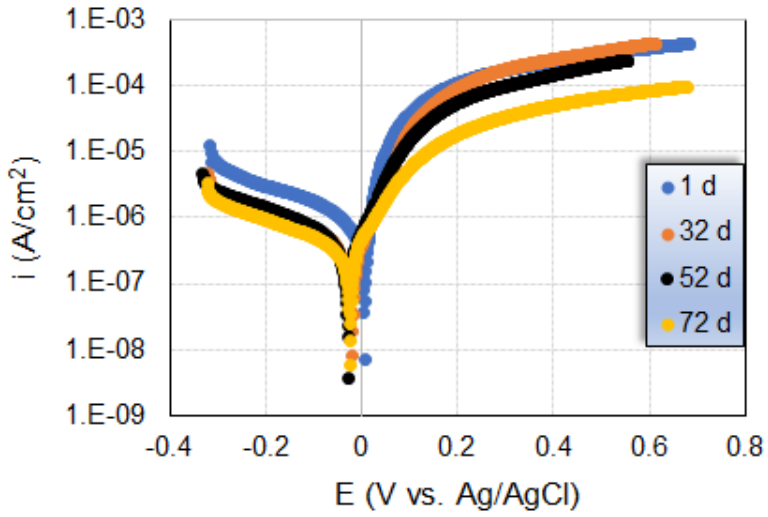

Figure 63. Tafel plots of CW602N after 1, 32, 52 and 72 days of exposure in TW3

Corrosion parameters extracted from the potentiodynamic investigation are summarized in Table 41. While R_p increased with time, i_{corr} fluctuated between 1 and 72 days of immersion. This was associated with increased Tafel slopes between 32 and 72 days.

Table 41. Corrosion parameters of CW602N after 1, 32, 52 and 72 days in TW3

	1d	**32d**	**52d**	**72d**
E_{corr} [mV vs. Ag/AgCl]	5.0	-18.0	-29.0	-24.0
i_{corr} [µA/cm²]	0.6	0.2	0.3	0.3
R_p [kΩ cm²]	22.2	42.7	51.3	53.1
B_c [mV/dec]	256.6	160.0	237.8	247.9
B_a [mV/dec]	31.5	65.0	82.9	88.9

Electrochemical Impedance spectroscopy (EIS)

CW511L

The EIS response of CW511L in TW3 was monitored up to 72 days of immersion. Nyquist and Bode diagrams are shown in Figures 64 and 65, respectively. The Nyquist diagram shows small and incomplete HF semi-circle which increased in size up to 52 days before decreased after 72 days of immersion. The low frequency impedance loop increased in size and did not intersect with the real axis which makes the determination of polarization resistance challenging for longer exposure durations.

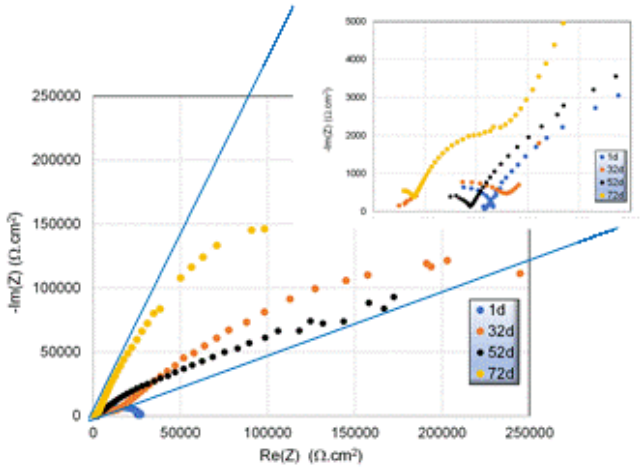

Figure 64. Nyquist diagram of CW511L at E_{corr}
up to 72 days of immersion in TW3 at room temperature.

The Bode representation shows additional features of the CW511L response with a phase angle that did not exceed 45°. The number of phase angle maxima, which indicates the number of processes involved, was not obvious to determine due to similarity in kinetic behavior. Two main processes i.e. charge transfer followed by diffusion process at LF were expected to be observed after 1 day of immersion. An additional process of adsorption seemed to appear with a negative phase angle. The response after 32 and 72 days of immersion was characterized by two well defined processes (two phase angle peaks). The impedance magnitude at LF seemed to increase with immersion time and was correlated to an increased R_p as presented in Table 39.

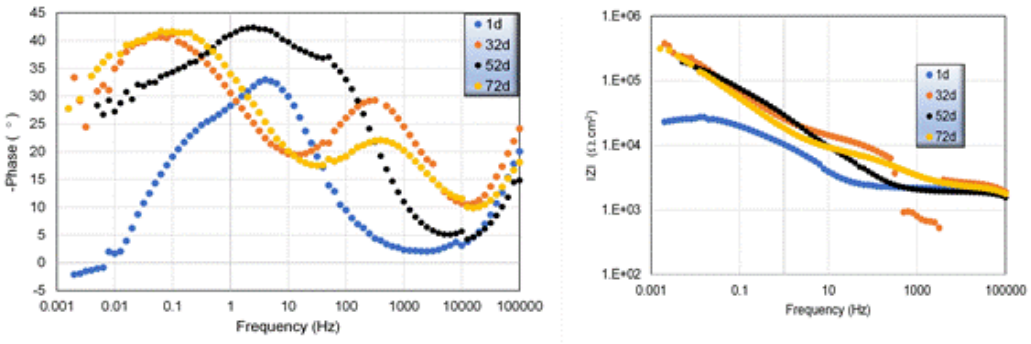

Figure 65. Bode diagrams of CW511L at E_{corr} up to 72 days of immersion in TW3 at room temperature.

CW724R

The EIS response of CW724R in TW3 was monitored for up to 72 days of immersion. Nyquist and Bode diagrams are shown in Figures 66 and 67, respectively. The Nyquist diagram shows a small and incomplete HF semi-circle which did not vary significantly in terms of size up to 72 days of immersion. More depressed semi-circles were observed at intermediate and low frequencies. Similar to CW511L, the low frequency impedance loop increased in size and did not intersect with the real axis which makes the determination of polarization resistance challenging after longer exposure durations.

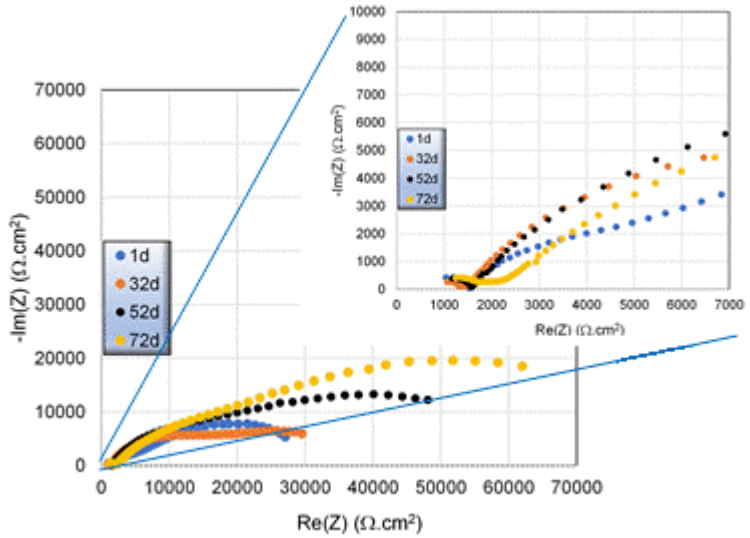

Figure 66. Nyquist diagram of CW724R at E_{corr} up to 72 days of immersion in TW3 at room temperature.

Figure 67 shows the Bode phase angle diagram. The two peaks are well defined after 1 day of immersion and were attributed to charge transfer and diffusion processes. The impedance magnitude at LF increased with time in the same way as the increase in polarization resistance R_p obtained from Tafel plot (Table 40).

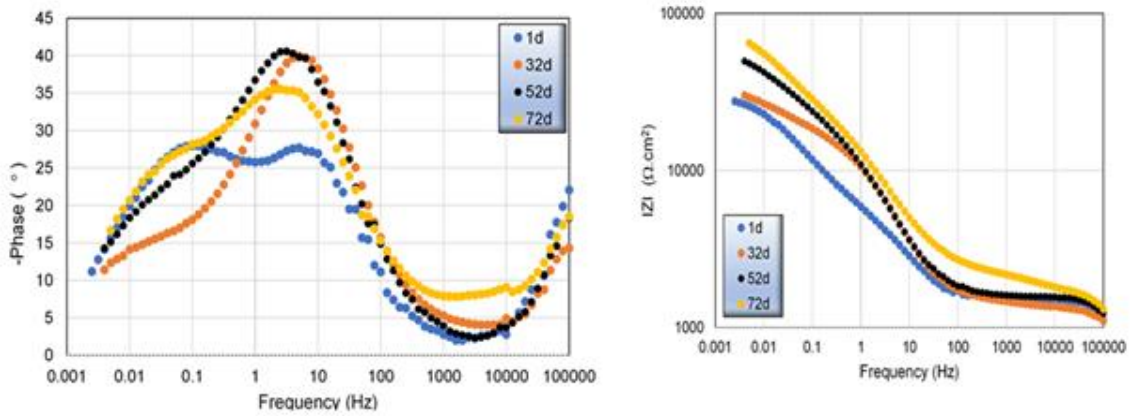

Figure 67. Bode diagrams of CW724R at E_{corr} up to 72 days of immersion in TW3 at room temperature.

CW602N

The EIS response of CW602N in TW3 was monitored for up to 72 days of immersion. Nyquist and Bode diagrams are shown in Figures 68 and 69, respectively. The Nyquist diagram shows a small and incomplete HF semi-circle which did not vary significantly in terms of size except for after 72 days of immersion. The low frequency impedance loop increased in size and appeared as a depressed semicircle.

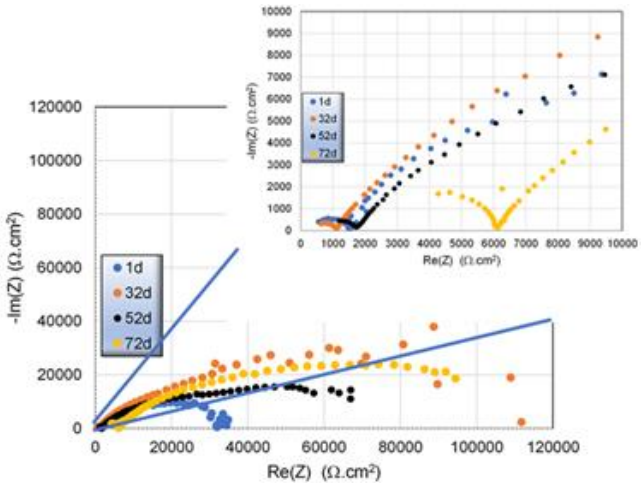

Figure 69. Nyquist diagram of CW602N at E_{corr}
up to 72 days of immersion in TW3 at room temperature.

Figure 70 shows the Bode phase angle diagrams. The two peaks seem to be mixed at different immersion times and were attributed to charge transfer followed by a diffusion process. The impedance magnitude at LF seemed to increase with time in the same way as an increased polarization resistance R_p obtained from the Tafel plot (Table 41).

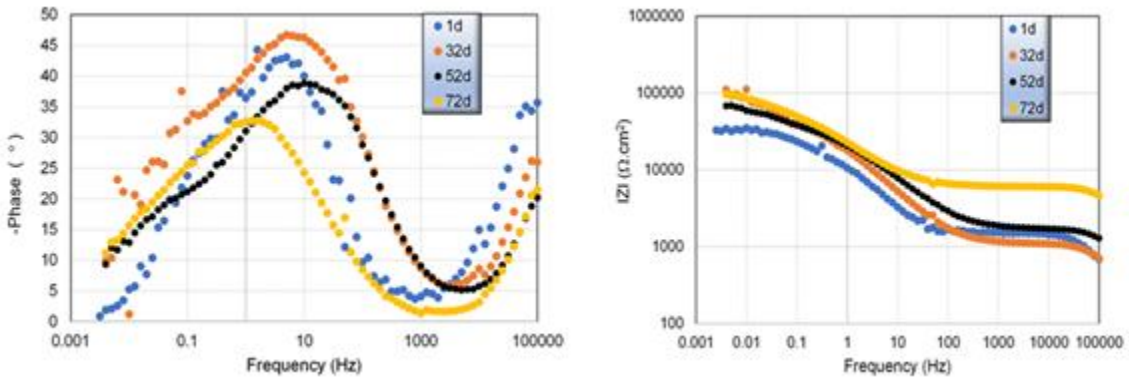

Figure 70. Bode diagrams of CW602N at E_{corr}
up to 72 days of immersion in TW3 at room temperature.

6.2.2 Weight loss

CW511L

The general corrosion rate of CW511L was determined by means of the weight loss method after different exposure periods in stagnant TW3. Very low corrosion rates were determined (<0.0042 mm/y) which indicates an excellent general corrosion resistance of this alloy in normal tap water (Figure 71). [37] The corrosion rates decreased during the first month followed by an increased rate to similar levels as observed after 16 days of exposure.

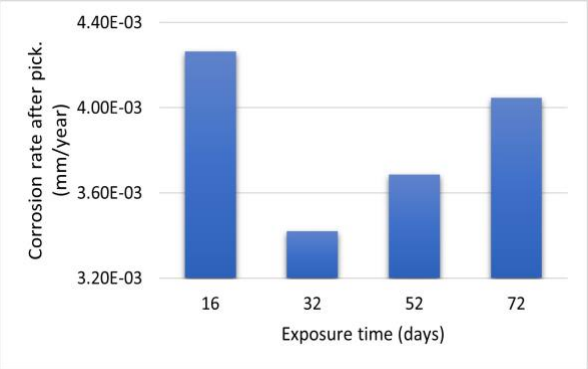

Figure 71. Corrosion rates determined for CW511L in TW3 using the weight loss method

CW724R

Similar corrosion rates for CW511L were determined for CW724R in TW3. The corrosion rate decreased with time to ≈0.0031 mm/y after one month (Figure 72), a rate that remained up to 72 days of exposure.

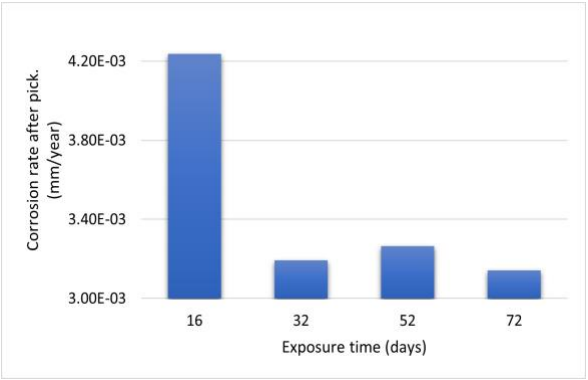

Figure 72. Corrosion rates determined for CW724R in TW3 using the weight loss method

CW602N

Due to a limited number of samples, the general corrosion rate of CW602N was determined for only one immersion time. A general corrosion rate of 0.0036 mm/y was measured after 72 days of immersion. This value will be considered as reference for comparison with other alloys at the same duration.

6.2.3 SEM-EDS

CW511L

SEM images of CW511L after 72 days of immersion in TW3 are shown in Figure 76. Two different surface areas were observed i.e. a smooth and a rough surface. Some pits were observed in some locations as shown in Figure 73, picture 2. EDS analysis was performed at three different locations (Figure 74).

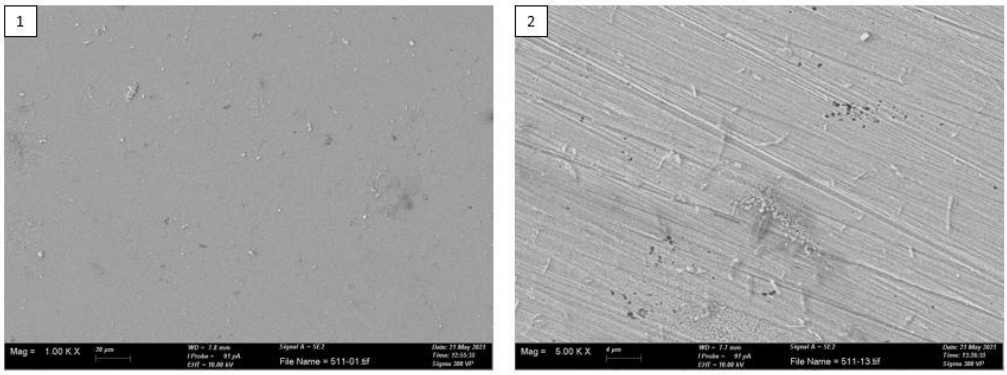

Figure 73. SEM images of CW511L exposed for 72 h in stagnant TW3 at 22 °C
1: 1000x magnification 2: 20 000x magnification.

EDS analysis (Table 42) on both the smooth area (Spectrum 1) and at the rough area (Spectrum 2 and 3), shows that the predominance of copper and oxygen (copper oxide) with a minor presence of zinc presence and some chlorine (Spectrum 2).

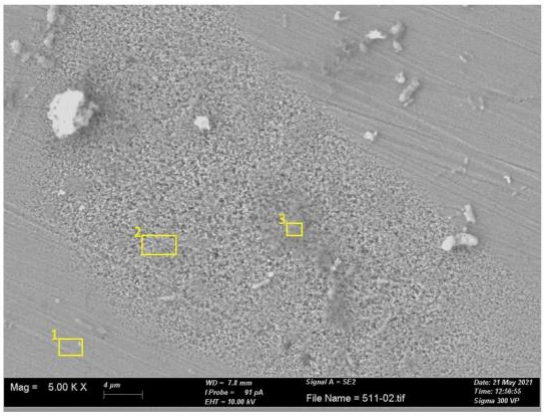

Figure 74. SEM image (5000x magnification) of CW724R exposed for 72 days to stagnant TW3 at 22 °C with marked areas for EDS analysis.

Table 42. Elemental analysis of CW511L after 72 days immersion at stagnant conditions in TW3 at 22 °C.

wt.-%	Cu	Zn	O	Cl
Spectrum 1	86.5	3.7	9.7	-
Spectrum 2	84.7	4.0	10.8	0.5
Spectrum 3	80.8	5.7	13.6	-

CW724R

SEM images of CW724R after 72 days of immersion in TW3 are shown in Figure 75. A uniform appearance was observed with corrosion products in a particular form. EDS analysis on selected locations shown in Figure 76 revealed a predominance of copper and oxygen (copper oxide) with minor amounts of zinc and silicon (Spectrum 2) (Table 43).

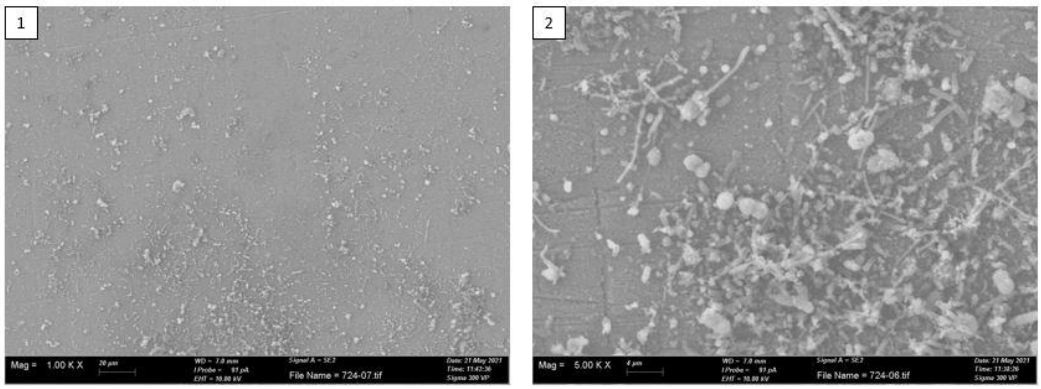

Figure 75. SEM images of CW724R exposed for 72 days at stagnant conditions in TW3 at 22 °C. 1: 1000x magnification 2: 5000x magnification.

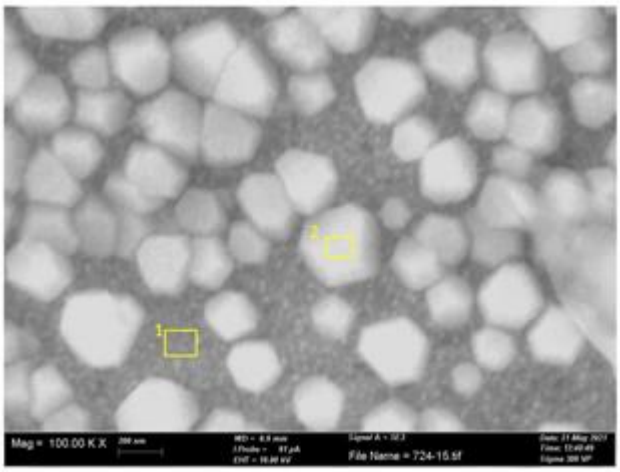

,

Figure 76. SEM image (100 000x magnification) of CW724R exposed for 72 days at stagnant conditions in TW3 at 22 °C with marked areas for EDS analysis.

Table 43. Elemental analysis of CW724R after 72 days immersion at stagnant conditions in TW3 at 22 °C.

wt.-%	Cu	Zn	O	Si
Spectrum 1	82.8	6.6	8.8	1.7
Spectrum 2	84.5	5.5	8.3	1.7

CW602N

SEM images of CW602N after 72 days of immersion in TW3 are shown in Figure 77. Two different corroded appearances were distinguished. EDS analysis (Table 44) performed at the two areas (Figure 78) showed different extent of corrosion with a composition dominated by copper and oxygen (possibly copper oxide) with minor amounts of zinc in the more corroded area (Spectrum 1) compared to the less corroded area (Spectrum 2).

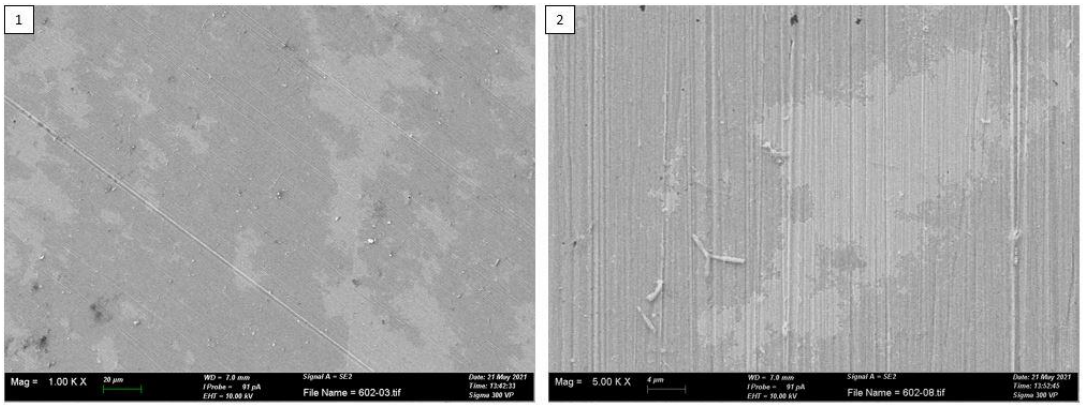

Figure 77. SEM images of CW602N exposed for 72 hours at stagnant conditions in TW3 at 22 °C. 1: 1000x magnification 2: 5000x magnification.

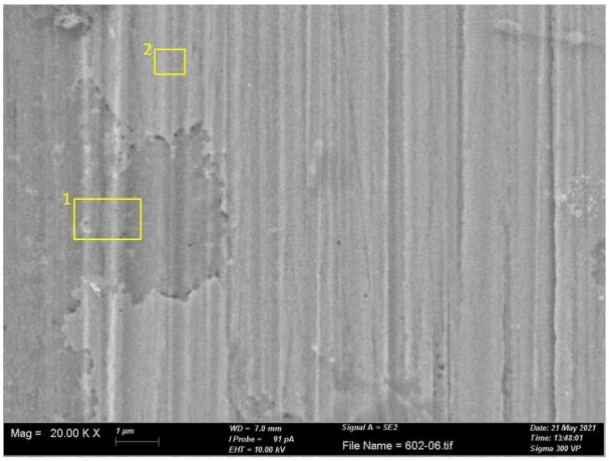

Figure 78. SEM image (20 000x magnification) of CW602N exposed for 72 days at stagnant conditions in TW3 at 22 °C and marked areas for EDS analysis.

Table 44. Elemental analysis of CW602N after 72 days immersion at stagnant conditions in TW3 at 22 °C.

wt.-%	Cu	Zn	O
Spectrum 1	86.5	4.8	8.8
Spectrum 2	63.7	35.0	1.3

6.2.4 XPS

XPS analysis of the composition of the outermost surface oxide was conducted to investigate changes in composition with time for the different alloys before and after exposure into the different test waters.

CW511L

XPS results obtained after different exposure durations to assess long-term changes in the surface oxide composition when exposed to the test water are presented in Figure 79. The surface oxide of the unexposed alloy was predominantly composed of more zinc-rich oxides compared with copper-rich oxides. Small quantities of oxidized lead and arsenic were observed within the outermost surface oxide. After 2 days, the fraction of zinc-rich corrosion products decreased at the same time as the fraction of copper-rich corrosion products increased and dominated the surface. The relative fraction of zinc-rich corrosion products increased up to 32 and 72 days of immersion with the presence of iron, lead, silicon and arsenic. At this immersion time, XPS results show that the surface layer starts to be a mixture of both copper (I) and (II) corrosion products (Table A1 in Appendix). These results are consistent with the OCP measurement after 32 days, which showed an inflexion point at which the alloy started to change its corrosion behavior. Indeed, lead and silicon reached their maximum in the surface oxide at this immersion time. Iron and arsenic were observed after 32 days in varying relative proportions with time. The results are also consistent with the corrosion rate findings (weight loss results, Figure 71) which showed changed rates after 32 days of immersion.

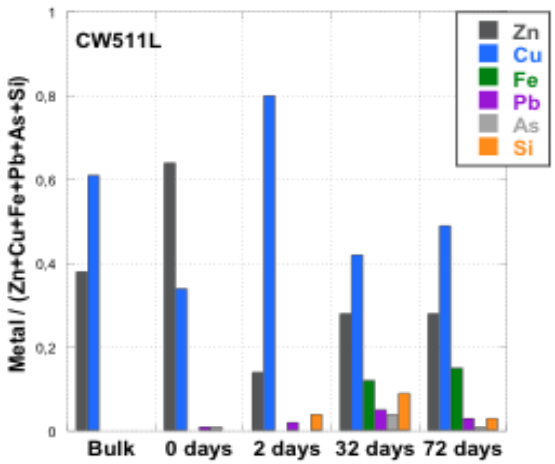

Figure 79. XPS analysis of the outermost surface oxide of CW511L after 0, 2, 32 and 72 days in TW3 at 22 °C.

CW724R

Figure 80 shows the XPS results obtained after different exposure durations for the CW724R alloy. The unexposed surface was composed of both copper- and zinc rich oxides. An increased fraction of the copper-rich corrosion products and a reduced amount of zinc-rich corrosion products was observed with time. The surface oxide was after 72 h predominantly composed of both copper (I) and (II) corrosion products (Table A1 in Appendix) with small amounts of zinc-rich corrosion products. Similar findings were observed in OCP that with time changed to

a similar potential as pure copper (Figure 60). An increased relative fraction of silicon was observed at the surface up to 32 days before reduced in amount. Arsenic was observed after 32 days and remained in the same relative amount up to 72 days. Lead was only observed after 2 days of exposure.

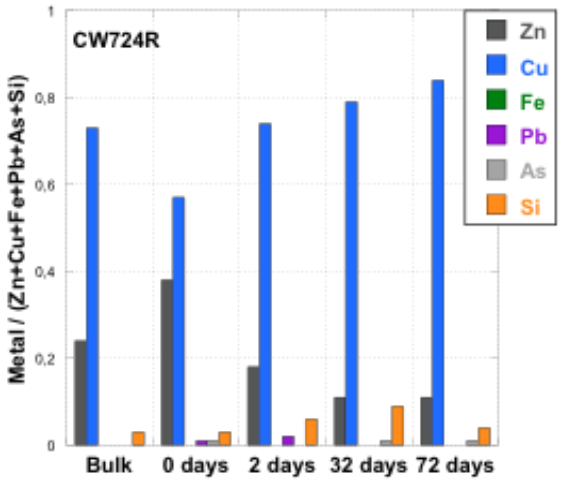

Figure 80. XPS analysis of the outermost surface of CW724R after 0, 2, 32 and 72 days exposure in TW3 at 22 °C.

CW602N

The XPS results for CW602N after different days of exposure are shown in Figure 81. After 2 days up to 72 days, a reduced relative amount of both copper- and zinc-rich corrosion products was observed. The surface layer composition showed a growth of copper (I) oxides (possibly Cu_2O) and a reduced presence of copper(II) corrosion products (Table A1 in Appendix). The relative amounts of arsenic remained the same between 2 and 72 days, whereas the relative amounts of lead decreased between 2 and 32 days while it increased from 32 to 72 days, opposite to the behavior of silicon. Thus, the results indicate that the CW602N changed its corrosion behavior after 32 days since also iron was observed within the outermost surface oxide at the stage.

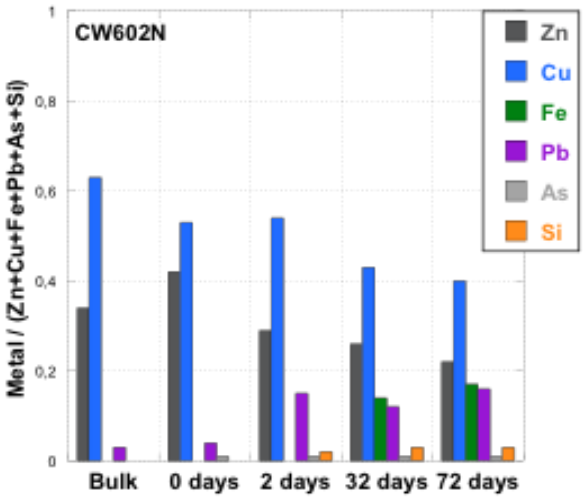

Figure 81. XPS analysis of the outermost surface oxide of CW602N after 0, 2, 32 and 72 days exposure in TW3 at 22 °C.

7. Discussion

Generated results in this master thesis work are in the following discussed from three perspectives including environmental factors, exposure duration and alloying elements. Both environmental variables and exposure duration are discussed for each alloy separately, followed by a comparison between each lead-free alloy (CW511L, CW724R) and the lead-containing brass (CW602N) in terms of effects of alloying elements.

7.1 CW511L

7.1.1 Effect of water chemistry

The effect of the test water composition on the corrosion performance was explored at room temperature for short-term immersion times that did not exceed 24 h. Based on the electrochemical investigations and the microscopic surface characterization at 24 h, TW1 was the most corrosive water followed by TW2 and TW3, respectively. With this ranking, the higher chloride concentration and alkalinity of TW1 was more corrosive to this alloy than a water characterized by a lower pH (TW2). A current plateau was observed only in the anodic branch of this alloy when immersed in TW1, which corresponds to a diffusion process. This process may be attributed to the diffusion of copper ions through the surface oxide or from the oxide to the bulk solution [38]. However, a simultaneous diffusion of both copper and zinc ions cannot be excluded and needs further analysis. Surface analysis by EDS showed a low content of Zn in the corroded areas, which may be related to a dezincification process. However, dezincification was minor since the LOM analysis of the cross section did not show any detectable depth. Both copper- and zinc-rich corrosion products (oxides) combined with the presence of chlorine and sulfur were observed. It was noticed that zinc rich corroded areas predominantly were connected with sulfur and copper-rich corroded areas with chlorine. While waters of lower pH, higher chloride content and higher alkalinity generally induce a higher extent of selective release of zinc [18,21], the CW511L remained resistant to such selective dissolution but rather showed localized corrosion (SEM images-Figures 32,34,35), though too minor to be detected in the potentiodynamic investigations.

7.1.2 Effect of water temperature

Regarding the temperature effect, the obtained results support the development of severe localized corrosion, which changed the test waters corrosiveness ranking to TW2>TW3>TW1. This ranking is based on the localized corrosion indicator, which is the pitting potential (E_{pit}) determined from potentiodynamic curves. However, a reduced general corrosion (observed on i_{corr} and R_p) with increased temperature was observed and was explained by a reduced content of dissolved oxygen (oxidant) (from 8 to 4 mg/L). This reduction in oxygen content is undesirable for the stability of the oxides present at the surface and favorable for localized corrosion to take place, observed via the pitting potential. Moreover, the corrosivity was higher in the water of low pH for this alloy, which was the case of TW2. Therefore, the corrosivity of the test water depends both on its composition and on temperature, from which follow different

corrosion forms. It is though expected that zinc-rich corrosion products present in the oxide are locally corroded due their lower reversible potential compared to copper-rich corrosion products. This should be investigated in future potentiostatic investigations.

7.1.3 Effect of test duration

In terms of exposure duration, the corrosion rate was assessed only in TW3 at 22 °C up to 72 days of immersion. Based on weight loss results, three stages were observed starting with a sharply reduced corrosion rate (due to corrosion product formation) preceding to a steady state stage followed by a re-increased rate after 32 days. In parallel, changes in OCP followed the same behavior but with values that after 32 days shifted in the positive direction. At this time, surface analysis (XPS) showed the development of a copper (I) and (II) corrosion products that seemed to be locally corroded after 32 days as observed by the potentiodynamic investigation (Figure 59). However, after 72 days of immersion, no pitting could be discerned in the Tafel plot, which is indicative of a good localized corrosion resistance for this alloy in TW3. A low zinc content observed by means of EDS-analysis may be related to local dezincification, though of non-measurable depth (cross sectional LOM analysis).

Changes of i_{corr} and R_p did not follow the corrosion rates determined from the weight loss samples. Similar results have been observed in the literature, preferentially after long-term exposures [39] and explained by changes in surface oxide composition induced by the electrochemical polarization during potentiodynamic investigations. Similar observations were made for CW511L with the presence of lead and iron in the outermost surface oxide (determined by means of XPS). These elements are known to be electroactive and possibly influence the potentiodynamic results. It is important to mention that one of the limitations of Tafel extrapolation and R_p is the assumption that electrochemical reactions are uniformly distributed over the surface. However, in the case of areas with corrosion products that may suffer from localized corrosion, measured i_{corr} values reflect an average instantaneous corrosion rate [25]. In this case, measurements of i_{corr} values may not reflect the corrosion rate as determined by means of using weight loss methods or match changes in OCP.

7.2 CW724R

7.2.1 Effect of water chemistry

Based on the electrochemical investigations and the microscopic surface characterization, TW2 was the most corrosive water to this copper alloy followed by TW1 and TW3 respectively. With this ranking, the effect of water pH dominated the other factors such as chloride concentration and alkalinity of TW1. The combination of a higher Cu/Zn ratio and lower pH seems to result in accelerated corrosion characterized by a significant extent of copper-rich corrosion products (Figure 30). Moreover, surface examination by means of SEM for samples exposed in TW2 showed a combination of thick corroded layers and localized corrosion appearing in the form of parallel crevices. Analysis by means of EDS showed both copper- and zinc-rich corrosion products dominated by the former with substantial low zinc content

particularly into TW2 compared to the other test waters. Other corrosive elements (Cl, S) were in addition to the silicon observed within the copper rich corroded areas. CW724R showed the lowest content of zinc after exposure in TW2, which may be attributed to a local dezincification. However, it seemed limited and non-severe due to the absence of detectable depths in the cross section samples analyzed by LOM. Curiously, small amounts of phosphorus were observed in the corrosion products formed upon exposure in TW1. Phosphorous has been reported to play an inhibitory role for dezincification [13].

7.2.2 Effect of water temperature

The increase in temperature to 50 °C induced severe localized corrosion changing the test waters corrosiveness ranking (based on E_{pit} values) to TW3>TW1>TW2. Similar to findings for CW511L, a reduced general corrosion was observed (from i_{corr} and R_p) with increased temperature due to a reduced dissolved oxygen content. Copper redeposition was observed for this alloy that is connected to its high bulk content and predominance of a copper-rich surface oxide making this alloy behaving as pure copper. On the other hand, the alloy showed the lowest anodic Tafel slope in TW3 (the highly corrosive water), indicative of highly active corrosion, findings in agreement with the literature [20]. A possible copper-rich corrosion product was observed in the LOM images (Figure 56). This seemed to be more enhanced in TW3 in which the E_{corr} was shifted to more positive values (compared to other waters), close to the E_{pit} potential zone of this alloy.

7.2.3 Effect of test duration

The effect of exposure duration was explored for this alloy up to 72 days in TW3. Based on changes in OCP with time and the weight loss results, three stages were observed starting with a sharply reduced corrosion rate (between 16 and 32 days) preceded by minor re-increased rates (32 days to 52 days) followed by a reduced rates after 52 days. The re-increased rate after 52 days can be related to pitting events observed in the potentiodynamic scan after this time period. Surface analysis by means of XPS showed an increased relative content of copper-rich and decreased fraction of zinc-rich corrosion products up to 72 days with presence of silicon. EDS analysis on this alloy after 72 days of immersion agrees well with the XPS findings in terms of the main elements. This predominant copper-rich corrosion products seemed to offer some corrosion protection, findings in concordance with reduced corrosion rates (weight loss). Moreover, a low zinc content was observed by means of EDS-analysis and may be related to some dezincification. However, the absence of any detectable corroded depths by means of LOM analysis imply negligible dezincification.

7.3 CW602N

7.3.1 Effect of water chemistry

Based on the electrochemical investigation, TW2 was the most corrosive water to this alloy followed by TW1 and TW3 respectively. Similar to findings for CW724R, this ranking seemed more affected by the low pH of the water compared to the other factors (chlorides and

alkalinity). For this alloy, EDS analysis showed lower zinc content associated with less lead present within the surface oxide and vice versa for all test waters (Table 30-32). This observation showed lead to have some role in the corrosion process of this alloy, which agrees with literature findings. [39] Similarly to observations for CW511L, the zinc-rich corrosion products were more prone to localized corrosion induced by sulfur-containing species. The electrochemical investigations of this alloy were characterized by a discrepancy between OCP and E_{corr}. Lead is known for its reversible potential at an intermediate position between zinc and copper participating in the mixed potential E_{corr} [34]. The E_{corr} value is extracted from the potentiodynamic plot during which the results can be influenced by micro-galvanic cells established between zinc and copper and between lead and copper which disable steady state conditions during the potentiodynamic scan. Further electrochemical characterization of these metals separately in the studied test water should clarify the extent of deviation in E_{corr} values.

7.3.2 Effect of water temperature

By increasing the temperature to 50 °C severe localized corrosion was observed which changed the test waters corrosiveness ranking (based on E_{pit} values) to TW3>TW1>TW2. Similar to findings for the other studied alloys, reduced general corrosion was observed (from i_{corr} and R_p) with increased temperature due to a decreased dissolved oxygen content. Furthermore, by observing the anodic Tafel slopes, the lowest value was obtained in TW3 (the most corrosive water at 50 °C), indicative of highly active corrosion.

7.3.3 Effect of test duration

The effect of exposure duration was explored for this alloy up to 72 days in TW3. Based on the OCP results, two stages were observed starting with a sharply decreased corrosion potential E_{corr} (between 1 and 8 days) preceded by a pseudo-steady state (fluctuating E_{corr}, i_{corr} and R_p) stage (8 days to 72 days). Surface analysis performed by XPS showed reduced relative amounts of copper and zinc in the outermost surface layer. The extent of lead varied to a minor extent after 2 days which may explain a reduced relative amount of zinc amount in at the surface up to 72 days. EDS-analysis showed a surface layer predominated by copper-rich corrosion products and low extent of zinc-rich corrosion products that may imply dezincification. However, non-detectable corrosion depths were observed on any samples during cross sectional LOM analysis.

7.4 Effect of lead

7.4.1 CW511L vs CW602N

The effect of the water chemistry on the short-term exposure of CW511L and CW602N was shown to be similar in relation to their good corrosion resistance in TW3 and observed differences in terms of the highest corrosive water. After 24 h of immersion, CW511L was the most affected in the water of high chloride (conductivity) and alkalinity while the CW602N was more affected in TW2 of low pH. Both alloys are α-brasses with higher content of the

following elements; lead, iron and nickel for CW602N. The possible participation of these elements in different electrochemical processes during short immersion time periods may explain the slight variations in corrosion rates and polarization resistance. However, LOM investigations showed a similar surface appearance for both alloys.

An increased test water temperature to 50 °C showed an agreement in terms of corrosion resistance of these alloys in the TW1. CW511L was more affected by the low pH of TW2 while CW602N was more affected by the high pH of TW3 of high conductivity and alkalinity.

The long-term exposures in TW3 could only be assessed for one immersion time (72 days) due to the limited samples. The obtained results showed similar corrosion resistance as observed for CW511L and similar OCP values. From the XPS results, some differences in terms of surface oxide composition were observed with higher relative copper and zinc content for CW511L than for CW602N and presence of lead for CW602N. However, those differences seemed not to result in any large difference in terms of corrosion performance based on the weight loss results. The relatively higher zinc content in the surface oxide of CW511L needs to be investigated in relation to its potentially negative effect to induce localized corrosion [40]. Some beneficial role of lead with regards to the dezincification was observed for CW602N. Since the alloys showed similar corrosion resistance and there may be a risk for lead release from CW602N into the water it would be more favorable to use CW511L.

7.4.2 CW724R vs CW602N

The effect of water chemistry at short-term exposures of CW724R and CW602N was similar terms of their corrosion resistance. After 24 h of immersion, both were more affected by the low pH of the TW2 followed by TW1 of high chloride and alkalinity. The two alloys (CW724R and CW602N) are α-κ and α brasses respectively with higher content of lead, iron and nickel in CW602N and of silicon and phosphorus in CW724R. The corrosion rates were higher for CW724R in TW1 and TW2, whereas the opposite results were observed in TW3. This can be related to the difference in Cu/Zn ratio in the alloys which resulted in copper-rich corrosion products which seems to enhance the cathodic process only in TW1 and TW2.

An increased test water temperature to 50 °C showed for both alloys a low corrosion resistance in TW3 characterized by its alkaline pH. CW724R was less resistant in the highly conductive TW1 in contrast with CW602N which was affected by the low pH of TW2. The resistance of lead brasses to localized corrosion at high temperatures was explained by their formation of insoluble salts that enhance the protective properties of the surface oxide. [41]

Since the long-term exposures in TW3 showed varying corrosion resistance of both alloys, their behavior was difficult to assess based on changes in OCP. Corrosion rates determined from the weight loss method showed a slightly improved corrosion resistance of CW724R compared with CW602N for samples immersed for 72 days. XPS analysis results showed an increased relative content of copper-rich corrosion products and decreased presence of zinc-rich corrosion products with time for CW724R and the absence of lead within the outermost

surface layer. The relative amounts of copper- and zinc-rich corrosion products within the outermost surface decreased with time for CW602N whereas the presence of other elements such as lead and iron increased at the surface. As previously mentioned, the positive role of lead with regard to the low zinc content was observed for CW602N. However, similar corrosion rates determined from the weight loss method of the two alloys make CW724R a good substitute to CW602N due to the absence of lead, that may be released into the water and result in health concerns.

8. Conclusion

Three dezincification resistant brasses (DZR) were studied in terms of their corrosion behavior in tap water considering different variables including water chemistry, temperature and exposure duration. The investigation included α-brasses (CW511L and CW602N) and a duplex α-κ brass (CW724R). Two of these alloys (CW511L and CW724R) are lead-free and the third one (CW602N) contains lead up to 1.7 wt.-%. A combination of electrochemical, microscopic and surface analytical techniques was adopted to explore corrosion types, mechanisms and rates. While these alloys passed the dezincification test as per ISO 6509-1:2014, the aim of this master thesis project was to assess their corrosion performance in tap water.

The water chemistry parameters were selected to investigate the effect of pH, chloride concentration and alkalinity on the corrosion resistance of the three DZR alloys in short-term exposures (24 h). Depending on the brass alloy, the corrosivity of the test waters varied. It was shown that CW511L was more sensitive to the water of higher chloride concentration and alkalinity than a water of low pH. However, the opposite results were obtained for both CW724R and CW602N. This difference in behavior can be attributed to the difference between these alloys in terms of surface oxide chemistry revealed by the XPS (and to some extent EDS) analysis. The presence of certain alloying elements in the surface layer merits further investigations to understand their influence on the corrosion process, i.e. lead for CW602N and silicon and phosphorous for CW724R. The high copper content of CW724R resulted in substantial copper-rich corrosion products that were more pronounced at low pH and resulted in considerably more localized corrosion observed by means of LOM but not during the potentiodynamic investigation.

The corrosivity of the test waters was also affected by the temperature when increased from 22 to 50°C during 24 h of immersion. While no features indicative of dezincification were observed, both general and localized corrosion were evident to a varying extent between the alloys. The initiation of the localized corrosion varied with the chemistry of the test water and the alloy composition. While similar findings were observed for CW724R and CW602N in relation to their high susceptibility to localized corrosion in the alkaline TW3, CW511L was more prone to pitting in TW2 of low pH.

The effect of exposure duration was explored in the alkaline TW3 for the three brasses up to 72 days. Based on the corrosion rate obtained by weight loss, an initially high corrosion rate was followed by a reduced rate with time for both CW511L and CW724R. With its high copper content, CW724R gradually changed its properties similar to pure copper (positive OCP potential) with surface oxides of good barrier properties predominantly composed of copper-rich corrosion products and to a less extent also zinc-rich corrosion products as observed by means of XPS analysis. Localized corrosion was observed for both CW511L and CW724R after 52 days which did not seem to propagate. The long-term corrosion behavior of the leaded brass CW602N was more fluctuating (OCP evolution) most probably related to the involvement of electroactive lead and iron in the surface layer (XPS analysis). The general

corrosion rate of this alloy was determined only at 72 days of immersion, showing a value in the same order of magnitude as determined for CW511L.

Finally, lead-free brasses showed a good corrosion behavior competitive to lead-containing brass. To avoid hazardous effects of lead, lead-free brass alloys should hence replace lead containing brasses on the market.

9. Future work

As a perspective of the present thesis, it will be important to conduct future work to investigate some unexplored aspects for better understanding of the corrosion mechanisms of the studied brass alloys. This may include the following suggestions:

- Complete the surface analysis by the determination the crystalline nature and composition of the surface oxide using XRD.
- Develop the kinetic model or electrical equivalent circuit to fit EIS results and extract the Faradaic process parameters (double layer capacitance and charge transfer resistance) as well as diffusion characteristics.
- Investigate galvanic interactions between lead, iron, zinc and copper considering the proportion between these elements in the surface oxide on the studied alloys.
- Study of pitting corrosion of DZR brasses using cyclic polarization technique to assess the repassivation behavior depending on the alloy and the environmental characteristics.
- Study factors affecting the copper re-deposition and its role in pitting initiation.
- Study the effect of water temperature for longer time peridos to explore the repassivation behavior of the studied alloys.
- Study the effect of organic matter (TOC), flow, disinfection (residual chlorine, microorganisms), water replenishment rate on the corrosion behavior.
- Study effects of coupling to copper (galvanic corrosion) taking place in tap water installations.

10. Acknowledgments

I would like to express my gratitude to the people who helped me with various aspects of this work. Thanks to my supervisors Charlotta Obitz, Annika Talus and Clara Linder at *RISE KIMAB* for the support and consultation. Thanks also to my examiner Prof. Inger Odnevall from *KTH Royal Institute of Technology* for the support and for the help with the XPS analysis.

In addition, I would really like to thank two other researchers at *RISE KIMAB*. Firstly, Abdelkader Meroufel for his guidance and insightful discussions throughout the whole project as well as providing useful feedback for the report. Secondly, Helen Pahverk for teaching and assisting in all the corrosion tests performed.

Finally, I would like to thank *Nordic Brass Gusum AB* and *Wieland Werke AG* for allowing me to use their brass alloys for this investigation.

11. References

[1] Öhman, M. “The effect of Group VA-elements as dezincification inhibitors for brass – and their influence for the susceptibility to IGA and SCC”. Swerea KIMAB, 2014.
[2] Choucri J, Zanotto F, Grassi V, Balbo A, Ebn Touhami M, Mansouri I, Monticelli C. “Corrosion Behavior of Different Brass Alloys for Drinking Water Distribution Systems.“ Metals.2019;9(6):649.
[3] Directive (EU) 2020/2184 of the European Parliament and of the Council of 16 December 2020 on the quality of water intended for human consumption (recast) *OJ L 435, 23.12.2020, p.1–62*
[4] Toulfatzis AI, Pantazopoulos GA, David CN, Sagris DS, Paipetis AS. “Machinability of Eco-Friendly Lead-Free Brass Alloys: Cutting-Force and Surface-Roughness Optimization”. *Metals*.2018;8(4):250.
[5] Kim, JG. Jung SB, Kwon OH, Dealloying Behavior of Unleaded Brasses Containing Bismuth in Potable Water, Corrosion 57 (2001), 291-294.
[6] Tang, M, Sinsheimer P, Sarver, E, Parks, J, Edwards M, Evaluating “Lead-Free” Brass Performance in Potable Water, Corrosion 75 (2019), 865-875.
[7] Moriarty M, Wu Y, Murray T, Hutchinson C, The effect of phase fraction, size and shape on the dezincification of duplex brasses, Corrosion Science 184 (2021), 109366.
[8] Corrosion of metals and alloys- determination of dezincification resistance of copper alloys with zinc-Part 1: test method. ISO 6509-1, (2014).
[9] Influence of metallic materials on water intended for human consumption- dynamic rig test for assessment of metal release- Part 1: design and operation. EN 15664-1 (2013).
[10] Jacobsson, D., Däcker, C-Å., Sundberg, R., Rod, O. A General Guide for Failure Analysis of Brass. Swerea KIMAB, 2010.
[11] R. M. Hussein and O. I. Abd. "Influence of Al and Ti Additions on Microstructure and Mechanical Properties of Leaded Brass Alloys", *Indian Journal of Materials Science*, vol. 2014, Article ID 909506, 5 pages, 2014.
[12] Copper Development Association Publication No. 117. “The Brasses- properties & applications”
[13] D.D. Davies, Dip. App. Chem., MIM. “A note on the dezincification of brass and the inhibiting effect of elemental additions”, Copper Development Association Inc., New York, NY 10016, 1993.
[14] E. Sarver,, Y. Zhang, and M. Edwards, Review of Brass Dezincification Corrosion in Potable Water Systems. Corr. Reviews, 28 (2010), 155-195.
[15] P. Zhou, M.J. Hutchison, J.W. Erning, J.R. Scully, K. Ogle, “An in situ kinetic study of brass dezincification and corrosion”, Electrochimica Acta, Volume 229, 2017, Pages 141-154, ISSN 0013-4686.
[16] Jones, Denny A. *Principles and Prevention of Corrosion*. New York: Macmillan Pub. Co, 1992, pp. 323-332.
[17] E. Sarver, M. Edwards, Controlling non-uniform copper and brass corrosion in building plumbing. Materials Performance 50 (2011), 60-65.
[18] Zhang, Y. and M. Edwards. “Effects of pH, chloride, bicarbonate, and phosphate on brass dezincification.” *Journal American Water Works Association* 103 (2011): 90-102.
[19] Koppar och kopparlegeringar: Copper and copper alloys. Svensk material- & mekanstandard, SMS handbok (1997), 1404-1782; 8
[20] Water Research Foundation, “The Performance of Non Leaded Brass Materials”, 2014.
[21] Carvalho, Maria L. Corrosion of copper alloys in natural seawater: effects of hydrodynamics and pH. Analytical chemistry. Université Pierre et Marie Curie - Paris VI, 2014. English. NNT: 2014, PA066304.

[22] Y. S. Tam & P. Elefsiniotis., "Corrosion control in water supply systems: Effect of pH, alkalinity, and orthophosphate on lead and copper leaching from brass plumbing", Journal of Environmental Science and Health Part A, 2009, 44:12, 1251-1260.
[23] M.E. Turner, Influence of Water Composition on the Dezincification of Duplex Brass Fittings. Proc. Soc. Water Treatment & Examination, (1961), 162.
[24] R. Feser, Uniform Corrosion of Metals in Acid, Neutral and Alkaline Electrolytes. In: Corrosion and oxide films. Encyclopedia of Electrochemistry. M. Stratmann, G.S. Frankel, A. Bard, vol. 4. DECHEMA, (2003). P.67.
[25] Cottis RA, Electrochemical methods. Shreir's Corrosion. Elesevier, (2010). P 1341.
[26] Corrosion of metals and alloys: Electrochemical test methods-guidelines for conducting potentiostatic and potentiodynamic polarization measurements. ISO 17475 (2006).
[27] F. Mansfled, Electrochemical Impedance spectroscopy, Wiley & Sons, (2008).
[28] Influence of metallic materials on water intended for human consumption- dynamic rig test for assessment of metal release- Part 2: test waters. ISO 15664-2, (2010).
[29] RAPP, T. Umweltbundesamt. Presentation at meeting. Stockholm, 2012-04-19.
[30] Paints and varnishes — Determination of resistance to liquids — Part 2: Water immersion method. ISO 2812-2. (2018).
[31] Corrosion of metals and alloys- Removal of corrosion products from corrosion test specimens. ISO 8407, (2021).
[32] G. Kear, B.D. Barker, F.C. Walsh, Electrochemical corrosion of unalloyed copper in chloride media—a critical review. Corrosion Science 46 (2004), 109-135.
[33] M. Damej, D. Chebabe, S. Abbout, H. Erramli, A. Oubair, N. Hajjaji. Corrosion inhibition of brass 60Cu–40Zn in 3% NaCl solution by 3-amino-1,2, 4-triazole-5-thiol. Heliyon 6(2020).
[34] B. Clark, C. Cartier, J. St. Claire, S. Triantafyllidou, M. Prevost, M. Edward, Effect of connection type on galvanic corrosion between lead and copper pipes. AWWA Journal 105 (2013), E576-E589.
[35] M. Orazem, B. Tribollet. Electrochemical Impedance Spectroscopy. John Wiley & Sons. (2008).
[36] A. Lasia, Electrochemical Impedance Spectroscopy and its applications. Springer. (2014).
[37] Fontana M (1986) Corrosion engineering, 3rd edn. McGraw-Hill, New York.
[38] Y. Feng, W.K. Teo, K.S. Siow, K.L. Tan, A.K. Hsieh, The corrosion behaviour of copper in neutral tap water. Part 1: Corrosion mechanisms. Corrosion Science 38 (1996), 369-385.
[39] Y. Zou, J. Wang, Y.Y. Zheng, Electrochemical techniques for determining corrosion rate of rusted steel in seawater. Corrosion Science 53 (2011), 208-216.
[40] J. Morales, G.T. Fernandez, P. Esparza, S. Gonzalez, R.C. Salvarezzat, A.J. Arviat, A comparative study on the passivation and localized corrosion of **α**, **β**, and **α-β** brass in borate buffer solutions containing sodium chloride. 1. Electrochemical data. Corrosion Science 37 (1995), 211.229.
[41] M. V. Rylkina, Yu. I. Kuznetsov, M. V. Kalashnikova, M. A. Eremina, Brass depassivation in neutral chloride media. Protection of metals 38 (2002), 340-346.

12. Appendix

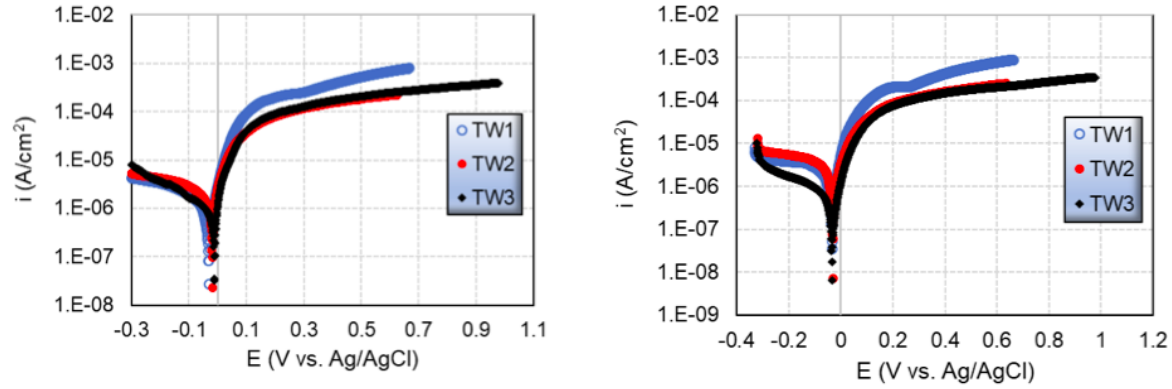

Figure A1. Tafel plots of CW511L after 1 h (left) and 6 h (right) of exposure at stagnant conditions in the different test waters at room temperature.

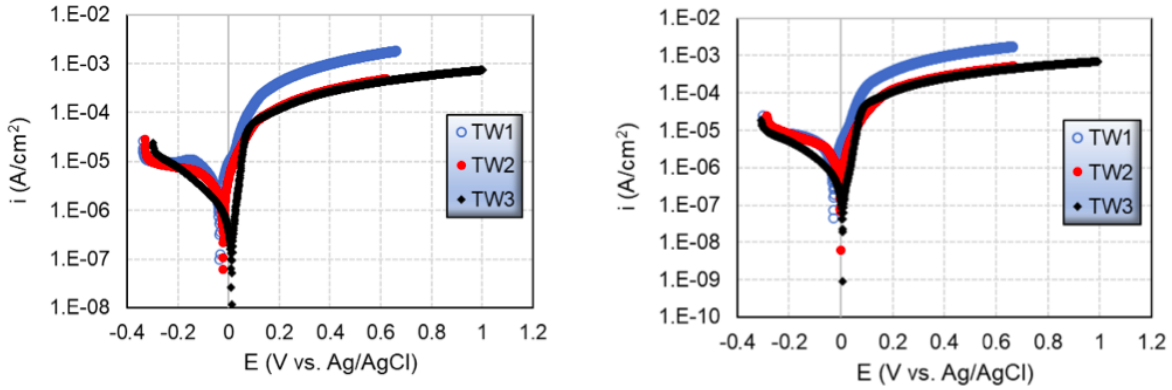

Figure A2. Tafel plots of CW724R after 1 h (left) and 6 h (right) of exposure at stagnant conditions in the different test waters at room temperature.

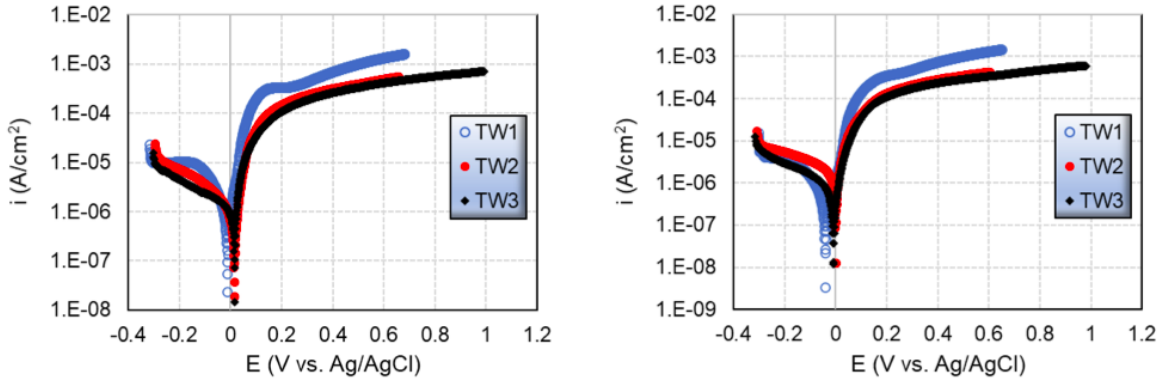

Figure A3. Tafel plots of CW602N after 1 h (left) and 6 h (right) of exposure at stagnant conditions in the different test waters at room temperature.

Table A1. Quantitative composition (wt.%) of surface layer obtained from XPS analysis

CW511L	Zn	Cu (0,I)	Cu(II)	Fe	Pb	As	Si	O
Bulk	*38.2*	*61.5*		*0.1*	*0.2*	*0.0*		
0 days	17.8	9.5			0.3	0.4		25.3
2 days	6.0	33.3			0.7		1.5	23.5
32 days	7.6	4.8	6.8	3.4	1.3	1.1	2.5	39.2
72 days	11.1	6.8	12.4	5.9	1.3	0.5	1.2	32.8

CW724R	Zn	Cu (0,I)	Cu(II)	Fe	Pb	As	Si	O
Bulk	*24.6*	*75.0*		*0.3*	*0.1*	*0.0*	*2.7*	
0 days	22.3	33.1			0.6	0.5	1.7	24.3
2 days	8.0	26.2	6.1		0.7	0.2	2.4	27.2
32 days	4.4	13.9	17.4			0.4	3.4	31.4
72 days	3.8	9.1	20.7			0.4	1.6	32.9

CW602N	Zn	Cu (0,I)	Cu(II)	Fe	Pb	As	Si	O
Bulk	*34.1*	*63.0*		*0.1*	*2.8*			
0 days	23.9	23.2	7.4		2.3	0.6		24.2
2 days	12.3	16.5	6.9		6.3	0.3	0.7	29.6
32 days	11.2	9.1	9.4	6.0	5.3	0.3	1.3	30.4
72 days	9.2	6.5	10.0	7.2	6.7	0.3	1.4	30.1